

DESIGN AND IMPLEMENTATION OF A 130KW, 750VDC BIDIRECTIONAL
PWM RECTIFIER SUPPLIED FROM 400V, 50HZ GRID

A THESIS SUBMITTED TO
THE GRADUATE SCHOOL OF NATURAL AND APPLIED SCIENCES
OF
MIDDLE EAST TECHNICAL UNIVERSITY

BY

TEVFIK PUL

IN PARTIAL FULFILLMENT OF THE REQUIREMENTS
FOR
THE DEGREE OF MASTER OF SCIENCE
IN
ELECTRICAL AND ELECTRONICS ENGINEERING

JUNE 2019

Approval of the thesis:

**DESIGN AND IMPLEMENTATION OF A 130KW, 750VDC
BIDIRECTIONAL PWM RECTIFIER SUPPLIED FROM 400V, 50HZ GRID**

submitted by **TEVFIK PUL** in partial fulfillment of the requirements for the degree of **Master of Science in Electrical and Electronics Engineering Department, Middle East Technical University** by,

Prof. Dr. Halil Kalıpçılar
Dean, Graduate School of **Natural and Applied Sciences**

Prof. Dr. İlkey Ulusoy
Head of Department, **Electrical and Electronics Eng.**

Prof. Dr. Muammer Ermiş
Supervisor, **Electrical and Electronics Eng., METU**

Examining Committee Members:

Assist. Prof. Dr. Ozan Keysan
Electrical & Electronics Engineering, METU

Prof. Dr. Muammer Ermiş
Electrical and Electronics Eng., METU

Assist. Prof. Dr. Emine Bostancı
Electrical & Electronics Engineering, METU

Prof. Dr. Işık Çadırcı
Electrical & Electronics Engineering, HU

Prof. Dr. Özgül Salor Durna
Electrical & Electronics Engineering, GU

Date: 28.06.2019

I hereby declare that all information in this document has been obtained and presented in accordance with academic rules and ethical conduct. I also declare that, as required by these rules and conduct, I have fully cited and referenced all material and results that are not original to this work.

Name, Surname: Tefvik Pul

Signature:

ABSTRACT

DESIGN AND IMPLEMENTATION OF A 130KW, 750VDC BIDIRECTIONAL PWM RECTIFIER SUPPLIED FROM 400V, 50HZ GRID

Pul, Tefik
Master of Science, Electrical and Electronics Engineering
Supervisor: Prof. Dr. Muammer Ermiş

June 2019, 137 pages

Design of a 130kVA of all SiC MOSFET based voltage source three phase PWM rectifier was made in the scope of this thesis study. Power losses of SiC MOSFET and Si IGBT having same voltage and current ratings were analyzed. Selection criteria of all materials used in rectifier panel was explained in detail. Unity power factor operation, bidirectional power flow, pure sinusoidal line current, regulated and adjustable output voltage were achieved by applying Phase Lock Loop algorithm and Voltage Oriented Control. Control methods mostly used in three phase PWM rectifiers which are Voltage Oriented Control and Direct Power Control were compared. Frequently used Pulse Width Modulation methods which are Sinusoidal Pulse Width Modulation and Space Vector Pulse Width modulation were contrasted. Phase Lock Loop algorithm, Voltage Oriented Control and Space Vector Pulse Width Modulation were implemented both on MATLAB/Simulink simulation environment and on Digital Signal Processor. Designed all SiC MOSFET based voltage source three phase PWM rectifier was tested at 130kVA of input power by using three phase voltage source traction inverter in the laboratory test bench as an active load. Power quality measurements such as Total Harmonic Distortion of line to line voltages, Total Harmonic Distortion of line currents and power factor were also performed using power quality analyzer.

Keywords: SiC MOSFET, Phase Lock Loop, Voltage Oriented Control, Space Vector
Pulse Width Modulation, Unity Power Factor

ÖZ

400V, 50HZ ŞEBEKEDEN BESLENEN 130KW, 750VDA İKİ YÖNLÜ DARBE GENİŞLİK MODÜLASYONLU DOĞRULTUCUNUN TASARIMI VE GERÇEKLENMESİ

Pul, Tefik
Yüksek Lisans, Elektrik ve Elektronik Mühendisliği
Tez Danışmanı: Prof. Dr. Muammer Ermiş

Haziran 2019, 137 sayfa

Bu tez çalışması kapsamında 130kVA tamamen SiC MOSFET tabanlı gerilim kaynaklı üç faz darbe genişlik modülasyonlu doğrultucunun tasarımı yapılmıştır. Aynı gerilim ve akım seviyesine sahip SiC MOSFET ve Si IGBT'nin güç kayıpları analiz edilmiştir. Doğrultucu panosunda kullanılan tüm malzemelerin seçim kriterleri detaylıca açıklanmıştır. Birlik güç faktörlü çalışma, iki yönlü güç akışı, tamamen sinus hat akımı, regüle edilmiş ve ayarlanabilen çıkış gerilimi, faz kilitleme döngüsü ve gerilim yönlü kontrol uygulanarak başarılmıştır. Gerilim yönlü kontrol ve direk güç kontrolü gibi üç faz darbe genişlik modülasyonlu doğrultuculara çoğunlukla kullanılan kontrol yöntemleri kıyaslanmıştır. Sinüs darbe genişlik modülasyonu ve uzay vektör darbe genişlik modülasyonu gibi sıklıklı kullanılan darbe genişlik modülasyonu yöntemleri karşılaştırılmıştır. Faz kilitleme döngüsü algoritması, gerilim yönlü kontrol ve uzay vektör darbe genişlik modülasyonu hem MATLAB/Simulink benzetim ortamında hem de sayısal işaret işlemcisi üzerinde gerçekleştirilmiştir. Tasarlanan tamamen SiC MOSFET tabanlı gerilim kaynaklı üç faz darbe genişlik modülasyonlu doğrultucu, laboratuvar test tezgahındaki üç faz gerilim kaynaklı çekiş invertörü aktif yük gibi kullanılarak 130kVA'lık giriş güç değerinde test edilmiştir. Hattan hata gerilimlerin toplam harmonik bozulması, hat akımlarının

toplam harmonik bozulması ve güç faktörü gibi güç kalitesi ölçümleri de, güç kalitesi analizörü kullanılarak yapılmıştır.

Anahtar Kelimeler: SiC MOSFET, Faz Kilitleme Döngüsü, Gerilim Yönlü Kontrol, Uzak Vektör Darbe Genişlik Modülasyonu, Birlik Güç Faktörü

To My Girlfriend, Gamze and To My Parents

ACKNOWLEDGEMENTS

I would like to thank my supervisor, Prof. Dr. Muammer Ermiş for his support, guidance, and encouragement on this thesis study.

I would also like to thank, Prof. Dr. Işık Çadırcı for her support and valuable advices throughout my research work.

I would like to express my gratitude to my girlfriend, Gamze Özer for her endless love, patience and encouragement throughout my life.

I would like to express my thankfulness to my parents, Muharrem and Zeliha, my sister, Merve and my brother in law, Çağrı for their patience, help and eternal encouragement throughout my life.

I wish to thank my colleague, Doğan Yıldırım for his technical support and endless encouragement at all stages of my thesis study.

I wish to thank my friends, Hakan Akşit, Behrang Hosseini and Cem Yolaçan for their contributions in my experimental study.

Finally, I would like to thank my company, ASELSAN for its financial support at the setup phase of my experimental study.

TABLE OF CONTENTS

ABSTRACT	v
ÖZ	vii
ACKNOWLEDGEMENTS	x
TABLE OF CONTENTS	xi
LIST OF TABLES	xiv
LIST OF FIGURES	xvi
LIST OF ABBREVIATIONS	xxi
CHAPTERS	
1. INTRODUCTION	1
1.1. Comparison of Three Phase Rectifier Topologies.....	1
1.2. Usage Areas of Three Phase PWM Rectifiers.....	5
1.3. Thesis Outline.....	9
2. SELECTION OF MATERIALS.....	11
2.1. Power Semiconductor Switching Devices	11
2.1.1. Introduction.....	11
2.1.2. Power Loss and Efficiency Comparison Between Si IGBT Modules and SiC MOSFET Module	14
2.2. Other Materials	22
2.2.1. Introduction.....	22
2.2.2. Current Sensor	23
2.2.3. Voltage Sensor.....	25
2.2.4. 3-Phases Line Contactor	26

2.2.5. Auxiliary Contactor	27
2.2.6. Soft-Start Contactor & Soft-Start Resistor	29
2.2.7. DC Power Supply	32
2.2.8. Heatsink	34
2.2.9. Laminated Bus Bars	36
2.2.10. Fan	39
2.2.11. Single Phase AC Line Reactor	40
2.2.12. DC-Link Capacitor	43
3. FUNCTIONS OF PRINTED CIRCUIT BOARDS USED IN RECTIFIER PANEL	49
3.1. Introduction	49
3.2. Main Board	50
3.3. Power Board	50
3.4. DSP Board	51
3.5. Fiber Optic Interface Board	52
3.6. SiC MOSFET Gate Driver Board	52
4. PHASE LOCK LOOP AND CONTROL STRATEGIES	55
4.1. Phase Lock Loop	55
4.2. Introduction to Control Strategies	61
4.3. Direct Power Control	61
4.4. Voltage Oriented Control	63
5. PULSE WIDTH MODULATION TECHNIQUES	67
5.1. Introduction	67
5.2. Sinusoidal Pulse Width Modulation	67

5.3. Space Vector Pulse Width Modulation	69
6. TESTS, MEASUREMENTS, AND RESULTS	75
7. SIMULATIONS	99
8. CONCLUSION AND FUTURE WORK	115
REFERENCES.....	119
APPENDICES	
A. Cree SiC MOSFET Characteristics.....	125
B. Infineon Si IGBT Characteristics.....	127
C. Semikron Si IGBT Characteristics.....	131
D. Mitsubishi Si IGBT Characteristics.....	135

LIST OF TABLES

TABLES

Table 2. 1. Parameters that found using the graphs on datasheets for 69kVA of input power	15
Table 2. 2. Calculated power losses of each module for 69kVA of input power	16
Table 2. 3. Parameters that found using the graphs on datasheets for 104kVA of input power	16
Table 2. 4. Calculated power losses of each module for 104kVA of input power	17
Table 2. 5. Parameters that found using the graphs on datasheets for 138.5kVA of input power	17
Table 2. 6. Calculated power losses of each module for 138.5kVA of input power .	18
Table 2. 7. Thermal resistance values given in the datasheets	19
Table 2. 8. Estimated junction temperature of each module for three different input power ratings	21
Table 2. 9. Some properties of current sensor	25
Table 2. 10. Some properties of voltage sensor	26
Table 2. 11. Some properties of 3-phases line contactor	27
Table 2. 12. Some properties of auxiliary contactor	29
Table 2. 13. Some properties of soft-start contactor	31
Table 2. 14. Some properties of soft-start resistor	32
Table 2. 15. Some properties of DC power supply	34
Table 2. 16. Some properties of heatsink	35
Table 2. 17. Comparison of insulation materials in terms of some important features	37
Table 2. 18. Some properties of DC-link bus bar	38
Table 2. 19. Some properties of 3-phases AC bus bar	39
Table 2. 20. Some properties of fan	40

Table 2. 21. Some properties of single phase AC line reactor	43
Table 2. 22. Some properties of DC-link capacitor	47
Table 5. 1. Vectors corresponding to eight switching states.....	70

LIST OF FIGURES

FIGURES

Figure 1. 1. Three phase diode bridge rectifier.....	1
Figure 1. 2. Three phase thyristor bridge rectifier	2
Figure 1. 3. Three phase two level voltage source rectifier	3
Figure 1. 4. Three phase three level voltage source rectifier	3
Figure 1. 5. Three phase two level current source rectifier	4
Figure 1. 6. Usage of single phase rectifiers in traction applications	6
Figure 1. 7. Usage of three phase voltage source PWM rectifiers in traction applications	7
Figure 1. 8. Usage of three phase voltage source PWM rectifier in rectification mode together with DC-DC converter for battery charging	8
Figure 1. 9. Usage of three phase voltage source PWM rectifier in inversion mode together with DC-DC converter for battery discharging	8
Figure 1. 10. Usage of three phase voltage source PWM rectifiers in wind turbine applications	9
Figure 2. 1. Efficiencies of each module according to different input power ratings	19
Figure 2. 2. Pictures of materials used in rectifier panel	22
Figure 2. 3. Location of materials inside designed all SiC MOSFET based voltage source three phase PWM rectifier panel	23
Figure 2. 4. Operation principle of auxiliary contactor	28
Figure 2. 5. Soft-start circuit used in the design	30
Figure 3. 1. Relation between the boards used in the rectifier panel	49
Figure 4. 1. PLL scheme.....	56
Figure 4. 2. Electrical interface of PCB type voltage sensor	57
Figure 4. 3. Voltage reading operation	57
Figure 4. 4. Clarke transformation.....	58

Figure 4. 5. Park transformation	59
Figure 4. 6. Usage of theta generated in PLL within inner current control loop	60
Figure 4. 7. Direct power control scheme	62
Figure 4. 8. Voltage oriented control scheme	65
Figure 5. 1. Sinusoidal pulse width modulation scheme.....	68
Figure 5. 2. Space vector diagram.....	70
Figure 5. 3. Turn-on times of vectors.....	71
Figure 5. 4. Line to neutral grid voltages, inductance of boost reactor, DC resistance of boost reactor, line currents and rectifier leg voltages	72
Figure 6. 1. Test bench.....	75
Figure 6. 2. Test equipment.....	76
Figure 6. 3. Oscilloscope images of line to neutral voltage, line current, DC-link voltage and DC-link current in rectification mode	77
Figure 6. 4. Oscilloscope images of line to neutral voltage and line current.....	78
Figure 6. 5. Oscilloscope images of DC-link voltage and DC-link current.....	78
Figure 6. 6. Oscilloscope images of line to neutral voltage, line current, DC-link voltage and DC-link current in inversion mode.....	79
Figure 6. 7. Probe connections of power quality analyzer	80
Figure 6. 8. Instant images of line to line voltages and line currents saved with power quality analyzer	81
Figure 6. 9. THD value of line to line voltage, V_{AB} and percentage of each harmonic according to fundamental value	81
Figure 6. 10. THD value of line current, i_A and percentage of each harmonic according to fundamental value	82
Figure 6. 11. RMS values of line to line voltages, RMS values of line currents, total active power of rectifier, total reactive power of rectifier, total apparent power of rectifier and power factor	82
Figure 6. 12. THD values of line to line voltages, V_{AB} , V_{BC} , V_{CA}	83
Figure 6. 13. THD values of line currents, i_A , i_B , i_C	83
Figure 6. 14. 10 minutes of records of line to line voltages, V_{AB} , V_{BC} , V_{CA}	84

Figure 6. 15. 10 minutes of records of line currents, i_A , i_B , i_C	85
Figure 6. 16. THD values of line to line voltages, V_{AB} , V_{BC} , V_{CA} for 10 minutes of record	86
Figure 6. 17. THD values of line currents, i_A , i_B , i_C for 10 minutes of record.....	87
Figure 6. 18. Grid frequency variation for 10 minutes of record	88
Figure 6. 19. Instant images of line to line voltages and line currents saved with power quality analyzer.....	89
Figure 6. 20. THD value of line to line voltage, V_{AB} and percentage of each harmonic according to fundamental value.....	89
Figure 6. 21. THD value of line current, i_A and percentage of each harmonic according to fundamental value.....	90
Figure 6. 22. RMS values of line to line voltages, RMS values of line currents, total active power of rectifier, total reactive power of rectifier, total apparent power of rectifier and power factor.....	90
Figure 6. 23. THD values of line to line voltages, V_{AB} , V_{BC} , V_{CA}	91
Figure 6. 24. THD values of line currents, i_A , i_B , i_C	91
Figure 6. 25. 10 minutes of records of line to line voltages, V_{AB} , V_{BC} , V_{CA}	92
Figure 6. 26. 10 minutes of records of line currents, i_A , i_B , i_C	93
Figure 6. 27. THD values of line to line voltages, V_{AB} , V_{BC} , V_{CA} for 10 minutes of record	94
Figure 6. 28. THD values of line currents, i_A , i_B , i_C for 10 minutes of record.....	95
Figure 6. 29. Grid frequency variation for 10 minutes of record	96
Figure 6. 30. Admissible value of percentage of each harmonic and admissible value of THD for line to neutral grid voltage.....	97
Figure 6. 31. Regulations for Total Demand Distortion (TDD) and each harmonic order	98
Figure 7. 1. Three phase voltage source PWM rectifier model build in Simulink...	100
Figure 7. 2. Three phase PLL model built in Simulink	101
Figure 7. 3. Line to neutral voltages, V_A , V_B , V_C	102
Figure 7. 4. Alpha & beta axis voltages.....	102

Figure 7. 5. Direct & quadrature axis voltages	103
Figure 7. 6. Theta generated in PLL loop	103
Figure 7. 7. Line to neutral voltage, V_A and theta.....	104
Figure 7. 8. Outer voltage control loop and inner current control loop models built in Simulink	106
Figure 7. 9. Sector selection model built in Simulink for SVPWM	107
Figure 7. 10. Switching states of active vectors and zero vectors if reference vector is in Sector 1	108
Figure 7. 11. Switching states of active vectors and zero vectors if reference vector is in Sector 2	109
Figure 7. 12. Switching states of active vectors and zero vectors if reference vector is in Sector 3	110
Figure 7. 13. Switching states of active vectors and zero vectors if reference vector is in Sector 4	111
Figure 7. 14. Switching states of active vectors and zero vectors if reference vector is in Sector 5	112
Figure 7. 15. Switching states of active vectors and zero vectors if reference vector is in Sector 6	113
Figure A. 1. I_{DS} vs V_{DS} characteristics of SiC MOSFET.....	125
Figure A. 2. I_{DS} vs V_{DS} characteristics of FWD.....	125
Figure A. 3. I_{DS} vs E_{ON} & E_{OFF} characteristics	126
Figure A. 4. T_J vs E_{ON} & E_{OFF} characteristics.....	126
Figure B. 1. I_C vs V_{CE} characteristics of Si IGBT.....	127
Figure B. 2. I_F vs V_F characteristics of FWD.....	128
Figure B. 3. I_C vs E_{ON} & E_{OFF} characteristics	129
Figure B. 4. I_F vs E_{REC} characteristics.....	130
Figure C. 1. I_C vs V_{CE} characteristics of Si IGBT.....	131
Figure C. 2. I_F vs V_F characteristics of FWD.....	132
Figure C. 3. I_C vs E_{ON} & E_{OFF} & E_{REC} characteristics.....	133
Figure D. 1. I_C vs V_{CE} characteristics of Si IGBT.....	135

Figure D. 2. I_F vs V_F characteristics of FWD	136
Figure D. 3. I_C vs E_{ON} & E_{OFF} & E_{REC} characteristic.....	137

LIST OF ABBREVIATIONS

ABBREVIATIONS

$\alpha\beta$	Alpha-Beta
AC	Alternating Current
Al	Aluminum
ADC	Analog to Digital Converter
CCS	Code Composer Studio
DSP	Digital Signal Processor
DC	Direct Current
DPC	Direct Power Control
dq	Direct-Quadrature
DTC	Direct Torque Control
EMI	Electromagnetic Interference
ESL	Equivalent Series Inductance
ESR	Equivalent Series Resistance
FOC	Field Oriented Control
FWD	Freewheeling Diode
GaN	Gallium Nitride
GPIO	General Purpose Input / Output
IGBT	Insulated Gate Bipolar Transistor
IC	Integrated Circuit
LPF	Low Pass Filter
MOSFET	Metal Oxide Semiconductor Field Effect Transistor
NO	Normally Open
NTC	Negative Temperature Coefficient
PCB	Printed Circuit Board
pf	Power Factor

PFC	Power Factor Correction
PI	Proportional Integral
PLC	Programmable Logic Controller
PLL	Phase Locked Loop
PR	Proportional Resonant
pu	Per Unit
PWM	Pulse Width Modulation
RMS	Root Mean Square
Si	Silicon
SiC	Silicon Carbide
SCR	Silicon Controlled Rectifier
SPWM	Sinusoidal Pulse Width Modulation
SVPWM	Space Vector Pulse Width Modulation
TDD	Total Demand Distortion
THD	Total Harmonic Distortion
UPS	Uninterruptible Power Supply
VOC	Voltage Oriented Control

CHAPTER 1

INTRODUCTION

1.1. Comparison of Three Phase Rectifier Topologies

Three phase rectifiers can be divided into two groups which are line commutated rectifiers and Power Factor Correction (PFC) rectifiers in general [1]. Line commutated rectifiers can be separated to two groups which are three phase diode bridge rectifiers and three phase thyristor bridge rectifiers. Figure 1. 1 and Figure 1. 2 are shown these topologies simply.

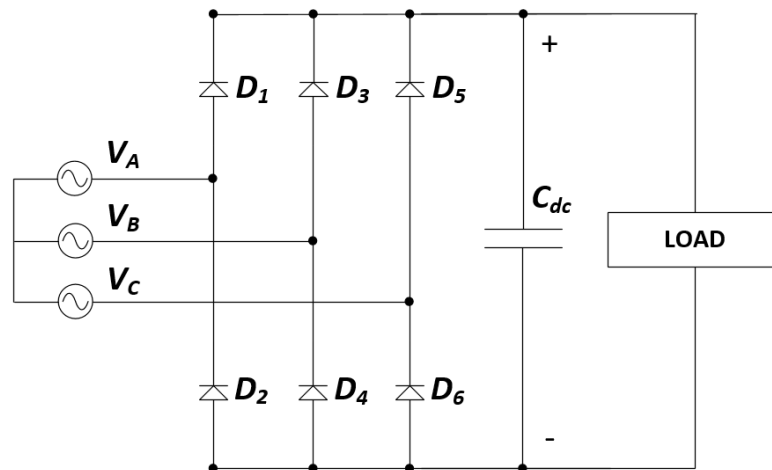


Figure 1. 1. Three phase diode bridge rectifier

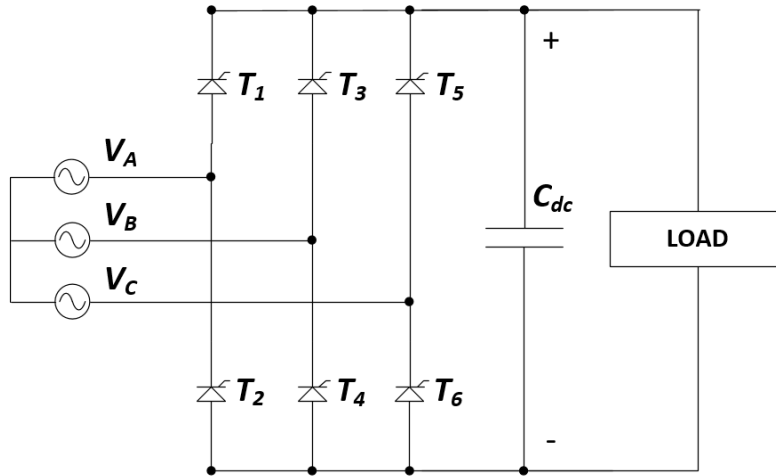


Figure 1. 2. Three phase thyristor bridge rectifier

These types of topologies are no longer preferred too much. Harmonic content of line current is significantly high because of non-sinusoidal distorted waveform. Allowed Total Harmonic Distortion (THD) value for line current according to regulations defined in IEEE 519-2014 standard [2] cannot be provided using these topologies. Besides, line to neutral voltage and line current do not become in phase which means unity power factor (pf) operation cannot be succeed nevermore. Furthermore, DC-Link voltage regulation cannot be achieved properly. To be able to overcome the problems mentioned above, PFC rectifiers are commonly used. Non-regenerative and regenerative topologies were found within PFC rectifiers. Non-regenerative topologies such as boost rectifier and Vienna rectifier are not popular because power transfer capability in both sides which are DC-Link and grid are expected. For this purpose, regenerative PFC rectifier topologies which are three phase voltage source rectifiers and three phase current source rectifiers became so popular in many applications. Three phase two level voltage source rectifier, three phase three level voltage source rectifier and three phase two level current source rectifier topologies were shown in Figure 1. 3, Figure 1. 4, Figure 1. 5 and respectively.

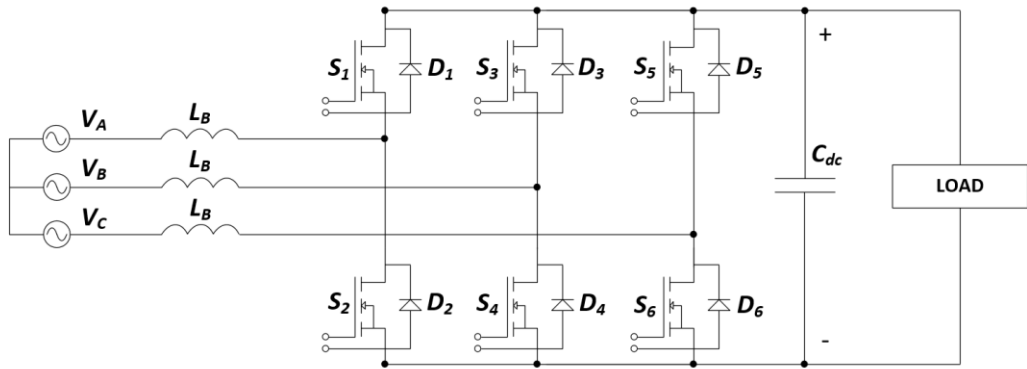


Figure 1. 3. Three phase two level voltage source rectifier

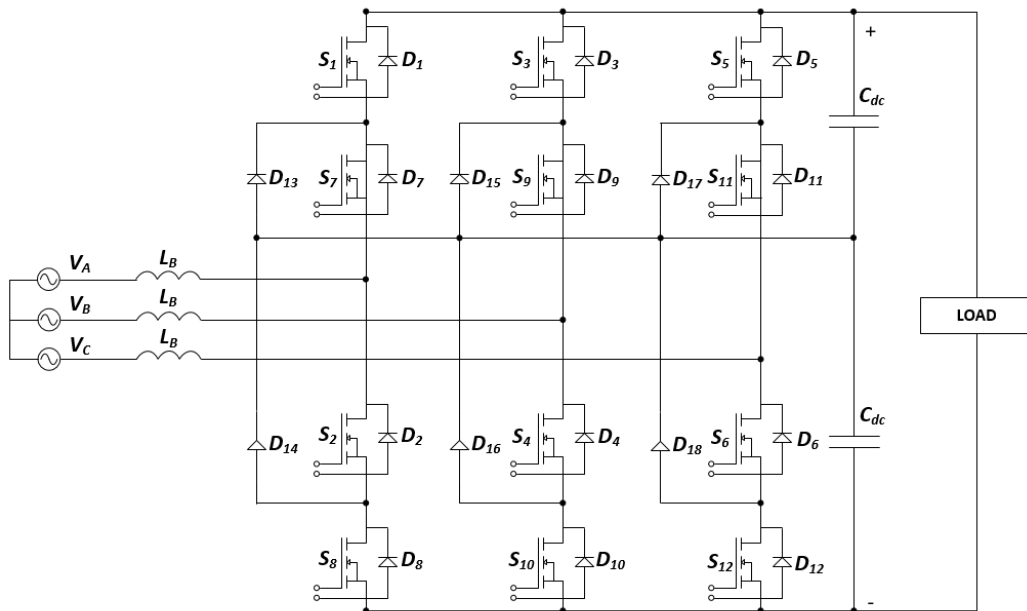


Figure 1. 4. Three phase three level voltage source rectifier

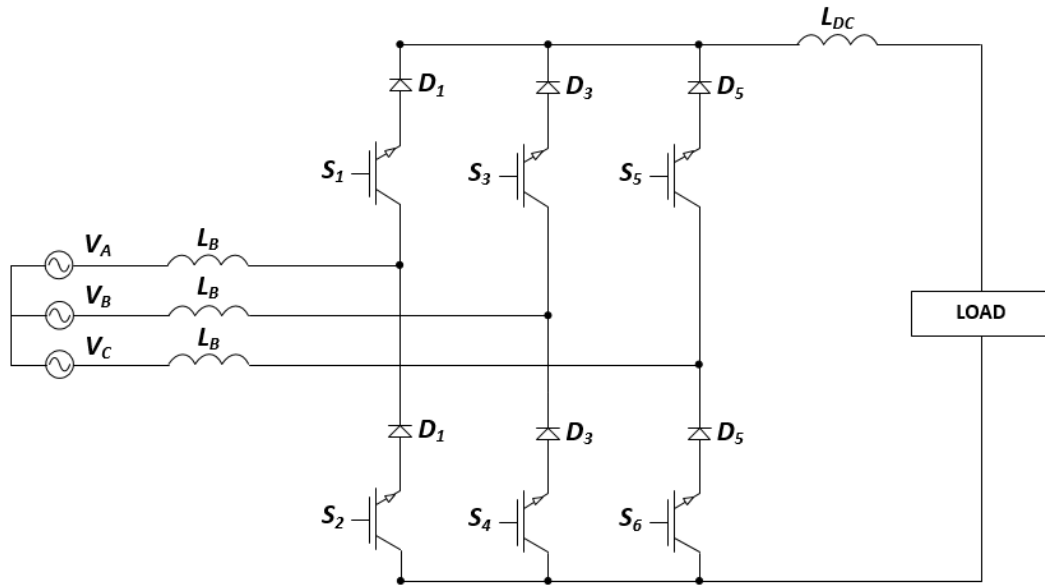


Figure 1. 5. Three phase two level current source rectifier

Three phase two level voltage source PWM rectifier were chosen and designed for fulfilling below requirements.

- ✓ Sinusoidal line currents having less harmonic content
- ✓ Obtaining line to neutral voltage in phase with line current which means unity pf operation
- ✓ Providing bidirectional power flow
- ✓ Adjusting and regulating DC-Link voltage in a controlled manner

Three phase two level current source rectifier topology were not chosen because of the fact that it is planned to use voltage source inverter as an active load in the test of rectifier that will be designed. Three phase three level voltage source rectifier was compared with three phase two level voltage source rectifier. In three level applications, power semiconductor switching device having lower blocking voltage can be chosen due to series connection of switches. In this way, voltage stress on switch can be lowered. Besides, lower switching frequencies can be preferred. However, gate drive circuit design and layout become difficult which results in complex control. Furthermore, six switches are used in two level topology. On the

other hand, twelve switches and six diodes are used in three level topology. Although unit price of switch decreases with the usage of lower voltage switches in three level topologies, total cost of switches and diodes used in three level topology are passed to total cost of switches used in two level topology. Moreover, possibility to place twelve switches and six diodes instead of six switches at same volume is too low. This situation inhibits compact mechanical design. In the applications that there is a size limitation of rectifier, three level topologies are not suitable.

1.2. Usage Areas of Three Phase PWM Rectifiers

AC to DC conversion which is also called rectification is an important issue in power electronics. Power converters which is an interface between AC supply and DC power system is called as rectifier in literature. Diode bridge rectifiers and thyristor bridge rectifiers which is also known as Silicon Controlled Rectifiers (SCR) were commonly used in many applications in the past. Design of these types of converters is simple, and robust designs can be obtained. Besides, cost effective solution can be get using diode or thyristor as a power semiconductor switching element. However, distorted line currents were formed, and so on line currents having considerably high harmonic content were obtained. These converters pollute AC supply side consistently. Reactive power was aroused and unity power factor operation cannot be provided. At the same time, DC-Link voltage is not able to controlled which means it cannot be adjusted to higher value than peak value of line to line supply voltage using three phase diode bridge rectifier. Moreover, both converters have unidirectional power capability. This means that these converters draw current from grid, however they cannot supply current to grid. In recent years, single phase PWM rectifiers and three phase PWM rectifiers become so popular together with increase of power regeneration demand to grid. At the same time, demand for obtaining line currents having Total Harmonic Distortion (THD) value smaller than allowable value stated in IEEE 519-2014 standard was increased. Since active switches such as SiC MOSFET and IGBT are used in PWM rectifier topologies, bidirectional power transfer can be achieved. When PWM rectifier is operated in rectification mode, current can be drawn from grid.

On the other hand, when PWM rectifier is operated in inversion mode, current can be supplied to grid. Both single phase PWM rectifiers and three phase PWM rectifiers are used in traction applications [3]. Figure 1. 6 explains usage of single phase rectifiers in traction applications.

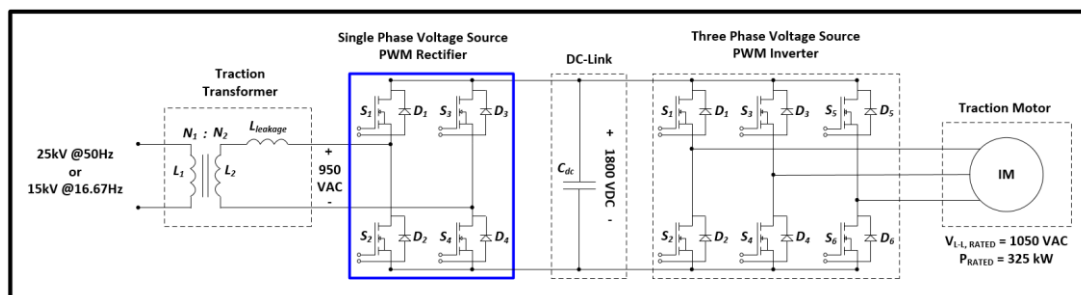


Figure 1. 6. Usage of single phase rectifiers in traction applications

In traction applications, three phase induction motors are driven by three phase voltage source PWM inverters. A DC voltage is required to supply three phase voltage source PWM inverter. In DC railway electrification systems such as 750VDC and 1500VDC, three phase voltage source PWM inverter can be fed from third rail or pantograph according to position of inverter within vehicles such as metro, tram, locomotive, regional train. However, there are also AC railway electrification systems commonly used in many countries. To be able to obtain DC voltage required to operate three phase voltage source PWM inverter, traction transformer and single phase voltage source PWM rectifier will be used together. First of all, main AC voltage which is 15kV at 16.67Hz frequency in countries like Austria, Germany, Sweden and which is 25kV at 50Hz frequency in countries like Turkey, Spain, Netherlands is decreased a specific value via traction transformer, and then secondary voltage of traction transformer will be applied to single phase voltage PWM rectifier. Generally, a second boost reactor is not used because of leakage inductance of traction transformer. This inductance is sufficient for boosting the DC-Link voltage to a determined value most of the time. Furthermore, usage of three phase voltage source PWM rectifiers in traction applications can be illustrated in Figure 1. 7.

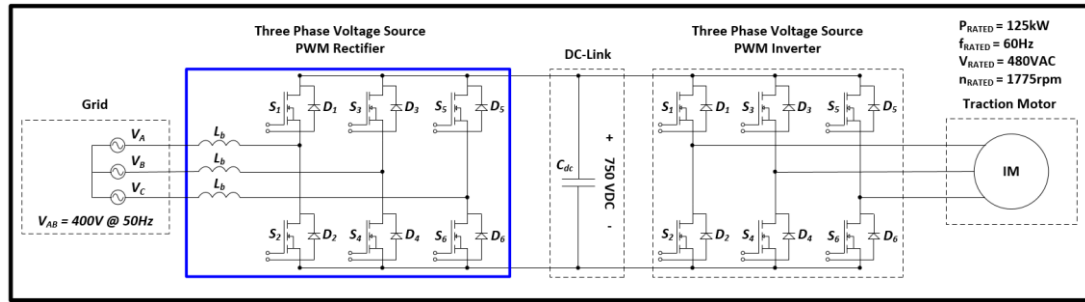


Figure 1. 7. Usage of three phase voltage source PWM rectifiers in traction applications

Three phase voltage source PWM rectifier can be used for DC-Link voltage regulation in places where grid connection is available. In the situation that vehicle accelerates, there is a reduction tendency in DC-Link voltage value. In this case, DC-Link voltage is come to desired value by drawing current from grid. In the situation that vehicle decelerates, there is a rise tendency in DC-Link voltage value. In this case, DC-Link voltage can be brought to desired value by supplying current to grid. This is called regeneration of power. Another usage area of three phase voltage source PWM rectifier is battery or super capacitor charging and discharging [4]. In recent years, energy storage components such as high voltage battery or supercapacitor became so popular in energy recovery applications. Supercapacitor is charged while buck-boost converter is in buck mode and three phase voltage source PWM rectifier is in rectification mode. On the other hand, supercapacitor is discharged while buck-boost converter is in boost mode and three phase voltage source PWM rectifier is in inversion mode. Charging and discharging states of supercapacitor were shown in Figure 1. 8 and Figure 1. 9 respectively.

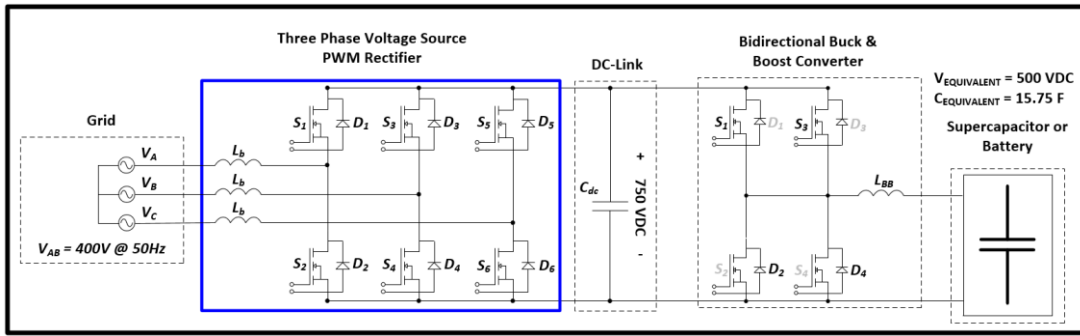


Figure 1. 8. Usage of three phase voltage source PWM rectifier in rectification mode together with DC-DC converter for battery charging

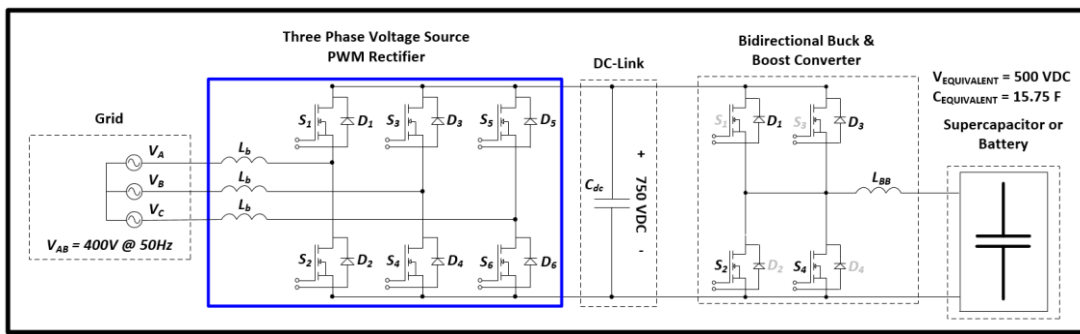


Figure 1. 9. Usage of three phase voltage source PWM rectifier in inversion mode together with DC-DC converter for battery discharging

Besides, three phase voltage source PWM rectifiers are used in wind turbine applications as a part of back to back converter [5]. Output voltage of synchronous generator changes according to rotation speed of micro turbine. This changeable frequency at turbine side is converted to 50Hz of fixed frequency using back to back converter placed between synchronous generator and grid. This operation was illustrated in Figure 1. 10.

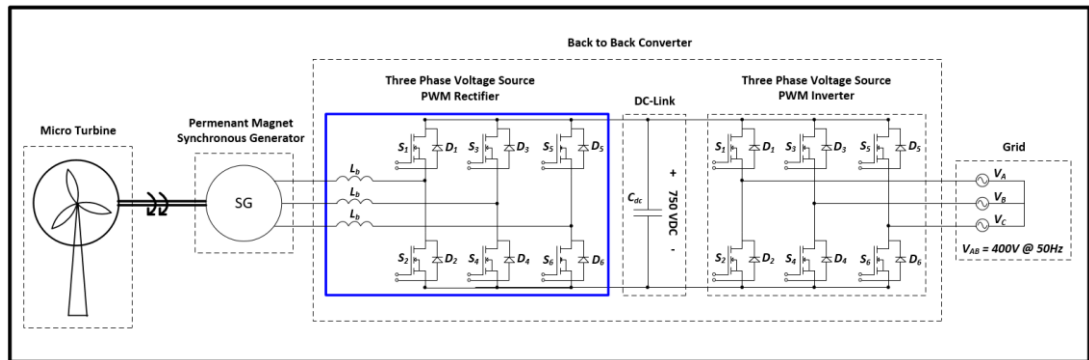


Figure 1. 10. Usage of three phase voltage source PWM rectifiers in wind turbine applications

Three phase PWM rectifiers are used in Uninterruptible Power Supply (UPS) applications, aircraft power supply applications, telecom & data server power supply applications and DC motor drive applications in addition to usage areas mentioned above in detail.

1.3. Thesis Outline

This thesis study comprises of eight chapters. Reason in the choice of three phase voltage source PWM rectifier was expressed in Chapter 1 by comparing rectifier topologies and explaining wide usage area of three phase PWM rectifiers. Selection criteria of both SiC MOSFET and other materials used in rectifier panel was clarified in Chapter 2. Besides, advantages of SiC MOSFET on Si IGBT were proved by calculating power losses and efficiencies at three different power ratings for SiC MOSFET and Si IGBTs having same ratings. Chapter 3 shows functions and electrical interfaces of five different types of printed circuit boards used in designed rectifier and correlations between them in detail. Basis of PLL algorithm and voltage based control methods which are VOC and DPC were illustrated in Chapter 4. On the other hand, frequently used modulation techniques which are SPWM and SVPWM were contrasted in Chapter 5. Performed tests, measurements and related results were given in Chapter 6. Furthermore, all Simulink models and simulation results were shared in Chapter 7. Finally, conclusions and planned future works were mentioned in Chapter 8.

CHAPTER 2

SELECTION OF MATERIALS

Selection of materials used in designed rectifier panel was explained in this chapter. This chapter was split into two subsections which are power semiconductor switching devices and other materials. Superior properties of SiC MOSFET modules in comparison with Si IGBT modules were given in part 2.1.1. Besides, selected SiC MOSFET modules were compared with Si IGBT modules having same voltage and current level in terms of power loss and efficiency at three different power levels in part 2.1.2. Moreover, selection criteria and some important properties of other materials such as current sensor, voltage sensor, 3-phases line contactor, auxiliary contactor, soft-start contactor, soft-start resistor, DC power supply, heatsink, laminated bus bars, fan, single phase AC line reactor, DC-Link capacitor were given in the subsection of other material.

2.1. Power Semiconductor Switching Devices

2.1.1. Introduction

In recent years, Insulated Gate Bipolar Transistor (IGBT) and Silicon Carbide Metal Oxide Semiconductor Field Effect Transistor (SiC MOSFET) are most common power semiconductor switching devices used in power stage design of the converters such as single phase PWM rectifier, three phase PWM rectifier, traction inverter, buck-boost converter etc. Together with improvement in SiC technology, commercial SiC MOSFET modules went into product range of companies such as Wolfspeed and ROHM Semiconductor. Si IGBT modules are already being sold in many companies such as Infineon, Semikron, Mitsubishi, ABB, Fuji Electric, Dynex Semiconductor etc.

Since both the Si IGBT and the SiC MOSFET modules are readily accessible, which

one should be used must be determined correctly. Most important selections in the power stage design of converter are material type and ratings of power semiconductor switching device. Before making a choice, following information was evaluated.

- ✓ SiC MOSFETs have ten times greater dielectric breakdown field than Si IGBT.
- ✓ SiC MOSFETs have three times greater bandgap than Si IGBT [6].
- ✓ SiC MOSFETs have thinner drift layer than Si IGBT, and so on higher doping concentration. This results in lower on-state resistance, $R_{DS, ON}$ [7].
- ✓ Drift velocity of SiC MOSFET has two times greater than Si IGBT. Therefore, SiC MOSFETs can operate at a considerably higher switching frequencies than Si IGBT.
- ✓ SiC MOSFETs have higher thermal conductivity compared to Si IGBTs [8].
- ✓ SiC MOSFET has no tail currents present on Si IGBT. By this means, turn-off energy, E_{off} of SiC MOSFET is significantly smaller than Si IGBT. Besides, freewheeling diode (FWD) within the Si IGBT module has high reverse recovery current. On the other hands, schottky barrier diode within the SiC MOSFET module has no reverse recovery current, and so on no reverse recovery loss. After all, SiC MOSFET modules has much smaller switching loss than Si IGBT modules due to lack of tail current and reverse recovery current.
- ✓ FWD on Si IGBT module can be breakdown by the reason of high reverse recovery current. This can lead to high surge voltages according to magnitude of stray inductance.
- ✓ Both Si IGBT modules and SiC MOSFET modules can be found in high blocking voltage ratings such as 1200V, 1700V and 3300V. Si IGBT modules has an advantage in terms of current ratings. SiC MOSFET modules having current rating up to 300A can be found for now.
- ✓ In terms of conduction losses, both modules have almost same. There is no distinct difference as in switching loss.

- ✓ Si IGBT modules has larger short circuit withstand time than SiC MOSFET [9]. Short circuit withstand time is a maximum duration that switch can be resisted without being degraded in the case of short circuit. A significantly high current comes to exist in short circuit condition. This surge current causes heat. This heat has to be dissipated over chip surface. Since chip area or die area is smaller in SiC MOSFET, excess heat cannot be dissipated easily compared to Si IGBT.
- ✓ If higher frequencies are chosen, size and weight of the passive components such as reactor and capacitor can be reduced dramatically. At the same time, dimensions of heatsink used for cooling can be decreased.
- ✓ Decreasing of converter's power losses and size reduction of both passive components and cooling unit allow to design converter whose efficiency and power density are higher.

In the lights of above information, it has been decided to use SiC MOSFET modules as a power semiconductor switching device in the power stage design of three phase PWM rectifier.

For apparent input power of 125kVA, Root Mean Square (RMS) value of line current was calculated as shown in (2.1) and (2.2).

$$S_{IN} = \sqrt{3} * v_{AB} * i_A \quad (2.1)$$

$$i_A = 125000 / (\sqrt{3} * 400) = 180.43 A_{RMS} \quad (2.2)$$

Since DC-Link voltage will be adjusted to 750VDC with voltage regulation, drain-source blocking voltage of SiC MOSFET module was chosen as 1700VDC by taking into account surge voltages that will be caused by stray inductances. Continuous drain current of SiC MOSFET was selected as 225A_{RMS} by considering safety margin. SiC MOSFET modules satisfying above requirements and whose part number is CAS300M17BM2 were selected from the company CREE. Another reason in selection of SiC MOSFET modules belonging to company CREE was that SiC

MOSFET gate driver board whose part number is PT62SCMD17 and belonging to company PRODRIVE TECHNOLOGIES is compatible to SiC MOSFET modules belonging to company CREE. By this means, there was no need to design gate driver board in the scope of this thesis study. Required parts from datasheet of SiC MOSFET module was given in Appendix.

2.1.2. Power Loss and Efficiency Comparison Between Si IGBT Modules and SiC MOSFET Module

Power losses of SiC MOSFET half bridge module used in all SiC MOSFET based voltage source three phase PWM rectifier were compared with Si IGBT half bridge modules of other companies which are Infineon, Semikron and Mitsubishi. Their part number are FF225R17ME4P_B11, SEMiX353GB176HDs and CM225DX-34T respectively. All chosen Si IGBT half bridge modules have 1700VDC collector-emitter saturation voltage and $225A_{RMS}$ continuous collector current according to datasheets. Required parts from datasheets of Si IGBT half bridge modules and SiC MOSFET half bridge module were given in Appendix. Efficiency comparison was made using obtained power losses at different input power ratings which are 69kVA, 104kVA and 138.5kVA. Besides, temperature rise from sink to junction was calculated for all modules. For SiC MOSFET half bridge module, SiC MOSFET conduction loss, diode conduction loss, SiC MOSFET switching loss and diode switching loss were calculated separately for three different input power ratings. At the same time, for Si IGBT modules, IGBT conduction loss, diode conduction loss, IGBT switching loss and diode switching loss were calculated separately for three different input power ratings. Conduction and switching loss calculations of Si IGBT and freewheeling diode were made according to [10]. In addition, conduction and switching loss calculations of SiC MOSFET and schottky barrier diode were made according to [11]. Conduction loss formulas of SiC MOSFET and diode for motor drive applications were given in (2.3) and (2.4).

$$P_{CM} = R_{DSon} * I_O^2 * \left(\frac{1}{8} + \frac{m_a * \cos\phi_1}{3 * \pi} \right) \quad (2.3)$$

$$P_{CD} = V_{F0} * I_O * \left(\frac{1}{2*\pi} - \frac{m_a*cos\phi1}{8} \right) + R_D * I_O^2 * \left(\frac{1}{8} - \frac{m_a*cos\phi1}{3*\pi} \right) \quad (2.4)$$

Conduction loss formulas of Si IGBT and freewheeling diode for motor drive applications were given in (2.5) and (2.6).

$$P_{CT} = V_{CE0} * I_O * \left(\frac{1}{2*\pi} + \frac{m_a*cos\phi1}{8} \right) + r_c * I_O^2 * \left(\frac{1}{8} + \frac{m_a*cos\phi1}{3*\pi} \right) \quad (2.5)$$

$$P_{CD} = V_{F0} * I_O * \left(\frac{1}{2*\pi} - \frac{m_a*cos\phi1}{8} \right) + r_D * I_O^2 * \left(\frac{1}{8} - \frac{m_a*cos\phi1}{3*\pi} \right) \quad (2.6)$$

Switching loss formulas of Si IGBT, SiC MOSFET and diode were given in (2.7) and (2.8).

$$P_{SW,T} = P_{SW,M} = (E_{on} + E_{off}) * f_{sw} \quad (2.7)$$

$$P_{SW,D} = E_{rr} * f_{sw} \quad (2.8)$$

For 69kVA input power, parameters that found using the graphs on datasheets [12] - [15] and calculated power losses for each module were shown in Table 2. 1 and

Table 2. 2 respectively.

Table 2. 1. Parameters that found using the graphs on datasheets for 69kVA of input power

Parameter	Cree	Infineon	Semikron	Mitsubishi
$R_{Dson} (m\Omega)$	14.5	-	-	-
$R_D (m\Omega)$	6	-	-	-
$V_{F0} (V)$	0.7	0.6	0.5	0.5
$V_{CE0} (V)$	-	0.6	0.6	0.45
$r_c (m\Omega)$	-	10.25	11.5	12
$r_D (m\Omega)$	-	8	7	14
$E_{on}(mJ)$	6	33	75	21
$E_{off}(mJ)$	2	42.5	41.67	30
$E_{rr} (mJ)$	0	47	25	21
$I_O(A)$	141.4	141.4	141.4	141.4
m_a	1	1	1	1
$cos\phi1$	1	1	1	1
$f_{sw}(kHz)$	5	5	5	5

Table 2. 2. Calculated power losses of each module for 69kVA of input power

Power Loss	Cree	Infineon	Semikron	Mitsubishi
P_{CM} (watt)	67	-	-	-
P_{CT} (watt)	-	71.47	77.24	73.53
P_{CD} (watt)	5.65	5.92	5.06	7.70
$P_{SW,M}$ (watt)	40	-	-	-
$P_{SW,T}$ (watt)	-	377.5	583.35	255
$P_{SW,D}$ (watt)	0	235	125	105
Total loss of SiC MOSFET (watt)	107	-	-	-
Total loss of Si IGBT (watt)	-	448.97	660.59	328.53
Total loss of diode (watt)	5.65	240.92	130.06	112.70
Total loss of module (watt)	112.65	689.89	790.65	441.23
Total loss of converter (watt)	337.94	2069.66	2371.96	1323.69
Efficiency (%)	99.51	97.088	96.67	98.12

For 104kVA input power, parameters that found using the graphs on datasheets and calculated power losses for each module were shown in Table 2. 3 and Table 2. 4 respectively.

Table 2. 3. Parameters that found using the graphs on datasheets for 104kVA of input power

Parameter	Cree	Infineon	Semikron	Mitsubishi
R_{DSon} (m Ω)	15	-	-	-
R_D (m Ω)	6	-	-	-
V_{F0} (V)	0.7	0.6	0.5	0.5
V_{CE0} (V)	-	0.6	0.6	0.45
r_c (m Ω)	-	9.33	10.16	10.33
r_D (m Ω)	-	6.83	6	11.73
E_{on} (mJ)	7.5	47.5	100	32.5
E_{off} (mJ)	4	60	60	41
E_{rr} (mJ)	0	56	35	25
I_O (A)	212.1	212.1	212.1	212.1
m_a	1	1	1	1
$\cos\phi$	1	1	1	1

$f_{sw}(kHz)$	5	5	5	5
---------------	---	---	---	---

Table 2. 4. Calculated power losses of each module for 104kVA of input power

Power Loss	Cree	Infineon	Semikron	Mitsubishi
P_{CM} (watt)	155.95	-	-	-
P_{CT} (watt)	-	133.19	141.86	134.55
P_{CD} (watt)	10.17	10.15	8.72	13.60
$P_{SW,M}$ (watt)	57.5	-	-	-
$P_{SW,T}$ (watt)	-	537.5	800	367.5
$P_{SW,D}$ (watt)	0	280	175	125
Total loss of SiC MOSFET (watt)	213.45	-	-	-
Total loss of Si IGBT (watt)	-	670.69	941.86	502.05
Total loss of diode (watt)	10.17	290.15	183.72	138.60
Total loss of module (watt)	223.62	960.85	1125.58	640.65
Total loss of converter (watt)	670.86	2882.55	3376.74	1921.94
Efficiency (%)	99.36	97.30	96.85	98.18

For 138.5kVA input power, parameters that found using the graphs on datasheets and calculated power losses for each module were shown in Table 2. 5 and Table 2. 6 respectively.

Table 2. 5. Parameters that found using the graphs on datasheets for 138.5kVA of input power

Parameter	Cree	Infineon	Semikron	Mitsubishi
R_{DSon} (m Ω)	15.5	-	-	-
R_D (m Ω)	5.75	-	-	-
V_{F0} (V)	0.7	0.6	0.5	0.5
V_{CE0} (V)	-	0.6	0.6	0.45
r_c (m Ω)	-	8.5	9.5	9.25
r_D (m Ω)	-	6.375	5.625	10.5
E_{on} (mJ)	9.5	62.5	137.5	45
E_{off} (mJ)	6	75	75	52
E_{rr} (mJ)	0	65	41.67	28
I_O (A)	282.8	282.8	282.8	282.8
m_a	1	1	1	1
$\cos\phi$	1	1	1	1

f_{sw} (kHz)	5	5	5	5
----------------	---	---	---	---

Table 2. 6. Calculated power losses of each module for 138.5kVA of input power

Power Loss	<i>Cree</i>	<i>Infineon</i>	<i>Semikron</i>	<i>Mitsubishi</i>
P_{CM} (watt)	286.48	-	-	-
P_{CT} (watt)	-	205.31	223.80	207.12
P_{CD} (watt)	15.45	15.43	13.33	20.70
$P_{SW,M}$ (watt)	77.5	-	-	-
$P_{SW,T}$ (watt)	-	687.5	1062.5	485
$P_{SW,D}$ (watt)	0	325	208.35	140
Total loss of SiC MOSFET (watt)	363.98	-	-	-
Total loss of Si IGBT (watt)	-	892.81	1286.30	692.12
Total loss of diode (watt)	15.45	340.43	221.68	160.70
Total loss of module (watt)	379.43	1233.24	1507.98	852.82
Total loss of converter (watt)	1138.3	3699.74	4523.94	2558.47
Efficiency (%)	99.18	97.40	96.84	98.19

Efficiencies of the all SiC MOSFET based voltage source three phase PWM rectifier were calculated using four different half bridge modules at three different input power ratings. Efficiencies according to different input power ratings were shown in Figure 2. 1.

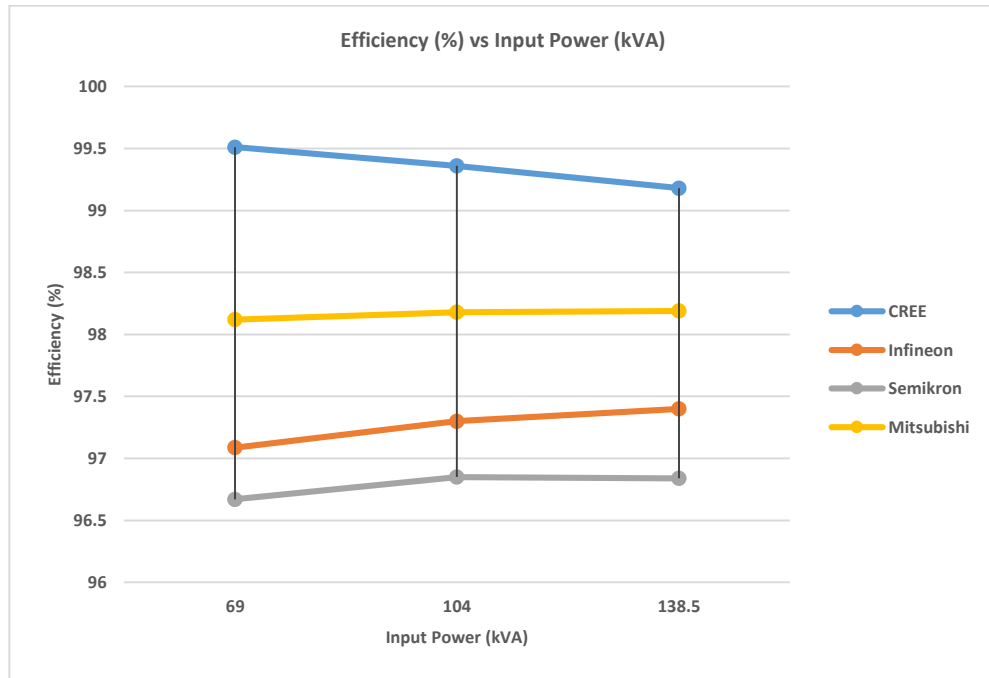


Figure 2. 1. Efficiencies of each module according to different input power ratings

In order not to damage power semiconductor switching devices, it is so important to analyze power module thermally. If temperature rise caused by power loss is so large, junction temperature will pass maximum allowable junction temperature of SiC MOSFET module or Si IGBT module. In this case, related module will be damaged. Before choosing power semiconductor switching devices, thermal analysis should be made properly. For calculating the temperature rise of modules from heatsink to junction, thermal resistance values given in the datasheets were used. Thermal resistances of SiC MOSFET, Si IGBT and diode were given in Table 2. 7.

Table 2. 7. Thermal resistance values given in the datasheets

Thermal Resistance	Cree	Infineon	Semikron	Mitsubishi
$R_{\theta,JC}$ of SiC MOSFET ($^{\circ}C/W$)	0.071	-	-	-
$R_{\theta,JC}$ of diode ($^{\circ}C/W$)	0.065	-	0.13	0.176
$R_{\theta,JC}$ of Si IGBT ($^{\circ}C/W$)	-	-	0.086	0.104
$R_{\theta,JH}$ of Si IGBT ($^{\circ}C/W$)	-	0.151	-	-
$R_{\theta,JH}$ of diode ($^{\circ}C/W$)	-	0.222	-	-
$R_{\theta,CH}$ of module ($^{\circ}C/W$)	-	-	0.04	0.0031

Different formulas were used to obtain temperature rise from heatsink to junction of SiC MOSFET, Si IGBT and diode because manufacturers give different thermal resistance values such as junction to case, junction to heatsink as seen in Table 2. 7. A general thermal model and specific thermal models according to manufacturers were given in Figure 2. 2 in order to be able explain junction temperature calculation better. Besides, related formulas according to manufacturers were given in (2.9), (2.10), (2.11), (2.12), (2.13), and (2.14).

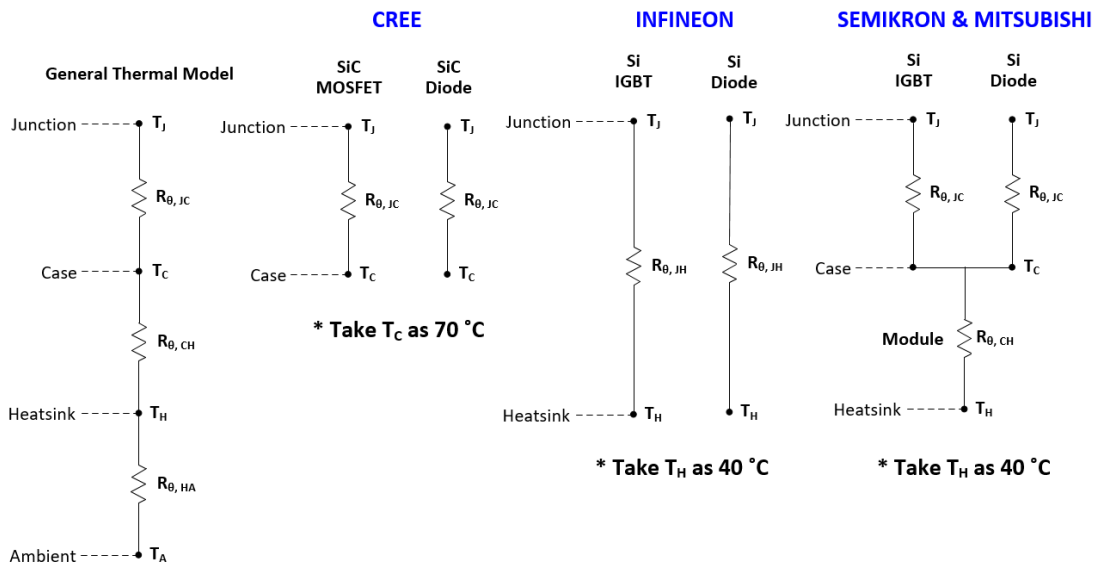


Figure 2. 2. Thermal Models

For CREE,

$$T_{J,SiC\ MOSFET} = (Total\ loss\ of\ SiC\ MOSFET * R_{\theta,JC}\ of\ SiC\ MOSFET) + T_C \quad (2.9)$$

$$T_{J,Diode} = (Total\ loss\ of\ diode * R_{\theta,JC}\ of\ diode) + T_C \quad (2.10)$$

For Infineon,

$$T_{J,Si\ IGBT} = (Total\ loss\ of\ Si\ IGBT * R_{\theta,JH}\ of\ Si\ IGBT) + T_H \quad (2.11)$$

$$T_{J,Diode} = (Total\ loss\ of\ diode * R_{\theta,JH}\ of\ diode) + T_H \quad (2.12)$$

For Semikron and Mitsubishi,

$$T_{J,Si\ IGBT} = (Total\ loss\ of\ Si\ IGBT * R_{\theta,JC}\ of\ Si\ IGBT) + (Total\ loss\ of\ module * R_{\theta,CH}\ of\ module) + T_H \quad (2.13)$$

$$T_{J,Diode} = (Total\ loss\ of\ diode * R_{\theta,JC}\ of\ diode) + (Total\ loss\ of\ module * R_{\theta,CH}\ of\ module) + T_H \quad (2.14)$$

Case temperature and sink temperature were taken as 70 °C and 40 °C respectively for the junction temperature calculation. Estimated junction temperature of each module were shown in Table 2. 8 for three different input power ratings. First column represents power switch and second column represents diode.

Table 2. 8. *Estimated junction temperature of each module for three different input power ratings*

	<i>Cree</i>		<i>Infineon</i>		<i>Semikron</i>		<i>Mitsubishi</i>	
<i>69kVA</i>	77°C	71°C	108°C	93°C	128°C	89 °C	75°C	61°C
<i>104kVA</i>	85°C	71°C	141°C	104°C	166°C	109°C	94°C	66°C
<i>138.5kVA</i>	96°C	71°C	175°C	115°C	211°C	129°C	115°C	71°C

According to datasheets of half bridge modules given in [12] - [15], maximum allowable junction temperature is 150°C for all modules. All modules may operate at 69kVA input power according to junction temperature data given in Table 2. 8. Si IGBT module belonging to Semikron does not operate at 104kVA input power because of its junction temperature (166°C). Besides, Si IGBT modules belonging to Infineon and Semikron do not operate at 138.5kVA input power because of their junction temperatures (175°C and 211°C respectively). SiC MOSFET module belonging to CREE and Si IGBT module belonging to Mitsubishi may operate at 138.5kVA input power. In the light of calculated power loss and junction temperature data, it is clear that SiC MOSFET module and Si IGBT module are almost same in terms of conduction loss. However, SiC MOSFET module has considerably lower switching loss than Si IGBT modules having same ratings. Because SiC MOSFET modules have no reverse recovery energy and turn-on & turn-off energies of SiC

MOSFET modules are very low. Si IGBT modules are not appropriate to operate at high switching frequencies because of their high switching losses.

2.2. Other Materials

2.2.1. Introduction

Criteria in selection of other materials except SiC MOSFET half bridge module and SiC MOSFET gate driver board and selected materials were explained in this part. SiC MOSFET half bridge module and SiC MOSFET gate driver board were expressed in Part 2.1 and Part 3.6 respectively. Figure 2. 3 shows pictures of materials used in rectifier panel which are voltage sensors, single phase AC line reactors, current sensors, soft-start contactor, soft-start resistor, 3-phases contactor, heatsink, laminated bus bars, discharge resistor and DC-Link capacitor.

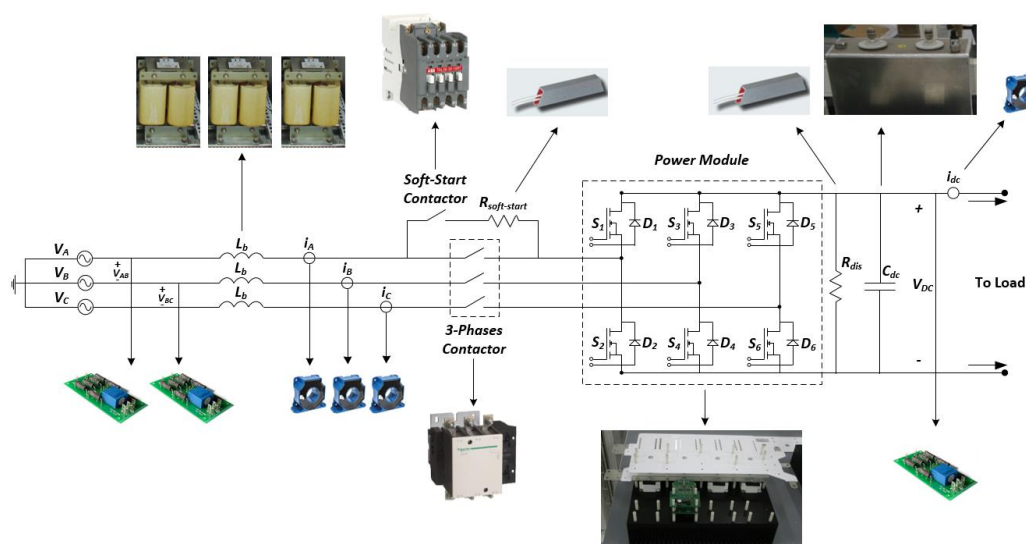


Figure 2. 3. Pictures of materials used in rectifier panel

Figure 2. 4 illustrates location of materials inside designed all SiC MOSFET based voltage source three phase PWM rectifier panel.

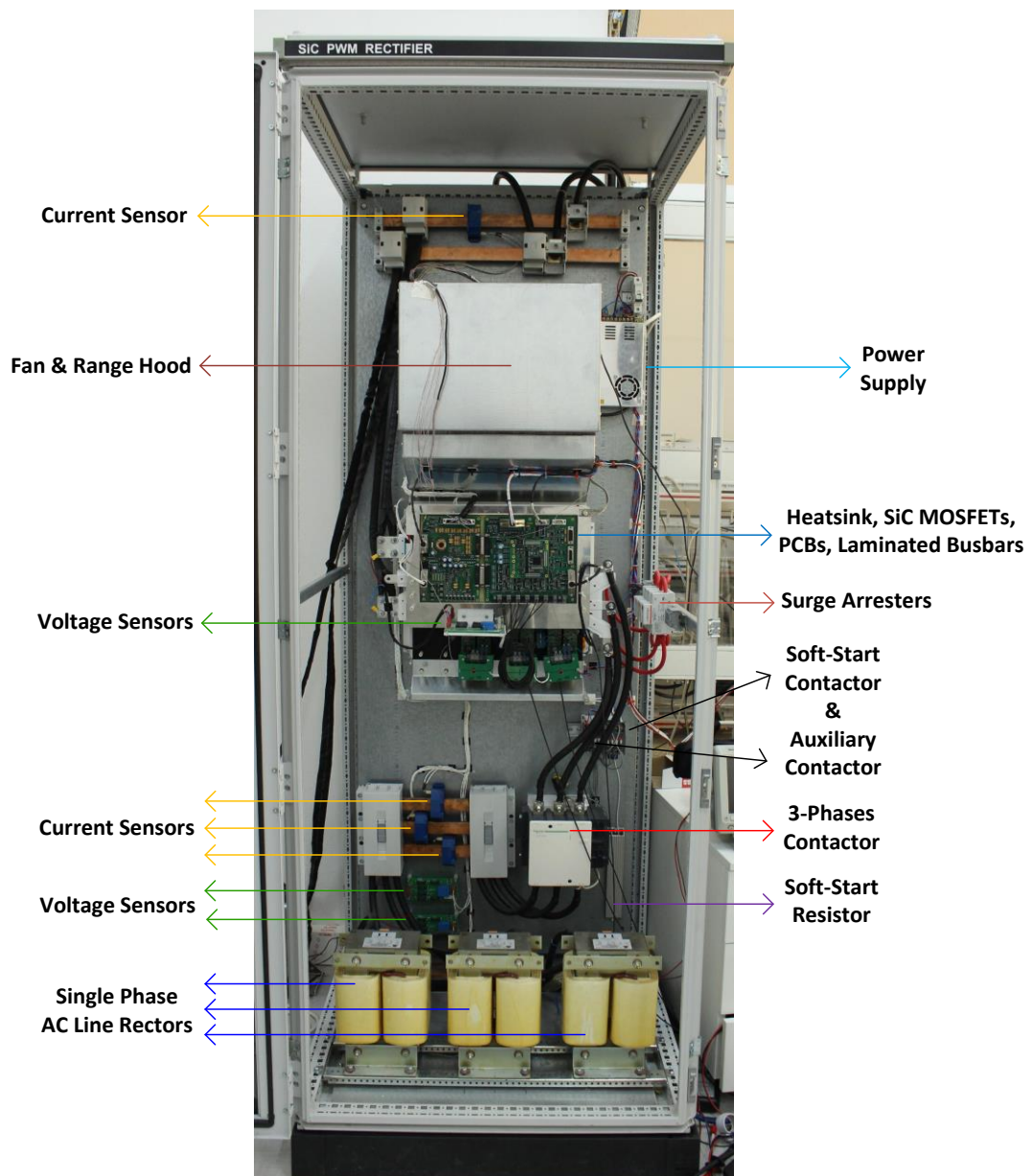


Figure 2. 4. Location of materials inside designed all SiC MOSFET based voltage source three phase PWM rectifier panel

2.2.2. Current Sensor

Different types of current sensors are used in the industry. Ohm's Law of Resistance, Faraday's Law of Induction and magnetic field sensors are mostly preferred for current sensing techniques [16]. Shunt resistors and copper traces can be given as example used ohm's law of resistance. Current transformers and Rogowski coil are

current sensors used Faraday's Law of Induction. Finally, hall-effect sensors are examples for magnetic field sensors. To be able select right current sensor, one should know advantages and disadvantages of different current sensor types. Shunt resistor has no galvanic isolation. Besides, a significantly high power loss occurs in high current applications. Although current transformer and Rogowski coil are isolated sensor, they can sense only AC currents. They are not appropriate when both DC and AC currents are wanted to measure with same sensors. Both galvanic isolation and AC/DC current measurements can provide with Hall-effect sensors. Hall-effect sensors are divided into two groups which are open loop hall-effect sensors and closed loop hall-effect sensors. Open loop hall-effect sensor can fail if high currents pass into it. Since flux of the magnetic core will be larger when current is getting larger, saturation may occur. In order to avoid high core flux, cancellation of fluxes is made in closed loop hall-effect sensors by creating counter flux on compensating winding. Closed loop hall-effect sensor was selected as a current sensor type because of the reasons mentioned above. Following requirements were taken into consideration in the selection of current sensor.

- ✓ Measuring minimum $220A_{RMS}$ of current
- ✓ Having measurement range up to minimum $\pm 400A$ of current
- ✓ Capability to measure both AC and DC currents
- ✓ Ability to operate with $\pm 15V$ of power supply
- ✓ Having overall accuracy less than 1%
- ✓ Having minimum 100kHz of bandwidth
- ✓ Ability to operate in $-40^{\circ}C/+85^{\circ}C$ of temperature range
- ✓ Having mass less than 300 gram

Current sensor belonging to company LEM whose part number is LF 510-S was chosen [17]. Some properties of this sensor were given in Table 2. 9.

Table 2. 9. *Some properties of the current sensor*

Picture	Parameter	Value
	Rated current	500A _{RMS}
	Measurement range	±800A
	Supply voltages	±14.25... ±25.2
	Overall accuracy	±0.6%
	Frequency bandwidth	200kHz
	Operating temperature	-40°C / +85°C
	Mass	240gram

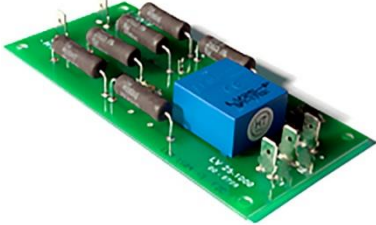
2.2.3. Voltage Sensor

It was aimed to use same voltage sensor for both line to line grid voltage measurement and DC-Link voltage measurement. The following requirements were determined by taking into account maximum voltage that will be seen.

- ✓ Measuring minimum 750V of voltage
- ✓ Having measurement range up to minimum ±1000V of voltage
- ✓ Capability to measure both AC and DC voltage
- ✓ Ability to operate with ±15V of power supply
- ✓ Having overall accuracy less than 1%
- ✓ Ability to operate in -40°C/+85°C of temperature range
- ✓ Having mass less than 100 gram
- ✓ Operation with principle of closed loop hall-effect
- ✓ Galvanic isolation

Voltage sensor belonging to company LEM whose part number is LV 25-1000 was chosen [18]. Some properties of this sensor were given in Table 2. 10.

Table 2. 10. *Some properties of the voltage sensor*

Picture	Parameter	Value
	Rated voltage	1000V
	Measurement range	$\pm 1500V$
	Supply voltages	$\pm 12 \dots \pm 15$
	Overall accuracy	$\pm \% 0.8$
	Principle	Closed loop hall-effect
	Operating temperature	$-25^{\circ}C / +70^{\circ}C$
	Mass	65gram

2.2.4. 3-Phases Line Contactor

3-phases line contactor are turned on after 560V of DC-Link voltage is obtained with diodes present in SiC MOSFET modules without turning on switches. Only soft-start contactor is turned on at this stage. To be able to keep schottky barrier diodes of SiC MOSFET modules as blocked, DC-Link voltages should be adjusted to a value higher than peak value of line to line grid voltage. After 560V of DC-Link voltage is reached, it is boosted to 750V of regulated voltage by turning on 3-phases line contactor. The following requirements were determined by taking into account maximum line to line to grid voltage and maximum line current that will be seen.

- ✓ Having three normally open (NO) main poles
- ✓ Having minimum 220A_{RMS} of rated operational current
- ✓ Having minimum 400VAC of rated operational voltage
- ✓ Having 24VDC of coil voltage
- ✓ Having a rigid enclosure
- ✓ Having a bus bar interface to be able connect cable lugs easily
- ✓ Ability to operate in $-40^{\circ}C/+85^{\circ}C$ of temperature range
- ✓ Having a weight less than 10kilogram

- ✓ Providing limitations of mechanical dimensions which are 250mm x 250mm x 250mm for height, width and depth respectively

3-phases line contactor belonging to company Schneider Electric whose part number is LC1F330 was chosen [19]. Some properties of this contactor were given in Table 2. 11.

Table 2. 11. *Some properties of the 3-phases line contactor*

Picture	Parameter	Value
	Main pole configuration	3 NO poles
	Rated operational voltage	440VAC
	Rated operational current	330A @ 440VAC
	Coil voltage	24VDC
	Operating temperature	-40°C / +70°C
	Weight	9.5kg
	Height	206mm
	Width	213mm
	Depth	219mm
	Power circuit connection	Bars suitable for lugs

2.2.5. Auxiliary Contactor

Main contacts of 3-phases line contactor which are A_1 and A_2 were not switched directly using contactor switching circuit found in power board. 3-phases line contactor was controlled with an auxiliary contactor. There was no need to choose an auxiliary contactor having high rated operational current because auxiliary contactor was only used for switching of main contacts of 3-phases line contactor. High currents on main power circuit passed through three poles of line contactor. Operation described above was illustrated in clearly Figure 2. 5.

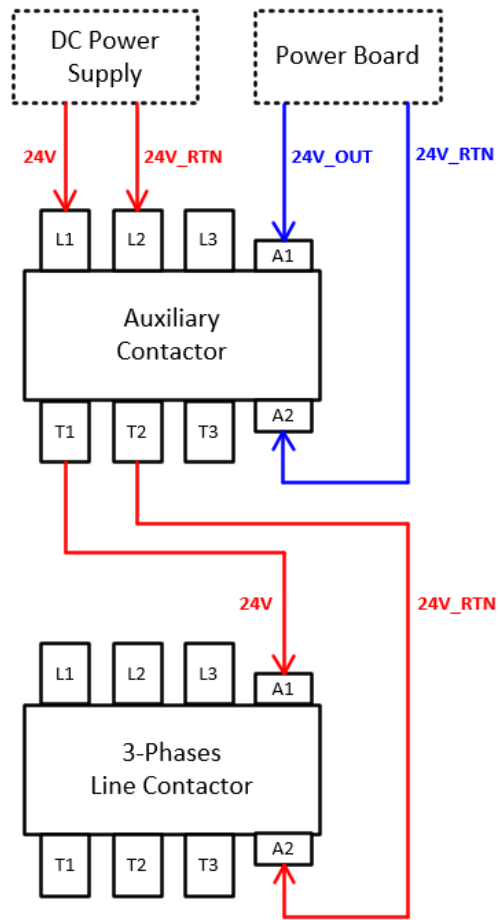


Figure 2. 5. Operation principle of the auxiliary contactor

Auxiliary contactor belonging to company ABB whose part number is TAL9-30-10 17-32VDC was chosen [20]. Some properties of this contactor were given in Table 2. 12.

Table 2. 12. *Some properties of the auxiliary contactor*

Picture	Parameter	Value
	Main pole configuration	3 NO poles
	Rated operational voltage	690VAC
	Rated operational current	7A @ 690VAC AC-3
	Coil voltage	24VDC
	Coil consumption	2.5W...8.5W
	Maximum electrical switching frequency	1200 cycles per hour @ AC-3
	Operating temperature	-40°C / +55°C
	Weight	520g
	Height	78mm
	Width	44mm
	Depth	97mm
	Terminal type	Screw terminals

2.2.6. Soft-Start Contactor & Soft-Start Resistor

A soft-start circuit composed of soft-start contactor and soft-start resistor connected each other in series is commonly used in many industrial power electronic converters to be able to decrease inrush current drawn by passive components such as DC-Link capacitor significantly. Since stresses on passive components decrease by reducing the inrush current, life time of materials is increased by using soft-start circuit shown in Figure 2. 6.

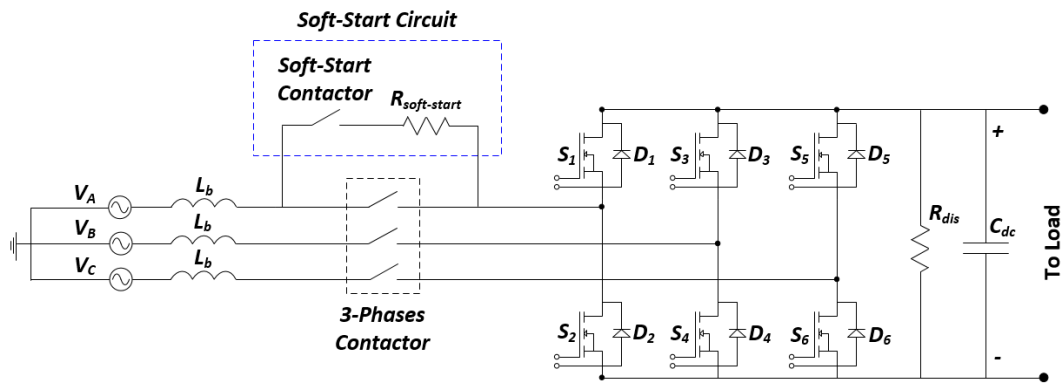


Figure 2. 6. Soft-start circuit used in the design

The following requirements were determined for soft-start contactor.

- ✓ Having minimum one normally open (NO) main poles
- ✓ Having minimum $10A_{RMS}$ of rated operational current
- ✓ Having minimum 400VAC of rated operational voltage
- ✓ Having 24VDC of coil voltage
- ✓ Having a rigid enclosure
- ✓ Ability to operate in $-40^{\circ}C/+85^{\circ}C$ of temperature range
- ✓ Having a weight less than 1kilogram
- ✓ Providing limitations of mechanical dimensions which are 100mm x 100mm x 100mm for height, width and depth respectively

Soft-start contactor belonging to company ABB whose part number is TAL26-30-10RT 17-32VDC was chosen [21]. Some properties of this contactor were given in Table 2. 13.

Table 2. 13. Some properties of the soft-start contactor

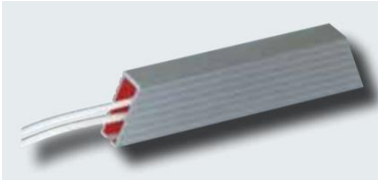
Picture	Parameter	Value
	Main pole configuration	3 NO poles
	Rated operational voltage	690VAC
	Rated operational current	13A @ 690VAC AC-3
	Coil voltage	24VDC
	Coil consumption	2.7W...9W
	Maximum electrical switching frequency	1200 cycles per hour @ AC-3
	Operating temperature	-40°C / +55°C
	Weight	750g
	Height	90mm
	Width	44mm
	Depth	110.6mm
	Terminal type	Ring terminals

For soft-start resistor, criteria were determined as follows.

- ✓ Having resistance value within 1kOhm-1.5kOhm of range
- ✓ No need to heatsink for power dissipation
- ✓ Operation in minimum 750VAC/DC of rated voltage
- ✓ Having a rigid enclosure
- ✓ Ability to operate in -40°C/+85°C of temperature range
- ✓ Having minimum 150W of rated power
- ✓ Providing limitations of mechanical dimensions which are 30mm x 50mm x 200mm for height, width and length respectively

Soft-start resistor belonging to company REO whose part number is K21102987030000 was chosen. Some properties of this resistor were given in Table 2. 14.

Table 2. 14. *Some properties of the soft-start resistor*

Picture	Parameter	Value
	Resistance	1300 Ω
	Rated operational voltage	900VAC/DC
	Rated power	200W
	Coil voltage	24VDC
	Operating temperature	-40°C / +85°C
	Height	21mm
	Width	40mm
	Length	210mm
	Terminal type	Cable

2.2.7. DC Power Supply

A DC power supply is required to supply following components within the all SiC MOSFET based voltage source three phase PWM rectifier panel.

- ✓ Three numbers of SiC MOSFET gate driver boards via fiber optic interface boars
- ✓ Control unit
- ✓ Main contacts of 3-Phases line contactor via auxiliary contactor
- ✓ DC diagonal module fan within range hood

Power consumption of each SiC MOSFET gate driver board in operational mode is 12.5W. Since three numbers of SiC MOSFET gate driver boards were used within power module, total power consumption coming from gate driver boars is 37.5W. Control unit draws almost 3A of current when it is supplied with 24VDC of voltage

and rectifier panel is operated at rated power. Therefore, power consumption of control unit is 72W. Furthermore, DC diagonal module fan used together with heatsink to be able to cool SiC MOSFET modules is in need of 24VDC of supply voltage. Power consumption of DC fan is 170W according to datasheet. Finally, coil consumption of 3-phases AC line contactor can be taken as 10W. Total power consumption of all SiC MOSFET based voltage source three phase PWM rectifier panel, P_{Total} was calculated in (2.15).

$$P_{Total} = 37,5W + 72W + 170W + 10W = 289.5W \quad (2.15)$$

The following requirements were determined by considering the calculation above.

- ✓ Having 24VDC of output voltage
- ✓ Having minimum 300W of power
- ✓ Having a fan for a proper cooling during operation
- ✓ Having a rigid enclosure
- ✓ Ability to be supply directly from 230VAC of socket
- ✓ Providing limitations of mechanical dimensions which are 50mm x 150mm x 250mm for height, width and length respectively

DC power supply belonging to company LEDWELL whose part number is LW 2415M was chosen [22]. Some properties of this power supply were given in Table 2.15.

Table 2. 15. *Some properties of the DC power supply*

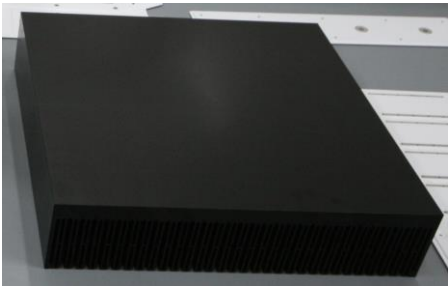
Picture	Parameter	Value
	Output voltage	24VDC
	Output current	15A
	Output power	350W
	Input voltage	230VAC
	Height	50mm
	Width	115mm
	length	215mm
	Cooling type	With fan

2.2.8. Heatsink

To be able to reduce size and volume of power converters and to make dense and compact design directly depend on sizes of passive components and cooling material. Decreasing of sizes of passive components was achieved by switching at high frequencies with SiC MOSFETs. Switching losses, and correspondingly total power losses increased as a result of switching at high frequencies. Junction temperature of SiC MOSFET increases depending on power losses and its thermal resistance. If junction temperature of the SiC MOSFET exceeds maximum allowable junction temperature defined in its datasheet, thermal runaway occurs and switch is damaged permanently. A proper cooling must be applied to prevent this situation. Air cooling and liquid cooling are frequently used as a cooling method in power electronic converters [23] - [24]. The idea lied behind cooling is that heat generated due to power loss sends away from the baseplates of switches via convection, conduction and radiation. Heatsink and liquid cooling plate are used for air cooling and liquid cooling respectively. Air cooling are divided into two groups as natural air cooling and forced air cooling. Natural cooling method is suitable for only low power applications. If it is used in high power applications, surface of heatsink is required to be increased significantly because fan is not used in this method. This causes the size and volume

of power converter to increase. A thermally conductive material called thermal grease is applied between base plate of switch and surface of heatsink. In this way, heat conduction to heatsink is ensured. Heatsinks are designed in such a way that they are composed of many fins aligned side by side. An important point in the alignment of fins is that they should be aligned by leaving enough space between them in the direction of air flow. Materials having high thermal conductivity such as aluminum and copper are commonly used within heatsink. Aluminum is preferred more compared to copper due to being lighter and cheaper. However, thermal conductivity of copper (400 W/m.K) is higher than that of aluminum (205 W/m.K). Furthermore, heat pipes embedded heat sink is used in addition to heat sink having only fins. Spreading of heat is provided better using heat pipes. On the other hand, air cooling method is less efficient than liquid cooling method in very high power applications around 1MW due to reduction in weight and size. Since maximum 150kVA of three phase PWM rectifier will be designed, usage of cold plate was not preferred. Forced air cooling was applied within rectifier panel via heatsink having aluminum fins. Standard extruded heatsink belonging to company Fischer whose part number is SK 650 was chosen. Some important properties of heatsink were given in Table 2. 16.

Table 2. 16. *Some properties of the heatsink*

Picture	Parameter	Value
	Number of fins	30
	Distance between fins	12.5mm
	Plate thickness	15mm
	Thermal resistance	0.37K/W - 0.1K/W
	Height	84mm
	Width	400mm
	Length	400mm

2.2.9. Laminated Bus Bars

Cables and laminated bus bars are frequently used in power connections within converters. Since quantity of cables increases, usage of cables becomes a problem with the increase in connection. Furthermore, cable diameter and cable weight increase in parallel with rise in current. Giving shape to the cable and bending within converter become difficult together with increment in cable diameter. Laminated bus bars are started to be preferred for high current, high power applications instead of cables or single copper bars. Cabling faults and voltage drop can be reduced using laminated bus bars. Moreover, size and cost advantages are able to provide via laminated bus bars compared to cables. Laminated bus bar is basically composed of conductors aligned one on the top of the other and insulation layers placed between conductors. Aluminum and copper are generally used as conductor material. Tin or nickel plating are usually applied on conductor. Insulation material is used for voltage isolation between two conductors. Insulation materials such as Nomex, Mylar (PET), Kapton and Tedlar are typically used in the industry. Furthermore, Inductance and so on impedance are reduced by placing two conductors in such a way that there is a thin insulation layer between them. Capacitance are increased under favor of this method. Inductance and capacitance of laminated bus bar can be calculated as in (2.16) and (2.17) respectively.

$$(nH) = 31.9 \times \frac{\text{Insulation thickness} \times \text{Length}}{\text{Width}} \quad (2.16)$$

$$C(pF) = 0.2225 \times \frac{\text{Width} \times \text{Length} \times \text{Dielectric constant}}{\text{Insulation thickness}} \quad (2.17)$$

According to formula in (2.16), inductance can be minimized by reducing insulation layer as much as possible and increasing width of the conductor. To be able to decrease inductance of laminated bus bar is vital. By this means, surge voltages coming from high rate of d_i/d_t are reduced. Inductance value less than 40nH is generally acceptable for laminated bus bars. Besides, dielectric breakdown strength, dielectric constant and continuous operating temperature are some parameters required to consider while

selecting insulation material type. Kapton is the best insulation material in terms of parameters mentioned above. However, it is much expensive compared to other materials. Dielectric breakdown strength for 3mil of insulation thickness, dielectric constant and continuous operating temperature are given in Table 2. 17 for Kapton, Mylar and Nomex [25].

Table 2. 17. Comparison of insulation materials in terms of some important features

Parameter	<i>Kapton</i>	<i>Mylar</i>	<i>Nomex</i>
Dielectric breakdown strength (for 3mil)	13.8kV	10kV	1.6kV
Dielectric constant	3.7	3.3	1.6
Continuous operating temperature	400°C	105°C	220°C

Laminated bus bars has also following advantages in addition to points above.

- ✓ Ability to provide integration with components such as SiC MOSFETs, IGBTs, decoupling capacitors and DC-Link capacitors easily
- ✓ Providing flux cancellation by placing conductors having reverse polarities one on the top of the other
- ✓ Having advantage thermally because of heat dissipation over a wide surface
- ✓ Better EMI and EMC performance compared to cables due to noise elimination

Selecting conductor size properly depending on current rating and adjusting clearance and creepage distances carefully are also important points in laminated bus bar design. Cross sectional area of the conductor should be determined correctly based on current that will be passed through it. Otherwise, temperature on conductor surface will increase swiftly. As a rule of thumb, conductor width should be selected three times higher than conductor thickness. It was decided to be used two different types of laminated bus bars within rectifier panel, one for DC-Link connection, and one for three phases connection. DC-Link bus bar and 3-Phases AC bus bar belonging to company EAGTOP whose part number are BSBC-1050-0200-01.A2352A and BSBC-

1050-0200-01.A2352 respectively were chosen. Some important properties of bus bars were given in Table 2. 18.

Table 2. 18. *Some properties of the DC-link bus bar*

Picture	Parameter	Value	
	Conductor material	Copper	
	Conductor thickness	1.5mm	
	Plating	Tin	
	Insulation material	Mylar (PET)	
	Insulation thickness	1.5mm	
	Length x width	485mm x 265mm	
	Rated voltage	1050VAC/DC	
	Rated current	200A	
	Operating temperature	-40°C / +105°C	
	Applied tests	Partial discharge	
		Dielectric	
	Power connections	Insulation resistance	
		Via spacers	

Table 2. 19. *Some properties of the 3-phases AC bus bar*

Picture	Parameter	Value	
	Conductor material	Copper	
	Conductor thickness	3mm	
	Plating	Tin	
	Insulation material	Mylar (PET)	
	Insulation thickness	1mm	
	Length x width	528mm x 212mm	
	Rated voltage	1050VAC/DC	
	Rated current	200A	
	Operating temperature	-40°C / +105°C	
	Applied tests	Partial discharge	
		Dielectric	
	Power connections	Insulation resistance	
		Via spacers	

2.2.10. Fan

Forced air cooling method was applied within the all SiC MOSFET based three phase voltage source PWM rectifier panel by using fan. The following requirements were determined.

- ✓ Having 24DC of input voltage to be able take advantage of DC power supply directly
- ✓ Having control input to be able adjust speed of the fan
- ✓ Having minimum 1000m³/h of air flow
- ✓ Being its power consumption less than 200W
- ✓ Ability to operate in -40°C/+85°C of temperature range
- ✓ Having sound level less than 85dB not to cause noise pollution

DC diagonal type fan belonging to company EBM-PAPST whose part number is K3G 200-BD46-04 was chosen [26]. Some important properties of fan were given in Table 2. 20.

Table 2. 20. *Some properties of the fan*

Picture	Parameter	Value
	Nominal input voltage	24VDC
	Input voltage range	16VDC...28VDC
	Power consumption	170W
	Air flow	1240m ³ /h
	Sound level	80dB
	Length	225mm
	Width	225mm
	Depth	89mm
	Operating temperature	-25C / +60°C
	Control input	0-10VDC

2.2.11. Single Phase AC Line Reactor

There may be low order and high order harmonics due to unbalance in grid voltages and high frequency switching. Besides, it may occur surge voltages in grid because of other converters connected to same grid and high frequency switching. AC line reactors are frequently used in many three phase rectifier applications to be able decrease low order and high order harmonics present in line current and to be able to protect grid. AC line reactors improve power factor (pf) and THD of line current by liken the line current to almost sinusoidal via harmonic elimination. Limitations associated with both THD value and percentage of each harmonic compared to fundamental stated in IEEE 519-2014 standard were satisfied in this way. Furthermore, stresses on DC-Link capacitor can be reduced by decreasing harmonics on line current and absorbing surge currents and voltages. Since DC-Link capacitor is

drawn less pulse current, its life time can be extended. Although there are many important advantages of AC line reactor, there are some drawbacks required to be paid attention such as voltage drop, power loss and unit price. Voltage drop on AC line reactor and its power loss can be calculated using (2.18) and (2.19).

$$\text{Voltage Drop, } \Delta V = (2 \times \pi \times f \times L) * I_{RMS} \quad (2.18)$$

$$\text{Power Loss, } P = I_{RMS}^2 * R_{DC} \quad (2.19)$$

Voltage applied to rectifier decreases due to voltage drop on AC line reactor connected in series with grid. A significantly high voltage drop can arise depending on magnitudes of frequency, f, inductance, L, and rated RMS current, I_{RMS} according to (2.18). Since the voltage applied to input terminals of rectifier decreased, intended DC output voltage cannot be obtained. Voltage drop can be compensated by choosing a relatively high value of DC-Link capacitor. Moreover, each reactor has a DC resistance in series with its inductance in the range of a few mΩs. A considerably high I^2R losses can occur depending on the magnitudes of DC resistance, R_{DC} , and rated RMS current, I_{RMS} according to (2.19). These losses cause the temperature rise within the reactor. If temperature rise exceeds the allowable value, isolation of the reactor is damaged. Finally, AC line chokes is generally more expensive than DC line chokes at the same inductance value.

Minimum inductance value of single phase AC line reactor was calculated using (2.20) before determining the requirements.

$$\text{Inductance, } L = (V_{SC} \%) \times \frac{V_{AN}}{2 \times \pi \times f \times i_{A,RMS}} \quad (2.20)$$

Short circuit voltage percentage, V_{SC} can be taken as 5% in order to satisfy IEEE 519-2014 standard even in highly disturbed grid conditions. For 130kVA of load test, rated value of line current, $i_{A,RMS}$ was calculated in (2.21).

$$i_{A,RMS} = \frac{S_{IN}}{\sqrt{3} * V_{AB}} = \frac{130000}{\sqrt{3} * 400} = 187.6 A_{RMS} \quad (2.21)$$

So, minimum inductance value of single phase AC line reactor was calculated using the values of short circuit voltage percentage, V_{SC} , and rated value of line current, $i_{A,RMS}$ in (2.22).

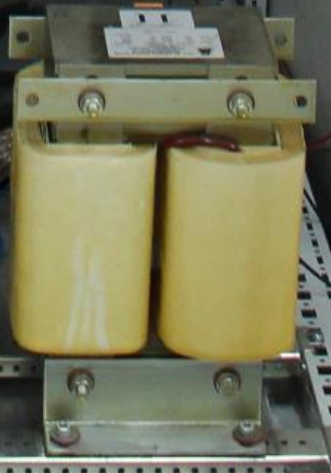
$$Inductance, L = 0.05 \times \frac{400/\sqrt{3}}{2 \times \pi \times 50 \times 187.6} \cong 0.2mH \quad (2.22)$$

The following requirements were determined by keeping in mind the points above.

- ✓ Being the structure of single phase iron core
- ✓ Having 400VAC of rated voltage
- ✓ Having minimum 216.5A_{RMS} of rated current considering maximum 150kVA of load test possibility
- ✓ Having 50Hz of fundamental frequency
- ✓ Having minimum 0.2mH of inductance with less than ±5% of tolerance
- ✓ Linearity of inductance up to minimum 275A_{RMS} of current
- ✓ No need to cooling (natural convection)
- ✓ Operation in 100% of duty cycle
- ✓ Having third harmonic content less than 1% of fundamental
- ✓ Having harmonic content at switching frequency less than 1% of fundamental
- ✓ Having H temperature class
- ✓ Having total power loss than 300W
- ✓ Having weight less than 35kg
- ✓ Providing limitations of mechanical dimensions which are 250mm x 200mm x 200mm for height, width and depth respectively
- ✓ Having a bus bar interface proving opportunity to connect cable lugs easily

An AC line reactor belonging to company MANGOLDT whose part number is 1042215 was chosen. Some important properties of reactor were given in Table 2. 21.

Table 2. 21. *Some properties of the single phase AC line reactor*

Picture	Parameter	Value
	Number of phases	Single phase
	Structure	Iron core with air gap
	Rated voltage	400VAC
	Rated current	220A _{RMS}
	Inductance	0.5mH \pm 3%
	Frequency	50Hz
	Linearity	Up to 287A _{RMS}
	Power loss	275W
	3 rd harmonic	0.88A \Rightarrow 0.4%
	Harmonic @ 15kHz	2.2A \Rightarrow 1%
	Duty cycle	100%
	Cooling	Natural convection
	Temperature class	H
	Allowable temperature rise	125°C
	Winding material	Aluminum
	Weight	30kg
	Height	265mm
	Width	195mm
Depth	180mm	
Power connection	Copper terminals suitable for cable lugs.	

2.2.12. DC-Link Capacitor

DC-Link capacitors are used between many different types of power converters. They may use between AC/DC converters such as three phase diode bridge rectifier, three phase thyristor bridge rectifier, single phase PWM rectifier, three phase PWM rectifier

and DC/AC converters such as three phase two level voltage source inverter. Furthermore, they may use between DC/DC converters such as buck & boost converter and DC/AC converters such as three phase two level voltage source inverter. At the same time, they may be found in DC side of three phase two level voltage source inverter in series connection with DC line choke. Since, three phase two level voltage source inverter was used as active load at load tests of all SiC MOSFET based voltage source three phase PWM rectifier in this thesis study, DC-Link capacitor was used between these two converters. DC-Link capacitors are basically used for reducing ripple voltage at DC-Link and to be able to draw pulse currents. Both low and high frequency ripple currents can be drawn by DC-Link capacitor depending on type of the converter used in AC/DC conversion and DC/AC conversion. If passive rectifiers such as three phase diode bridge rectifier, three phase thyristor bridge rectifier are used in AC/DC side, low frequency ripple currents are generally injected by DC-Link capacitor. On the other hand, if active rectifiers such as single phase PWM rectifier, three phase PWM rectifier are used in AC/DC side, high frequency ripple currents are mostly drawn by DC-Link capacitors. Three phase two level voltage source PWM inverter draws high frequency ripple current as well. For this reason, both ripple current drawn by rectifier and ripple current drawn by inverter should be taken into consideration while calculating the ripple RMS current of DC-Link capacitor [27]. Aluminum (Al) electrolytic capacitors and metallized film capacitors are mostly preferred as DC-Link capacitors. To be able to choose right type of capacitor, pros and cons of two capacitor types should be examined in detail.

- ✓ In terms of capacitance per volume, Al electrolytic capacitor has superior properties.
- ✓ Operating voltage of Al electrolytic capacitors is quite less than film capacitors. Al electrolytic capacitors may be found up to 600VDC. However, there are found film capacitors having almost 2000VDC of rated operating voltage.

- ✓ Al electrolytic capacitors have high Equivalent Series Resistance (ESR) value. For this reason, they have low ripple current carrying capacity. Besides, high ESR value causes high I^2R power losses. On the other hand, film capacitors have low ESR values, and so on high ripple current carrying capacity.
- ✓ Al electrolytic capacitors should be connected in series because of their low operating voltages in order to obtain for example 2000VDC of DC-Link. Balancing resistors that will be connected to Al electrolytic capacitors in parallel should be used in order to provide voltage balance. Total ESR value also increases due to series connection of Al electrolytic capacitors.
- ✓ Al electrolytic capacitors show a big change of capacitance in low temperature conditions. However, capacitance value of film capacitor is able to remain stable even at -40°C .
- ✓ Al electrolytic capacitors have polarity. If it is not paid attention, they may be connected improperly. On the other hand, film capacitors have no polarity.
- ✓ In terms of construction, Al electrolytic capacitors may be dangerous. Since they have liquid construction, explosion may occur in conditions of liquid compression. In other respects, film capacitors have dry construction.
- ✓ Energy storage capacity of Al electrolytic capacitors is more compared to film capacitors.
- ✓ Film capacitors have significantly high life time than Al electrolytic capacitors. It is expected to operate for almost thirty years from film capacitors.
- ✓ Film capacitors are more expensive in comparison with Al electrolytic capacitors.
- ✓ Most important property of metallized film capacitors is that they have self-healing which means they can stay operational in short circuit condition. Area exposed to high short circuit current is able to separated itself behaving like open circuited. In this way, remaining parts continue to operate.

Metallized film capacitor was chosen as DC-Link capacitor because of high ripple current and high rated DC voltage requirements. The following requirements were taken into account while choosing metallized film capacitor.

- ✓ Having minimum 4mF of capacitance with $\pm 10\%$ tolerance
- ✓ Having ESR value less than $0.5\text{m}\Omega$
- ✓ Having Equivalent Series Inductance (ESL) value less than 70nH
- ✓ Having minimum 900VDC of rated voltage
- ✓ Having minimum 150V of ripple voltage
- ✓ Having minimum 100A_{RMS} of ripple current
- ✓ Having dissipation factor less than 3×10^{-4}
- ✓ Having minimum 80.000 hours of life time at 70°C of hotspot
- ✓ Having thermal resistance value less than 2K/W
- ✓ Ability to operate in $-40^\circ\text{C}/+85^\circ\text{C}$ of temperature range
- ✓ Having self-healing property
- ✓ Having the weight less than 20kg
- ✓ Providing limitations of mechanical dimensions which are 300mm x 300mm x 150mm for height, length and width respectively

A DC-Link capacitor belonging to company ELECTRONICON whose part number is E56.A26-475200 was chosen. Some important properties of capacitor were given in Table 2. 22.

Table 2. 22. *Some properties of the DC-link capacitor*

Picture	Parameter	Value
	Capacitance	4.7mF \pm 10%
	Rated DC voltage	1100VDC
	Ripple voltage	200V
	Maximum ripple current	150A _{RMS}
	ESR	0.3m Ω
	ESL	100nH
	Thermal resistance, R _{TH}	1.2K/W
	Life time @70°C	100000 hours
	Operating temperature	-25°C / +70°C
	Weight	15kg
	Height	260mm
	Length	340mm
	Width	140mm
	Material	Polypropylene
	Construction	Dry type, resin moulded
	Dissipation factor, tg δ_0	2x10 ⁻⁴
	Self-healing	✓
Pressure switch	✓	

Calculating the hotspot temperature is an issue required to be taken into account in the selection of DC-Link capacitor. Whether hotspot temperature of DC-Link capacitor exceeds its maximum allowable operating temperature or not should be controlled. For this reason, power losses of DC-Link capacitor which are joule losses, P_J and

dielectric losses, P_D were calculated in (2.23) and (2.24) respectively for $150A_{RMS}$ of ripple current.

$$P_J = I_{RMS}^2 \times ESR = 150A_{RMS}^2 \times 0.3m\Omega = 6.75W \quad (2.23)$$

$$P_D = Q \times \tan\delta_0 = \frac{I_{RMS}^2}{C \times W} \times \tan\delta_0 = \frac{150A_{RMS}^2}{(4.7 \times 10^{-3}) \times (2 \times \pi \times 100)} \times (2 \times 10^{-4})$$

$$= 1.52W \quad (2.24)$$

After calculating power losses, temperature rise from junction to ambient, ΔT was calculated as shown in (2.25).

$$\Delta T = (P_J + P_D) \times R_{TH} = (6.75W + 1.52W) \times (1.2^\circ C/W) \cong 10^\circ C \quad (2.25)$$

Finally, hotspot temperature, T_{HS} was calculated in (2.26) by taking ambient temperature, T_A as $40^\circ C$.

$$T_{HS} = \Delta T + T_A = 10^\circ C + 40^\circ C = 50^\circ C \quad (2.26)$$

Since hotspot temperature of DC-Link capacitor is less than its maximum allowable operating temperature which is $70^\circ C$, it can be said that selected DC-Link capacitor is thermally appropriate.

CHAPTER 3

FUNCTIONS & ELECTRICAL INTERFACES OF PCBs USED IN RECTIFIER PANEL AND CORRELATIONS BETWEEN THEM

3.1. Introduction

Five different printed circuit boards (PCBs) which are power board, main board, DSP board, fiber optic interface board and SiC MOSFET gate driver board were used in the design of all SiC MOSFET based voltage source three phase PWM rectifier. These PCBs were not designed. Related electrical interfaces of these ready boards were used directly in this thesis study. Power board, main board and DSP board are found in a control unit. Control unit was supplied from a DC power supply. SiC MOSFET half bridge module was driven with two channel SiC MOSFET gate driver board. This gate driver board has electrical interface. Differential input signals which are $V_{IN+, HIGH}$, $V_{IN-, HIGH}$, $V_{IN+, LOW}$, $V_{IN-, LOW}$ should be applied to SiC MOSFET gate driver board to be able to produce gate driving voltages for both sides. However, main board has a fiber optic interface for transmission of PWM signals. Fiber optic interface board was used to convert fiber signals to electrical signals. Relation between the boards mentioned above was illustrated in Figure 3. 1 in detail.

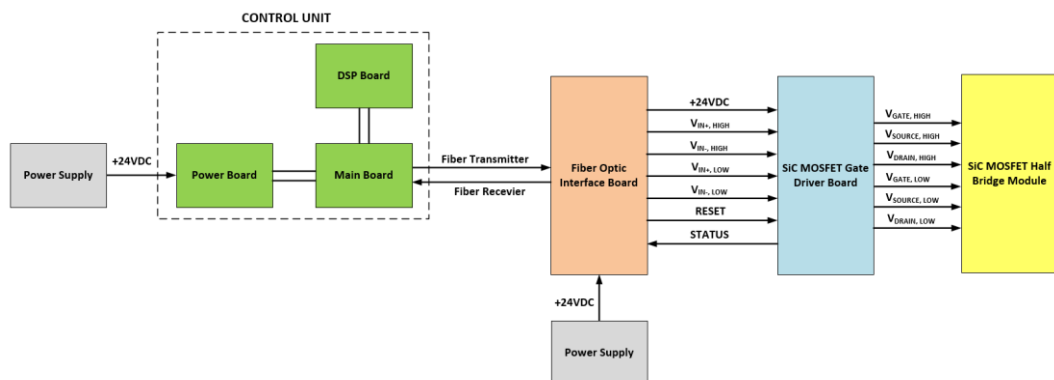


Figure 3. 1. Relation between the boards used in the rectifier panel

Following parts explain functions of each board in depth.

3.2. Main Board

Main board has the functions below.

- ✓ PWM signal transmission and receiving via fiber optic connectors
- ✓ Current reading
- ✓ Voltage reading
- ✓ Thermistor sensing

Main board provides fiber optic transmission of PWM signals to fiber optic interface board. Since fiber optic connectors have extremely high bandwidth, fiber optic cables can be carried through long distances. Besides, noise cannot be coupled to fiber optic cables easily because their electromagnetic interference (EMI) immunity are significantly high. For this reason, fiber optic connectors are commonly used in recent years. Furthermore, four current sensors used for line currents, i_A , i_B , i_C and DC-Link current, i_{DC} and three voltage sensors used for line to line voltages, V_{AB} , V_{BC} and DC-Link voltage, V_{DC} were read in this board. Current outputs of current and voltage sensors were converted to differential digital signals using measuring resistances and Analog to Digital Converter (ADC) Integrated Circuits (ICs). And then, these digital signals were sent to DSP board. There is also thermistor sensing circuit on main board. Three Negative Temperature Coefficient (NTC) thermistors were placed near SiC MOSFET half bridge modules on heatsink. Temperatures of SiC MOSFET modules were monitored using this circuitry.

3.3. Power Board

Power board has the functions below.

- ✓ Reverse voltage protection
- ✓ Inrush current limiter
- ✓ Producing $\pm 15V$ of current and voltage sensor supplies
- ✓ Producing $+3.3V$ of DSP supply

- ✓ On/off control of contactors
- ✓ Filtering of input voltage which is +24VDC

There are protection circuits on power board against reverse plugging of power connector and drawing inrush current. Besides, isolated DC-DC converters were present on power board. $\pm 15V$ of current and voltage sensor supplies are produced using 24V/15V DC-DC converter. At the same time, 24V/5V isolated DC-DC converter and 5V/3.3V buck converter IC are found on power board to produce +3.3V DSP supply. Moreover, on/off control circuits are found on power board to switch three phase line contactor and soft-start contactor in a controlled manner.

3.4. DSP Board

DSP board has dual-core microcontroller belonging to company TEXAS INSTRUMENTS whose part number is TMS320F28377D. DSP board has the functions below.

- ✓ CAN communication
- ✓ RS-422 serial communication
- ✓ Having configurable General Purpose Input / Outputs (GPIOs)

CAN high, CAN low and CAN ground signals are produced on DSP board. CAN communication was used in monitoring of important parameters continuously on MATLAB/Simulink model using CAN/USB converter. CAN communication was also used for changing parameters such as DC-Link voltage, reference current, i_q , parameters of PI controllers used both in outer voltage control loop and inner current controller loop while all SiC MOSFET based voltage source three phase PWM rectifier is operating. This property provides an opportunity not to lose time while loading software to flash of DSP consistently. Moreover, Signals of TXD+, TXD-, RXD+, RXD-, GND are produced on DSP board for RS-422 serial communication. This property allows software loading without using emulator.

3.5. Fiber Optic Interface Board

Fiber optic interface board has the functions below.

- ✓ Conversion from fiber to electrical
- ✓ Conversion from electrical to fiber
- ✓ Conversion of single ended signal to differential signals
- ✓ Filtering of input voltage

First of all, input voltage is filtered on fiber optic interface board. This filtered voltage is sent to SiC MOSFET gate driver board. Besides, optical signals come from main board are taken with fiber optic receivers and then converted to single ended electrical signals. These single ended signals are converted to differential signals which are $V_{IN+, HIGH}$, $V_{IN-, HIGH}$, $V_{IN+, LOW}$, $V_{IN-, LOW}$ and sent to SiC MOSFET gate driver board as a differential input signals for high side and low side. A signal to be able reset SiC MOSFET gate driver board is produced on fiber optic interface board depending on request comes from main board. Furthermore, there is a circuitry to be able take status information comes from SiC MOSFET gate driver board. Status signal is converted to optical signal and then sent to main board via fiber optic transmitter. By this means, operation of all SiC MOSFET based voltage source three phase PWM rectifier is stopped by cutting PWM signals.

3.6. SiC MOSFET Gate Driver Board

SiC MOSFET gate driver board [28] used in all SiC MOSFET based voltage source three phase PWM rectifier has two channels. Therefore, it is suitable for driving MOSFETs both in high side and low side. +20V/-6V of gate driving voltages are produced on this board. It has 20A of peak output current capability. Besides, it is appropriate for switching frequencies up to 125kHz.

SiC MOSFET gate driver board has the functions below.

- ✓ Under and over voltage monitoring of isolated supplies produced in primary side

- ✓ Unver voltage monitoring of gate driving voltage produced in secondary side
- ✓ V_{DS} monitoring
- ✓ Adjusting blanking time
- ✓ Adjusting dead time

Isolated supply voltages produced in primary side for using in gate drive circuits in secondary side are monitored on SiC MOSFET gate driver board against situations of under voltage or over voltage. Besides, gate driving voltages used to turn on SiC MOSFET in both sides are monitored with the help of circuit present on secondary side. Fault signal is produced if positive gate driving voltage which is normally +20V decreases under +18V.

A MOSFET has a $V_{DS, ON}$ voltage when it turned on depending on drain current, I_D and on state resistance, $R_{DS, ON}$. Over current situation are determined by monitoring this voltage. Voltage of V_{DS} increases linearly while drain current, I_D is increasing in linear region. However, voltage of V_{DS} increases up to DC-Link voltage in the case of short circuit because it goes into saturation region. A circuitry is used in secondary side of SiC MOSFET gate driver board to compare voltage of V_{DS} with a determined voltage level. If voltage of V_{DS} exceeds this trip level, short circuit condition is sensed. Fault signal is produced and PWM signal is cut off. Trip level of V_{DS} adjusts by changing value of a resistor assembled on SiC MOSFET gate driver.

A time passes for turning on of MOSFET completely after applying turn on signal because internal capacitances of MOSFET which are C_{DS} and C_{GS} is required to charge. Until a SiC MOSFET is conducted on completely, voltage of V_{DS} is quite high compared to voltage of $V_{DS, ON}$. For this reason, if V_{DS} monitoring circuit is active continuously, misdetection can occur. Short circuit can be sensed although there is no short circuit condition. To be able to inhibit this situation, a blanking time is used. V_{DS} monitoring circuit is activated after a specific blanking time passed. Default blanking time on SiC MOSFET gate driver board is 1 μ s. This time can be adjusted with a

capacitor assembled on SiC MOSFET gate driver board. This value has not been changed throughout thesis study.

A dead time is used to ensure that MOSFET on low side is turned on after MOSFET on high side is completely turned off or vice versa. By this means, shoot-through is prevented without turning on MOSFETs on both sides at the same time. Default dead time on SiC MOSFET gate driver board is 500ns. This time can be adjusted with two resistors depending on whether they are both assembled or not or which one is assembled.

CHAPTER 4

PHASE LOCK LOOP ALGORITHM AND VOLTAGE BASED CONTROL METHODS

4.1. Phase Lock Loop Algorithm

It is necessary to provide synchronization between grid connected converters and grid to obtain unity power factor (pf) operation. Improving the power quality provides to be increased the efficiency of grid connected converters such as Three Phase Pulse Width Modulation Rectifiers. There are many reasons not to be able to implement a Phase Locked Loop (PLL) algorithm having high immunity. Line voltage sags, line voltage spikes, unbalanced between line voltages, line frequency variations, harmonics in line currents are some disturbances for that [29]. PLL algorithm is basically used to adjust and know phase angle of line voltage accurately. This phase is used both in PLL algorithm as a feedback and in inner current control loop. Therefore, performance of the inner current control loop directly depends on the success of PLL algorithm. In this thesis work, Direct-Quadrature (dq) axis based PLL algorithm was applied using Digital Signal Processor (DSP) belonging to Texas Instruments company (TMS320F28377D). Besides, PLL model was established and tested using MATLAB/Simulink simulation environment. Code Composer Studio (CCS) 6.1.1 was used for code development. Developed and built code was loaded to flash memory of microprocessor on DSP board via RS422 serial communication. There are many different types of PLL techniques in literature. Reference frames or coordinates used for line voltages representation varies from one technique to other. Some PLL techniques directly use stationary, time dependent abc reference frame. Other techniques use either stationary, time dependent Alpha-Beta($\alpha\beta$) reference frame or synchronous, time independent dq reference frame. Using abc reference frame directly is not proper to be able to achieve an immune PLL algorithm [30]. For

this reason, dq axis based PLL algorithm was chosen. Figure 4. 1 shows PLL scheme implemented on microcontroller step by step.

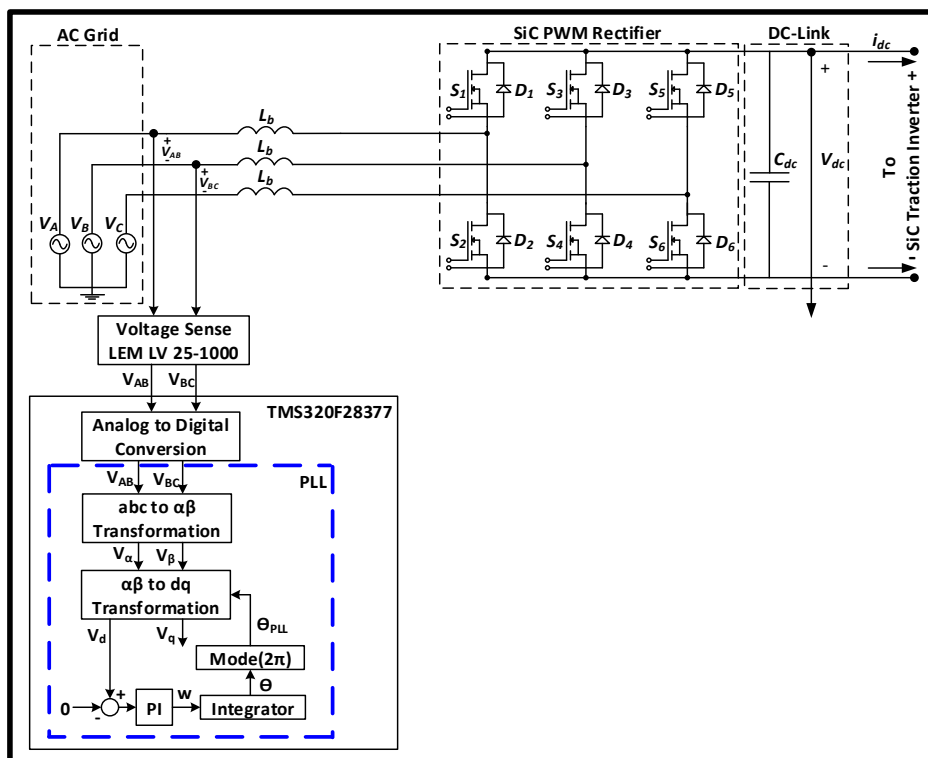


Figure 4. 1. PLL scheme

First of all, two pieces of printed circuit board type voltage sensors belonging to LEM company (LV 25-1000) were used to sense V_{AB} and V_{BC} line voltages. Depending on applied voltage from primary terminals, these voltage sensors give current output from secondary terminal in milliamp (mA) range using a specific conversion ratio (1000V/25mA). Supply voltages of voltage sensors ($\pm 15\text{VDC}$) were provided from power board located on power module. Current output terminal (measuring terminal) were also connected to connector on power board. Current output was converted to voltage output using measuring resistance on main board, and then analog voltage output were converted to digital signal using Analog to Digital Converter (ADC) ICs on main board. These differential digital signals generated on main board were sent to DSP board and sensed as a real voltage value. Electrical interface of printed circuit

board type voltage sensor and above operation were shown in Figure 4. 2 and Figure 4. 3 respectively.

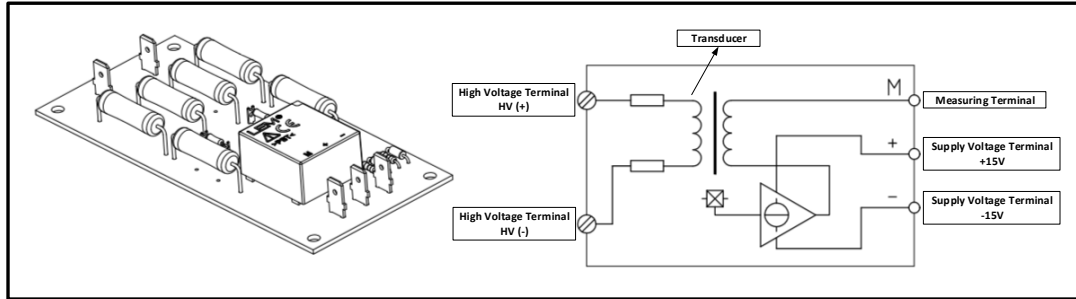


Figure 4. 2. Electrical interface of PCB type voltage sensor

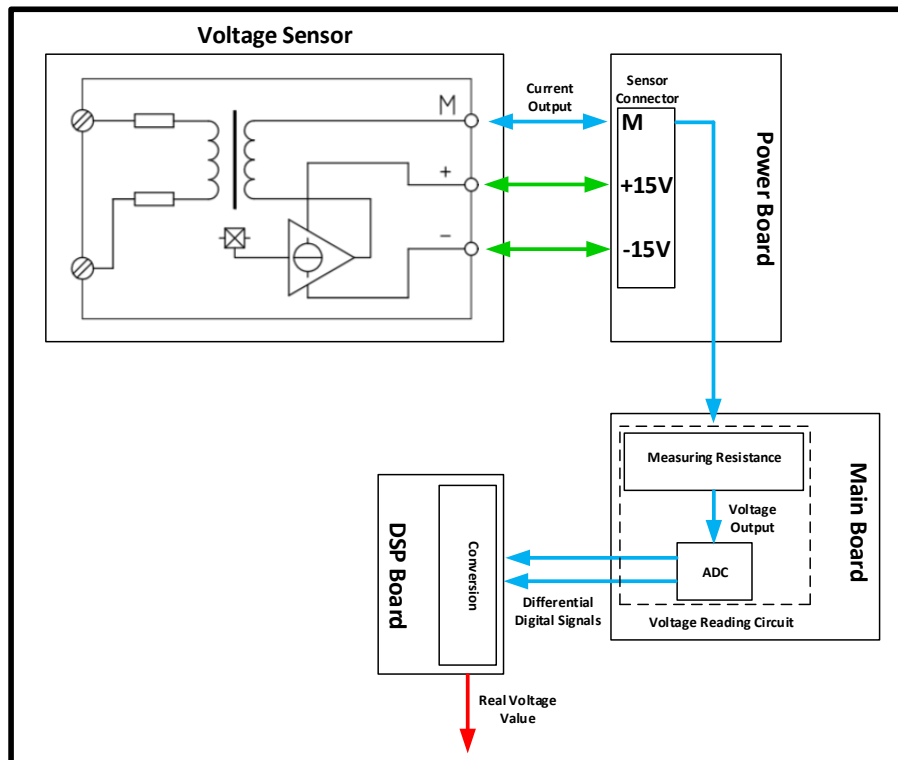


Figure 4. 3. Voltage reading operation

After sensing V_{AB} and V_{BC} line voltages using voltage sensors, these grid voltages were transformed to V_{α} and V_{β} voltages in stationary reference frame. V_{α} and V_{β} voltages are also time dependent like V_{AB} and V_{BC} grid voltages. ABC to $\alpha\beta$ transformation is known as Clarke Transformation in literature. After Clarke

Transformation, V_α and V_β should be perpendicular. Physical and mathematical explanations of Clarke Transformation was shown in Figure 4. 4, (4.1), and (4.2) respectively.

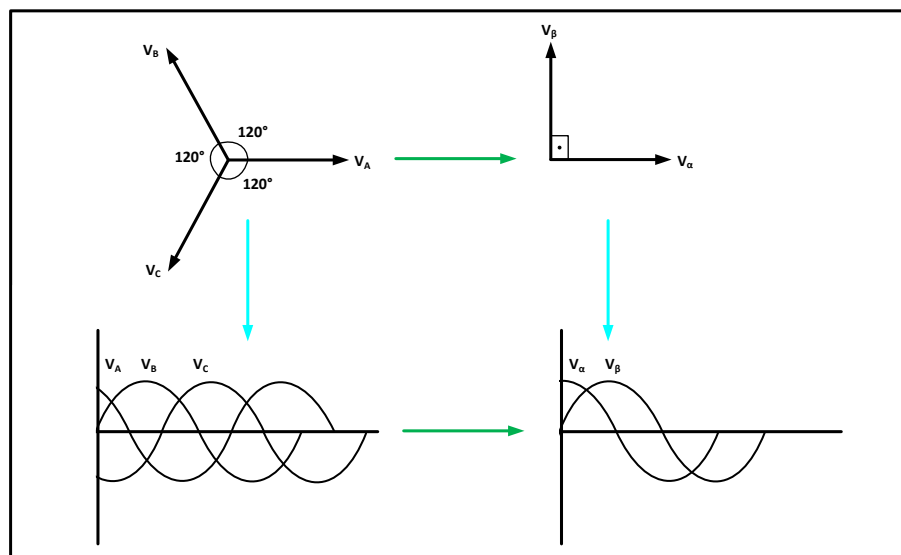


Figure 4. 4. Clarke transformation

$$V_\alpha = \frac{2}{3} * (V_a - \frac{1}{2} (V_b + V_c)) \quad (4.1)$$

$$V_\beta = \frac{1}{\sqrt{3}} * (V_b - V_c) \quad (4.2)$$

After Clarke Transform, V_α and V_β voltages in stationary reference frame were transformed to V_d and V_q voltages in synchronous (rotating) reference frame. V_d and V_q voltages are time independent DC components. They should be orthogonal. $\alpha\beta$ to dq transformation is known as Park Transformation in literature. Physical and mathematical explanations of Park Transformation was shown in Figure 4. 5, (4.3), and (4.4) and respectively.

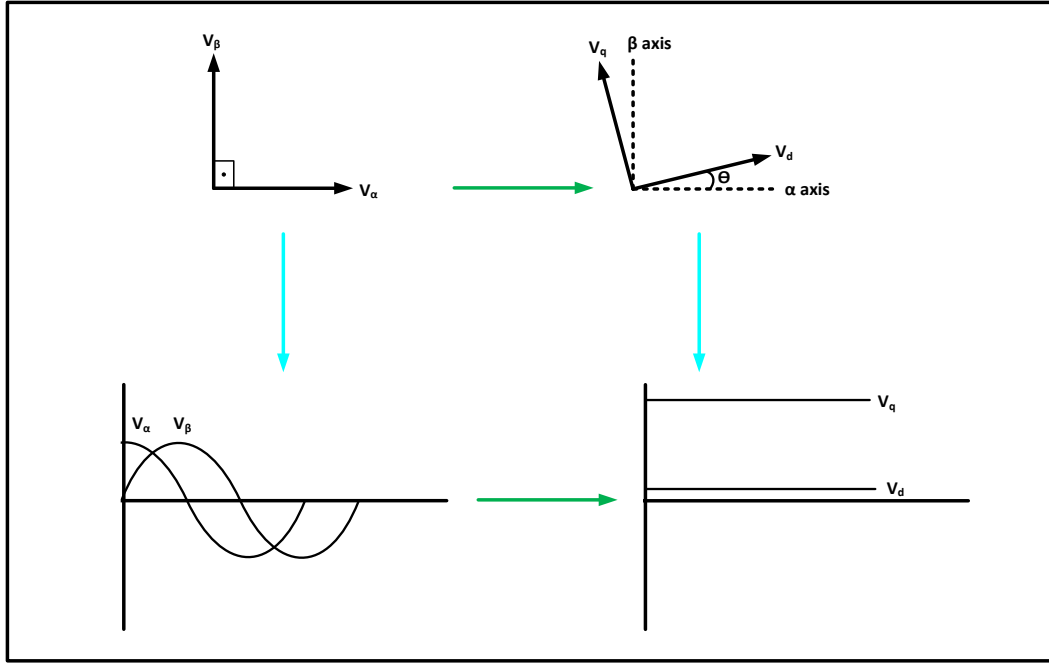


Figure 4. 5. Park transformation

$$V_d = V_\alpha * \cos(\omega t) + V_\beta * \sin(\omega t) \quad (4.3)$$

$$V_q = V_\beta * \cos(\omega t) - V_\alpha * \sin(\omega t) \quad (4.4)$$

After Park Transformation, PI controller was adjusted in a way that V_d should be zero. By this means, V_q follows grid voltage vector. Output of PI controller gives angular frequency, ω . To be able to obtain, phase angle, Θ , it is required to take the integral of angular frequency, ω by using the (4.5).

$$\theta = \int \omega * dt \quad (4.5)$$

However, this angle goes infinite because of the fact that integral has no limit. To prevent this situation, mode operation was made according to 2π and then, real phase angle, Θ_{PLL} was obtained. This phase angle, Θ_{PLL} was formed using line to line grid voltages V_{AB} and V_{BC} . Since inner current control loop uses line currents I_A , I_B and I_C for transformations, Θ_{PLL} cannot be used directly in inner current control loop. Instead of Θ_{PLL} , Θ_{PWM} was used by extracting $\pi/6$ from Θ_{PLL} and making mode operation

according to 2π . Angle, Θ_{PWM} was used both park transformation and inverse park transformation in inner current control loop as shown in Figure 4. 6.

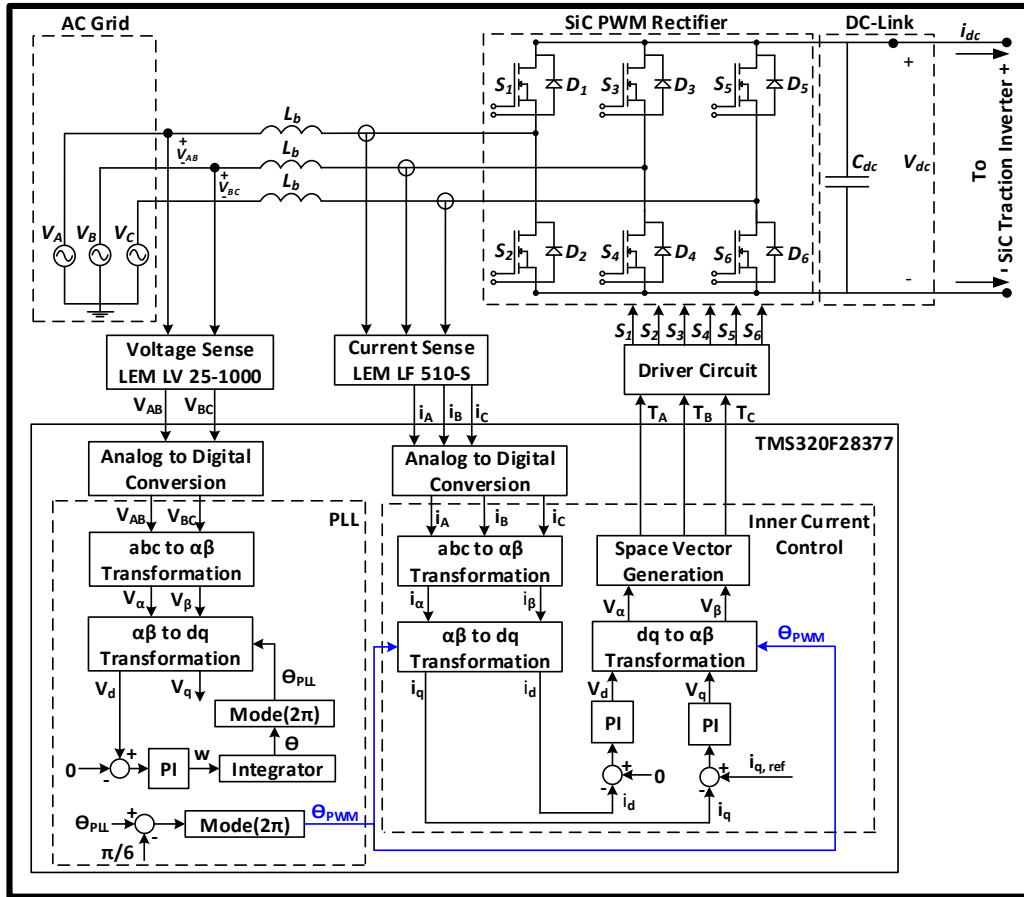


Figure 4. 6. Usage of theta generated in PLL within inner current control loop

While developing code in CCS 6.1.1, Clarke, Park and Inverse Park transformations were made using available code blocks called macro instead of writing (4.1), (4.2), (4.3) and (4.4) one by one. Furthermore, in the case of unbalanced between line voltages, second harmonic are formed in general. To be able to eliminate this component, several methods such as Low Pass Filter (LPF), resonant filter and moving average filter are proposed in literature. All these filters decelerate dynamic response of the system. Besides, LPF can cause phase shift. Resonant filters are better than LPF in terms of phase shift. Optimization of LPF should be made carefully not to face with a considerable phase shift. To conclude, PLL algorithm is crucial for three phase PWM

rectifiers to be able control converters properly independent of the control techniques to be applied. To be able apply Direct Power Control (DPC) properly, active and reactive power should be calculated instantaneously. For example, to be able to calculate active power correctly, line currents and line voltages should be known accurately via PLL algorithm. On the other hand, to be able apply Voltage Oriented Control (VOC) properly, park and inverse park transformations should be made correctly using the phase angle, Θ_{PWM} generated by PLL algorithm.

4.2. Introduction to Voltage Based Control Methods

Direct Power Control (DPC) and Voltage Oriented Control (VOC) are commonly used voltage based control methods to control three phase voltage source PWM rectifiers. There are also virtual flux based control methods in literature. However, in the scope of this thesis work, voltage based control methods were only examined. Analogy can be made between DPC for rectifiers and Direct Torque Control (DTC) for induction machines. At the same time, there is a similarity between VOC for rectifiers and Field Oriented Control (FOC) for induction machines. VOC was implemented on using microprocessor on DSP board. Furthermore, before starting code development, Success of the VOC method was tried on MATLAB/Simulink simulation environment. Following parts will explain the both control methods in detail.

4.3. Direct Power Control

DPC is basically based on active and reactive power control. Reference value of active power is determined by multiplying measured DC-Link voltage and reference current which is output of Proportional Integral (PI) controller used in voltage control loop. Reference value of reactive power should be taken zero for unity power factor (pf) operation. Feedback values of active and reactive power are calculated instantaneously by measuring line currents via current sensors, line voltages by means of voltage sensors and using PLL. Hysteresis controllers take errors of active and reactive power and outputs of hysteresis controllers are fed to switching table.

Switching states (T_A , T_B , T_C) are determined according to switching table. Control method mentioned above is shown in Figure 4. 7 in detail.

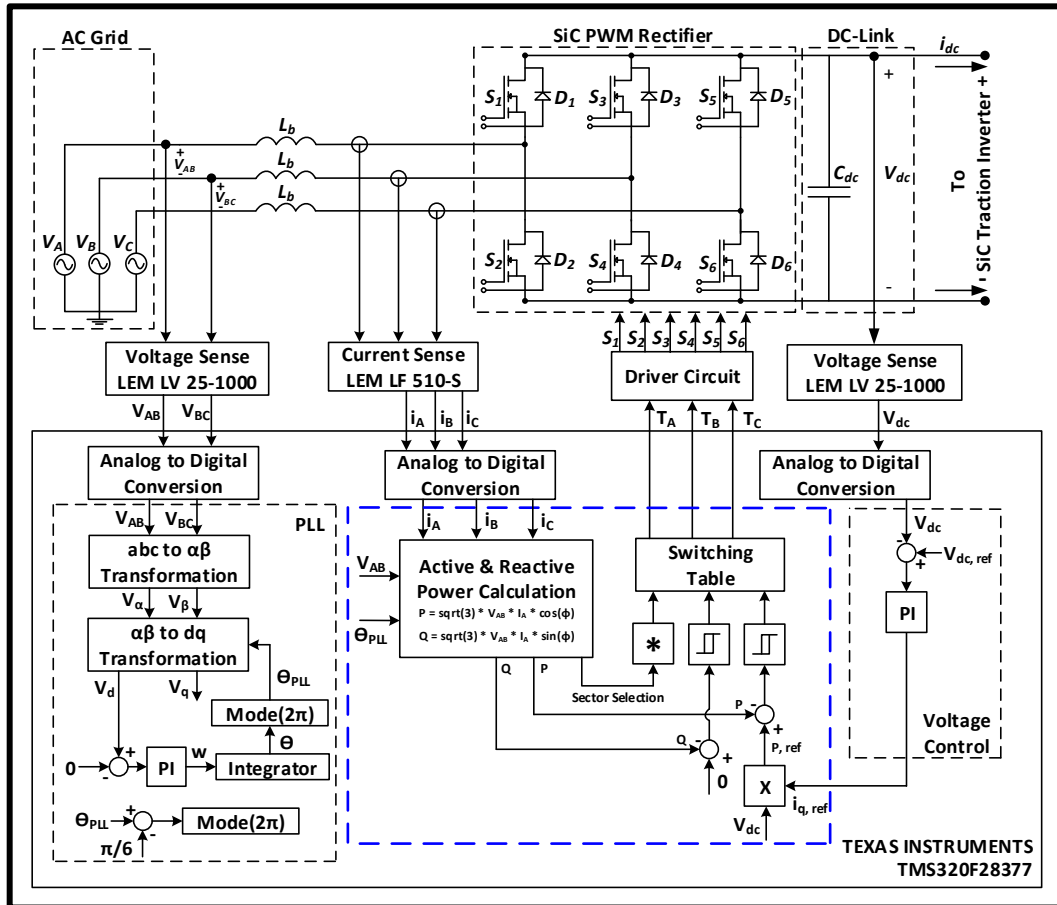


Figure 4. 7. Direct power control scheme

DPC method requires to know active and reactive power information at any time to be able control the rectifier. A considerably high sampling frequency has to be used to determine these ever-changing power values. Furthermore, switching frequency is not constant in DPC method, it changes consistently. This situation makes difficult to design a suitable boost reactor, L_b [31]. A significantly high inductance value has to be chosen for boost reactor, L_b . However, choosing higher inductance value causes larger component size. This results in mechanical design which is not dense and not compact. Moreover, calculations of active and reactive power cannot be made properly at switching instants. This condition complicates control of the rectifier.

Advantages of DPC method are that it does not need to inner current control loop and Pulse Width Modulation (PWM) blocks such as Sinusoidal PWM (SPWM) and Space Vector PWM (SVPWM). Implementation of these modulation techniques is quite complicated compared to switching table used in this control method. DPC method does not need to Clarke, Park and Inverse Park transformations because of the fact that there is no inner current control loop. Inner current control loop has good dynamic response at transients and good static response at steady state if its control parameters are optimized properly. DPC was not chosen as a control method in this thesis study because of its drawbacks mentioned above.

4.4. Voltage Oriented Control

VOC is basically based on two control loops which are called outer voltage control loop and inner current control loop. Voltage regulation at DC-Link and bidirectional power capability provides cooperation of these two control blocks. Voltage control loop takes DC-Link voltage measured via voltage sensor as a feedback. Error gets subtracting reference value, $V_{dc, ref}$ from DC-Link voltage, V_{dc} . Error is fed to PI controller. Output of PI controller which is $i_{q, ref, pu}$ goes to inner current loop as an input. Outer voltage control loop is completed at this stage. Both Proportional Resonant (PR) controller and PI controller are used as a regulator in inner current control loop. PI controllers were preferred in the scope of this thesis study. First of all, inner current control loop needs to real value of line currents which are i_A , i_B , i_C . Current measurements were performed using current sensors that work with principle of closed loop hall effect belonging to LEM company (LF 510-S). Current readings on DSP board is same as voltage readings clarified in Figure 4. 3. Current carrying cable is passed into this hall effect current sensor. Magnetic field is produced around current carrying conductor. Current sense is made with the help of hall cell placed into the air gap of a magnetic circuit. According to primary current, current sensor gives current output in mA range using a determined conversion ratio (500A/100mA). After reading real value of line currents, these values were not used directly in transformations and in PI regulators. Per unit (pu) line currents which are $i_{A, pu}$, $i_{B, pu}$,

$i_{C, pu}$ were obtained to provide immunity to noise by dividing reference current values. Relation is shown in (4.6).

$$i_{A, pu} = \frac{i_A}{i_{ref}}, i_{B, pu} = \frac{i_B}{i_{ref}}, i_{C, pu} = \frac{i_C}{i_{ref}} \quad (4.6)$$

At the same time, line currents were limited to reference value. Per unit alpha and beta axis components which are $i_{\alpha, pu}$ and $i_{\beta, pu}$ were obtained using Clarke Transformation. Mathematical explanations of Clarke Transformation were shown in (4.7) and (4.8).

$$i_{\alpha, pu} = \frac{2}{3} * (i_{a, pu} - \frac{1}{2} (i_{b, pu} + i_{c, pu})) \quad (4.7)$$

$$i_{\beta, pu} = \frac{1}{\sqrt{3}} * (i_{b, pu} - i_{c, pu}) \quad (4.8)$$

After Clarke transformation, per unit direct and quadrature axis components which are $i_{d, pu}$ and $i_{q, pu}$ were obtained using Park transformation. Phase angle, θ_{PWM} generated in PLL algorithm was used in Park Transformation. Mathematical explanations of Park Transformation were shown in (4.9) and (4.10).

$$i_{d, pu} = i_{\alpha, pu} * \cos(\theta_{PWM}) + i_{\beta, pu} * \sin(\theta_{PWM}) \quad (4.9)$$

$$i_{q, pu} = i_{\beta, pu} * \cos(\theta_{PWM}) - i_{\alpha, pu} * \sin(\theta_{PWM}) \quad (4.10)$$

Difference between voltage control loop output which is $i_{q, ref, pu}$ and q-axis component of Park Transformation which is $i_{q, pu}$ was used in PI controller as an error. At the same time, difference between reference value of d-axis current which is zero and d-axis component of Park Transformation which is $i_{d, pu}$ was used in PI controller as an error. Outputs of PI controllers give $V_{d, pu}$ and $V_{q, pu}$. These values were used in Inverse Park Transformation to get alpha and beta axis components again which are $V_{\alpha, pu}$ and $V_{\beta, pu}$. Phase angle, θ_{PWM} generated in PLL algorithm was also used in Inverse Park Transformation. Mathematical explanations of Inverse Park Transformation were shown in (4.11) and (4.12).

$$V_{\alpha, pu} = V_{d, pu} * \sin(\theta_{PWM}) + V_{q, pu} * \cos(\theta_{PWM}) \quad (4.11)$$

$$V_{\beta, pu} = V_{q, pu} * \sin(\theta_{PWM}) - V_{d, pu} * \cos(\theta_{PWM}) \quad (4.12)$$

While developing code in CCS 6.1.1, Clarke, Park and Inverse Park Transformations used in inner current control loop were made using available code blocks called macro

as in PLL part instead of writing (4.7), (4.8), (4.9), (4.10), (4.11), and (4.12) one by one. Outputs of dq to $\alpha\beta$ transformation which are $V_{\alpha, pu}$ and $V_{\beta, pu}$ were used in SVPWM block to constitute switching states which are T_A, T_B, T_C . SVPWM block will be explained in modulation techniques part in detail. Control method mentioned above is shown in Figure 4. 8 in detail.

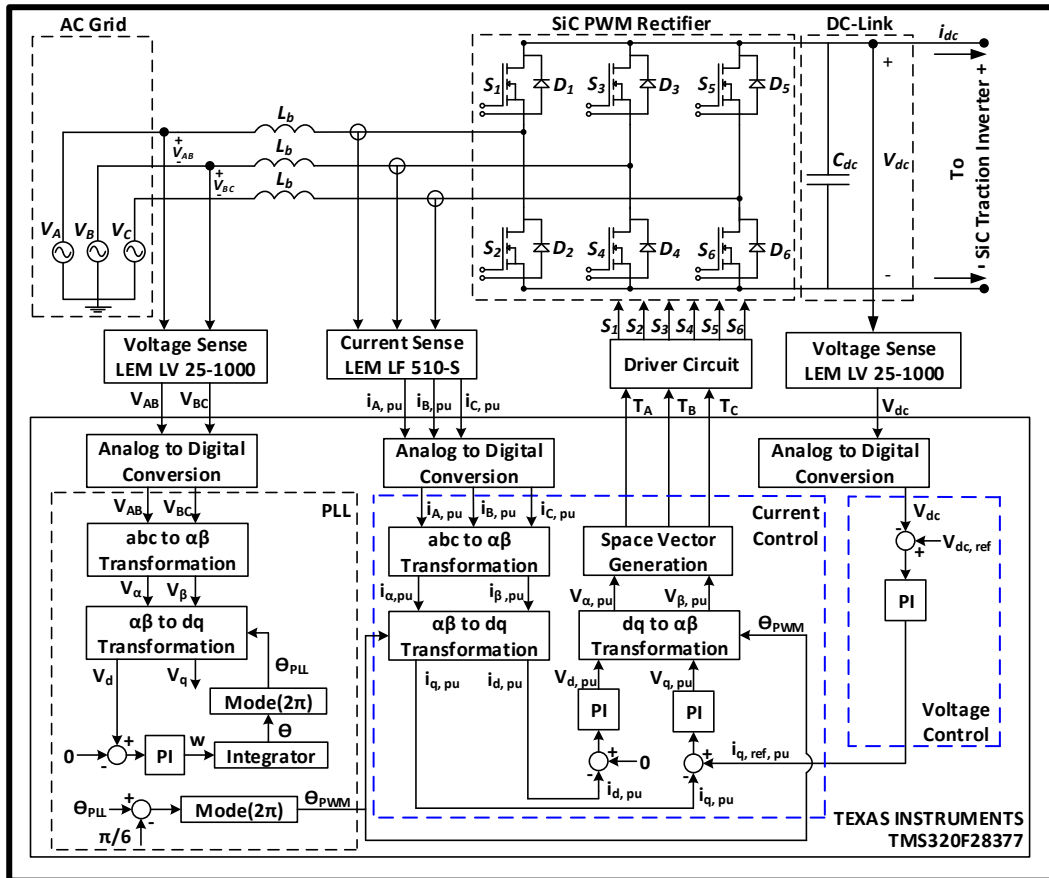


Figure 4. 8. Voltage oriented control scheme

Switching frequency is constant in VOC method compared to DPC method. This situation makes easy to design a suitable boost reactor, L_b . Advanced modulation techniques such as SVPWM can be implemented using VOC method. Usage of this kind of modulation technique is beneficial for harmonic reduction, however it is difficult to apply [32]. Main disadvantage of this method compared to DPC is inner current control loop. PI controller

parameters have to be well-optimized. Performance of inner current control loop directly depends on PI controller parameters and phase angle, θ_{PWM} created in PLL. However, if VOC method is applied successfully, dynamic response of the system at transients and static response of the system at steady state are better than DPC method. VOC was chosen as a control method in this thesis study because of its benefits mentioned above.

CHAPTER 5

PULSE WIDTH MODULATION TECHNIQUES

5.1. Introduction

Sinusoidal Pulse Width Modulation (SPWM) and Space Vector Pulse Width Modulation (SVPWM) are commonly used as a PWM technique in three phase PWM rectifier applications. Both PWM techniques have some advantages and disadvantages in terms of harmonics, THD performance, switching losses, DC bus utilization, power factor, number of switching, simplicity of implementation and control easiness. Following parts explain both modulation techniques in detail.

5.2. Sinusoidal Pulse Width Modulation

A reference signal which is also called control signal is compared with triangular carrier signal to form PWM signals in SPWM technique. Sinusoidal signal is used as control signal in three phase PWM rectifier applications. Frequency of sinusoidal signal is equal to grid frequency. On the other hand, switching frequency is adjusted by frequency of carrier signal. SPWM technique applied in three phase PWM rectifier was illustrated in Figure 5. 1.

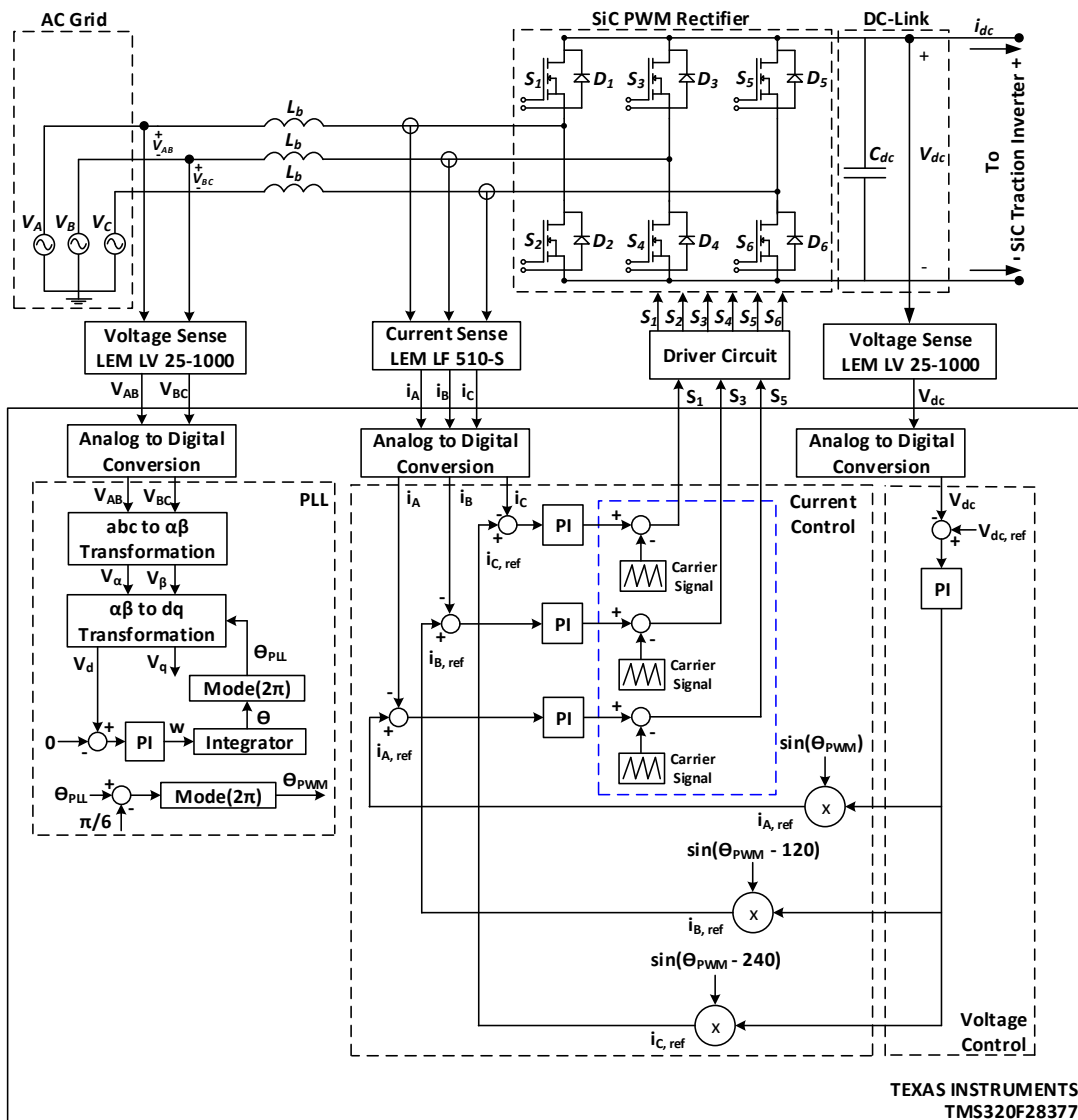


Figure 5. 1. Sinusoidal pulse width modulation scheme

Outer voltage control loop compares reference DC-Link voltage, $V_{dc,ref}$ with measured DC-Link voltage. Output of PI controller within outer voltage control loop is multiplied with sinusoidal waveforms shifted by 120° from each other to form reference line currents which are $i_{A,ref}$, $i_{B,ref}$, $i_{C,ref}$. Phase angle generated by PLL loop is used to be able to make line to neutral grid voltage and grid current in phase. Inner current control loop compares reference line currents with measured line current which are i_A , i_B , i_C . Outputs of PI controllers within inner current control loop are used

as control signals for SPWM. PWM signals are generated by comparing these sinusoidal control signals with triangular carrier signals. SPWM technique has following advantages and disadvantages.

- ✓ Its implementation is quite simple.
- ✓ Its control is easy.
- ✓ Unity power factor operation is not achieved.
- ✓ High THD value is obtained.

5.3. Space Vector Pulse Width Modulation

Space Vector Pulse Width Modulation (SVPWM) uses alpha axis and beta axis voltages (V_α , V_β) coming as a result of outer voltage control and inner current control loop. A space voltage vector, V_S , comprising vectorial sum of alpha and beta voltage vectors is formed. Representation, magnitude and phase angle of space vector were given in (5.1), (5.2), and (5.3) respectively.

$$V_S = V_\alpha + jV_\beta \quad (5.1)$$

$$|V_S| = \sqrt{V_\alpha^2 + V_\beta^2} \quad (5.2)$$

$$\theta = \arctan^{-1}\left(\frac{|V_\beta|}{|V_\alpha|}\right) \quad (5.3)$$

There are eight possible switching states of switches in three phase system. Each switching states is expressed a with one vector in SVPWM technique. Vectors corresponding to switching states were shown in Table 5. 1. Vectors which are V_1 , $V_2 \dots V_6$ are known as active vectors within space vector diagram. On the other hand, vectors which are V_0 and V_7 are known as zero vectors. Space vector diagram is separated to six sectors using these eight vectors. SVPWM technique is basically based on that a space voltage vector can be expressed using two adjacent active vectors and zero vectors. A space voltage vector, six active vectors, two zero vectors and sectors were shown in Figure 5. 2 in detail.

Table 5. 1. Vectors corresponding to eight switching states

Vector	S_1	S_3	S_5
V_0	0	0	0
V_1	1	0	0
V_2	1	1	0
V_3	0	1	0
V_4	0	1	1
V_5	0	0	1
V_6	1	0	1
V_7	1	1	1

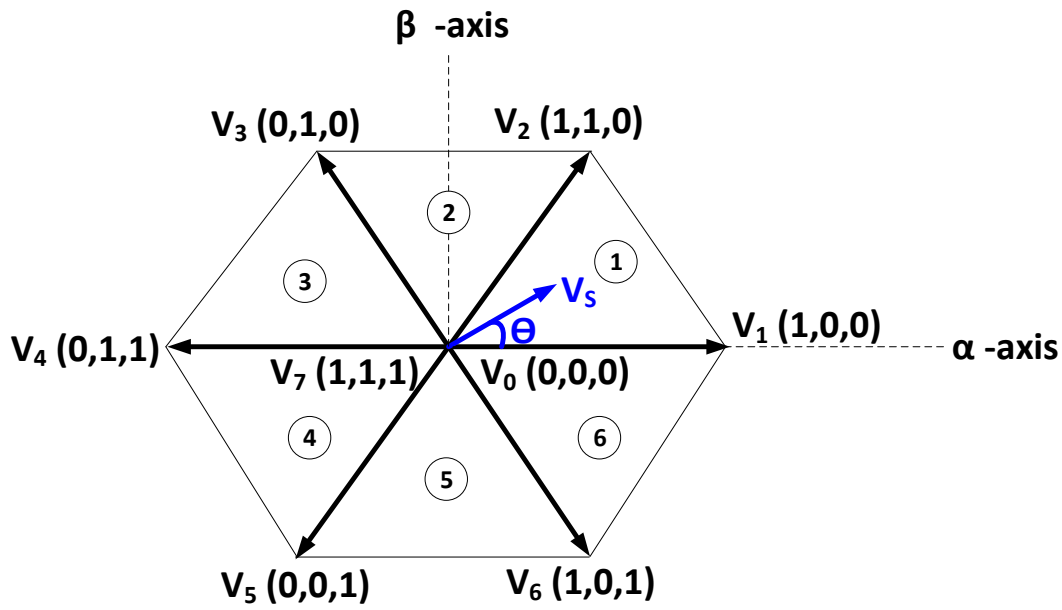


Figure 5. 2. Space vector diagram

A space voltage vector in Sector 1 are expressed using active vectors of V_1 and V_2 and zero vectors of V_0 and V_7 within one period, T_S as shown in (5.4).

$$V_S(t) = \frac{t_0}{T_S} V_0 + \frac{t_1}{T_S} V_1 + \frac{t_2}{T_S} V_2 + \frac{t_7}{T_S} V_7 \quad (5.4)$$

Times which are t_0 , t_1 , t_2 , t_7 are shown turn-on time of vectors. To be able reduce harmonics, symmetrical switching was made as shown in Figure 5. 3 [33] – [34].

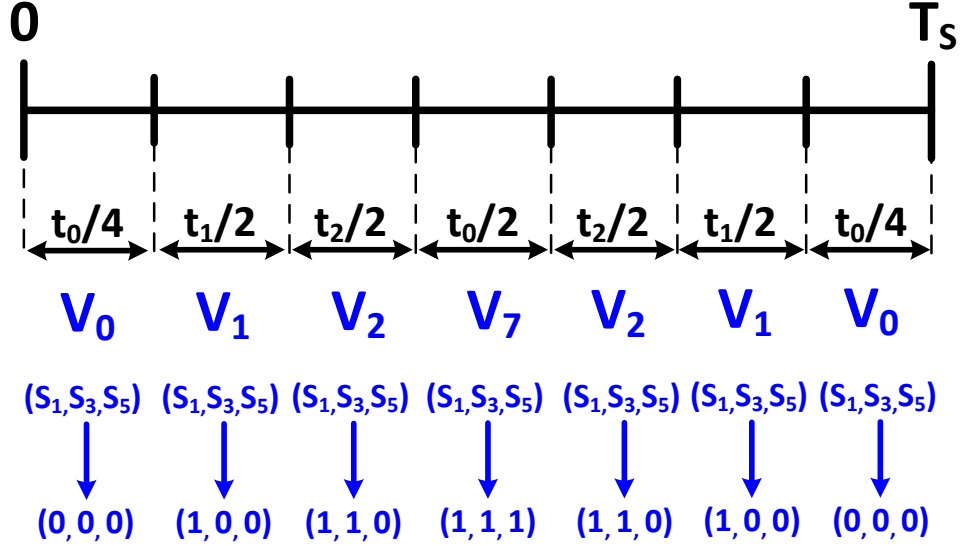


Figure 5. 3. Turn-on times of vectors

Firstly, angle of the space vector voltage, Θ is determined to be understood which sector it is in. Then, turn-on times of each vector which are t_1 , t_2 , t_0 are determined as in (5.5), (5.6), and (5.7) respectively for a space voltage vector within Sector 1.

$$t_1 = \frac{|V_S| \times \sin\left(\frac{\pi}{3} - \theta\right)}{|V_1| \times \sin\left(\frac{\pi}{3}\right)} \times T_S \quad (5.5)$$

$$t_2 = \frac{|V_S| \times \sin(\theta)}{|V_2| \times \sin\left(\frac{\pi}{3}\right)} \times T_S \quad (5.6)$$

$$t_0 = T_S - t_1 - t_2 \quad (5.7)$$

Line to neutral grid voltages shown in Figure 5. 4 which are V_A , V_B , V_C can be expressed as in (5.8), (5.9) and (5.10) respectively by using inductance of boost reactor, L_b , DC resistance of boost reactor, R_{dc} , line currents, i_A , i_B , i_C and rectifier leg voltages, V_{RA} , V_{RB} , V_{RC} .

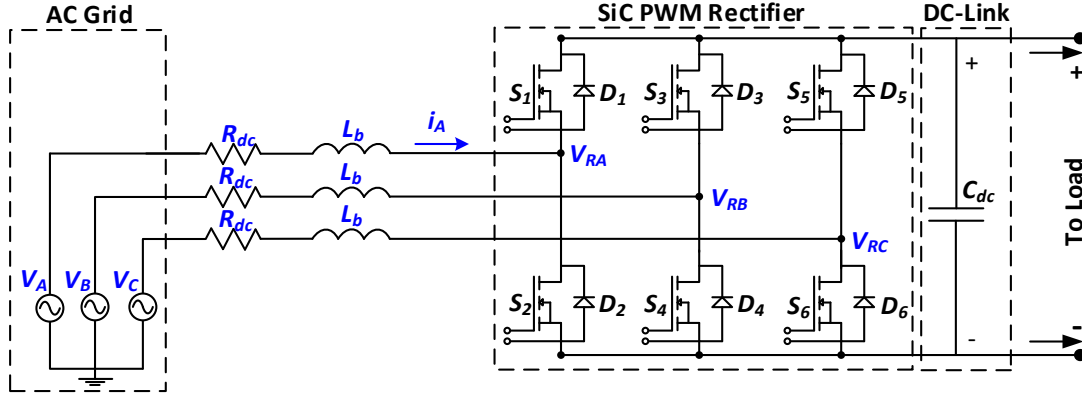


Figure 5. 4. Line to neutral grid voltages, inductance of boost reactor, DC resistance of boost reactor, line currents and rectifier leg voltages

$$V_A = 230 \times \sqrt{2} \times \sin(\theta) = R_{dc} \times i_A + L \times \frac{di_A}{dt} + V_{RA} \quad (5.8)$$

$$V_A = 230 \times \sqrt{2} \times \sin\left(\theta - \frac{2\pi}{3}\right) = R_{dc} \times i_B + L \times \frac{di_B}{dt} + V_{RB} \quad (5.9)$$

$$V_A = 230 \times \sqrt{2} \times \sin\left(\theta - \frac{4\pi}{3}\right) = R_{dc} \times i_C + L \times \frac{di_C}{dt} + V_{RC} \quad (5.10)$$

Furthermore, rectifier leg voltages, V_{RA} , V_{RB} , V_{RC} can be expressed using switching states, S_1 , S_3 , S_5 and DC-Link voltage, V_{dc} as shown in (5.11), (5.12) and (5.13) respectively.

$$V_{RA} = \left[S_1 - \frac{1}{3} (S_1 + S_3 + S_5) \right] \times V_{dc} \quad (5.11)$$

$$V_{RB} = \left[S_3 - \frac{1}{3} (S_1 + S_3 + S_5) \right] \times V_{dc} \quad (5.12)$$

$$V_{RC} = \left[S_5 - \frac{1}{3} (S_1 + S_3 + S_5) \right] \times V_{dc} \quad (5.13)$$

Maximum value of rectifier leg voltages can be $2V_{dc}/3$ according to switching states given in Figure 5. 2 in detail. . For this reason, magnitudes of active vectors which are $V_1, V_2 \dots V_6$ are equal to $2V_{dc}/3$.

SVPWM technique has following advantages and disadvantages.

- ✓ Number of switching is reduced to 30% of that of SPWM at same switching frequency.
- ✓ Since number of switching is decreased, switching losses are less in SVPWM according to SPWM.
- ✓ Harmonics are considerably reduced in comparison with SPWM. SVPWM technique provides shifting of frequency of dominant harmonic to a higher value. In this way, harmonics are filtered.
- ✓ Its implementation is quite complicated compared to SPWM.
- ✓ Better THD performance and unity power factor can be obtained in SVPWM due to decreased harmonics [35].
- ✓ Its control is harder according to SPWM.
- ✓ Better DC bus utilization is provided via SVPWM. 15% more of output voltage can be obtained with SVPWM technique [36].
- ✓ Wider linear modulation range is obtained with SVPWM.

SVPWM was preferred as modulation technique in designed all SiC MOSFET based voltage source three phase PWM rectifier by paying attention to points above. Implementation of SVPWM technique was made both in MATLAB/Simulink simulation environment and in Digital Signal Processor (DSP) in the scope of this thesis study. SVPWM macro present in the library of Code Composer Studio (CCS) 6.1.1 was used directly in the stage of software development. On the other hand, SVPWM was designed step by step in MATLAB/Simulink without using ready SVPWM block present in Simulink.

CHAPTER 6

TESTS, MEASUREMENTS, AND RESULTS

Designed all SiC MOSFET based voltage source three phase PWM rectifier were tested using ready all SiC MOSFET based voltage source three phase PWM inverter as an active load in the test infrastructure of laboratory located in Middle East Technical University Electrical and Electronic Engineering Department. Test bench present in laboratory are shown in Figure 6. 1 in detail.

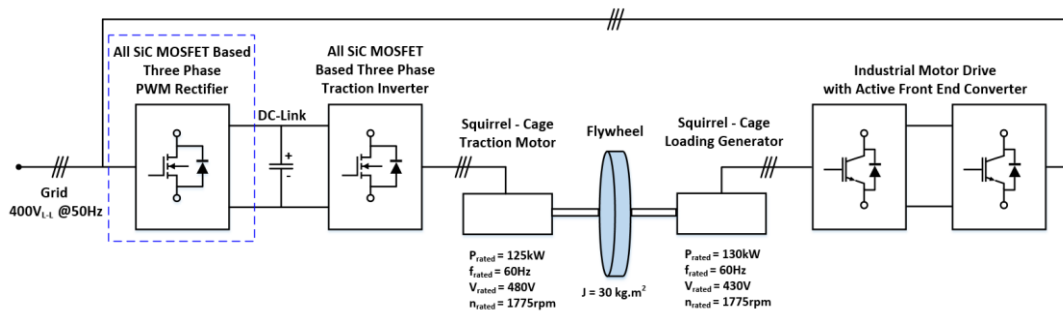


Figure 6. 1. Test bench

All SiC MOSFET based voltage source three phase PWM rectifier are supplied from 400 V_{LL} of grid voltage in distribution panel. 400V_{LL} of grid voltage are come to distribution panel via 1250kVA power rating of dry type transformer which transforms 34.5kV_{LL} of medium voltage to 400V_{LL} of low grid voltage. Both All SiC MOSFET based voltage source three phase PWM rectifier and All SiC MOSFET based three phase traction inverter are connected to same DC-Link line. All SiC MOSFET based three phase traction inverter drives 125kW of squirrel cage traction motor whose specifications are given in Figure 6. 1. 130kW of squirrel cage generator whose specification are given in Figure 6. 1 is used as load for squirrel cage traction motor. Squirrel cage traction motor and squirrel cage generator are connected each other with the help of double flex couplings, bearing and flywheel. Squirrel cage generator is controlled with an industrial motor drive with active front end converter.

By this means, power flow to grid is provided. A lot of different tests were performed using test bench. First of all, generator side was activated using Programmable Logic Controller (PLC) communications to form load against traction motor. Then, DC-Link voltage was brought and kept at 750VDC of constant value using All SiC MOSFET based voltage source three phase PWM rectifier. All tests were performed at 750VDC of DC-Link voltage. As a first test, generator side was operated at 1800rpm using industrial motor drive with active front end converter and PLC communications. At this speed, All SiC MOSFET based voltage source three phase PWM rectifier was provided 131.25kW of power to All SiC MOSFET based three phase traction inverter. Line to neutral voltage, line current, DC-Link voltage and DC-Link current were measured using two current probes, two current amplifiers, two high voltage differential probes and digital oscilloscope. Details about test equipment, channel assignments of digital oscilloscope according to measured data were given in Figure 6. 2 in detail.

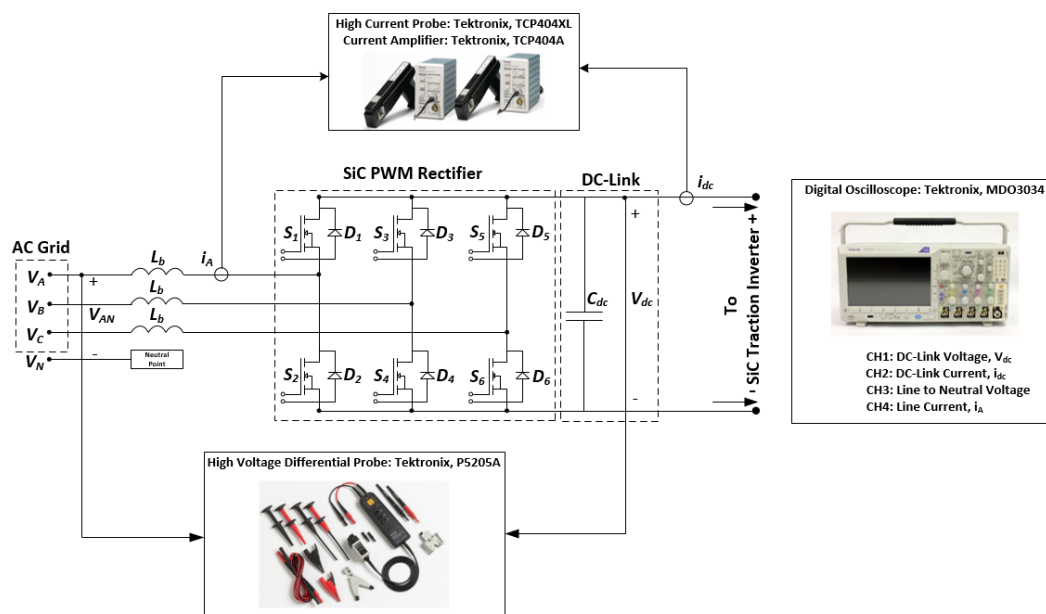


Figure 6. 2. Test equipment

Waveforms of line to neutral voltage, line current, DC-Link voltage and DC-Link current saved in digital oscilloscope were shown in Figure 6. 3. Input and output power

of All SiC MOSFET based voltage source three phase PWM rectifier were calculated in (6.1) and (6.2) according to oscilloscope measurements.

$$S_{IN} = \sqrt{3} * V_{AB,RMS} * i_{A,RMS} = \sqrt{3} * 400 * 190.95 = 132.3kVA \quad (6.1)$$

$$P_{OUT} = V_{DC} * i_{DC} = 750 * 175 = 131.25kW \quad (6.2)$$

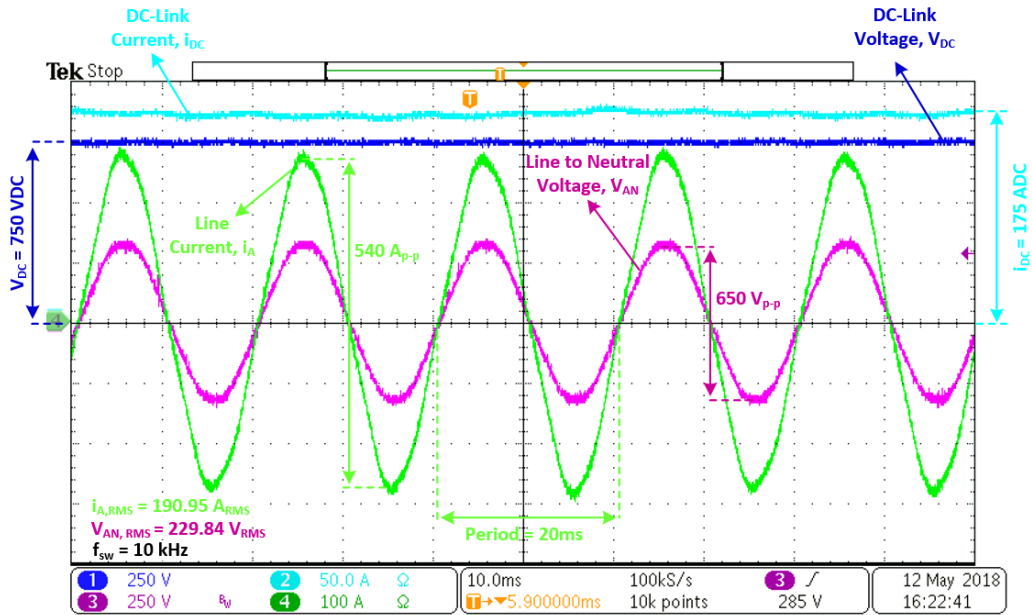


Figure 6. 3. Oscilloscope images of line to neutral voltage, line current, DC-link voltage and DC-link current in rectification mode

Grid side waveforms (line to neutral voltage and line current) and DC-Link side waveforms (DC-Link voltage and DC-Link current) were saved separately as well. Figure 6. 4 and Figure 6. 5 show grid side and DC Link side respectively. Unity power factor operation are seen in Figure 6. 4 clearly.

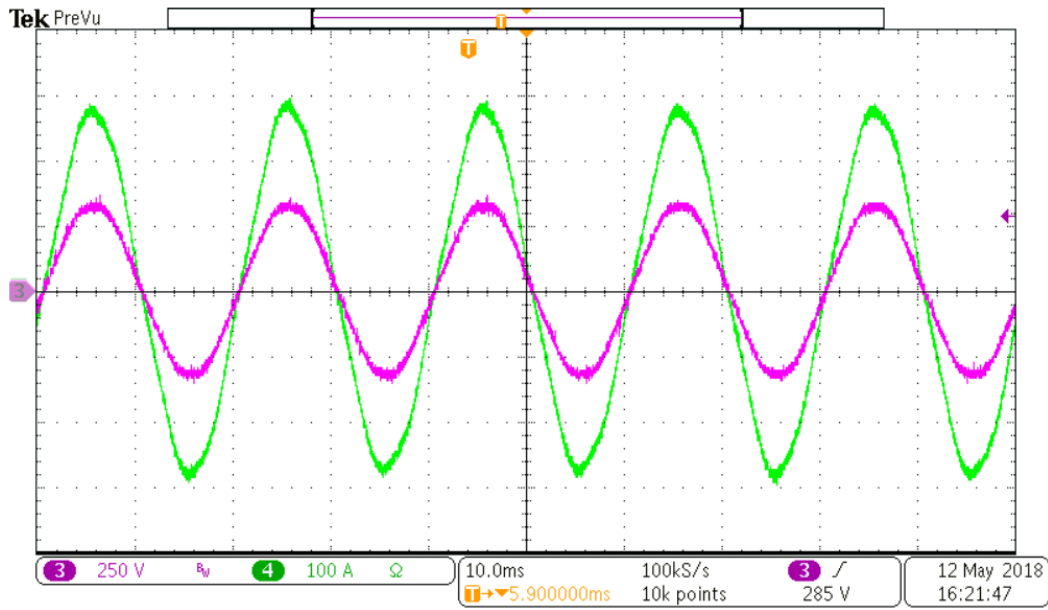


Figure 6. 4. Oscilloscope images of line to neutral voltage and line current

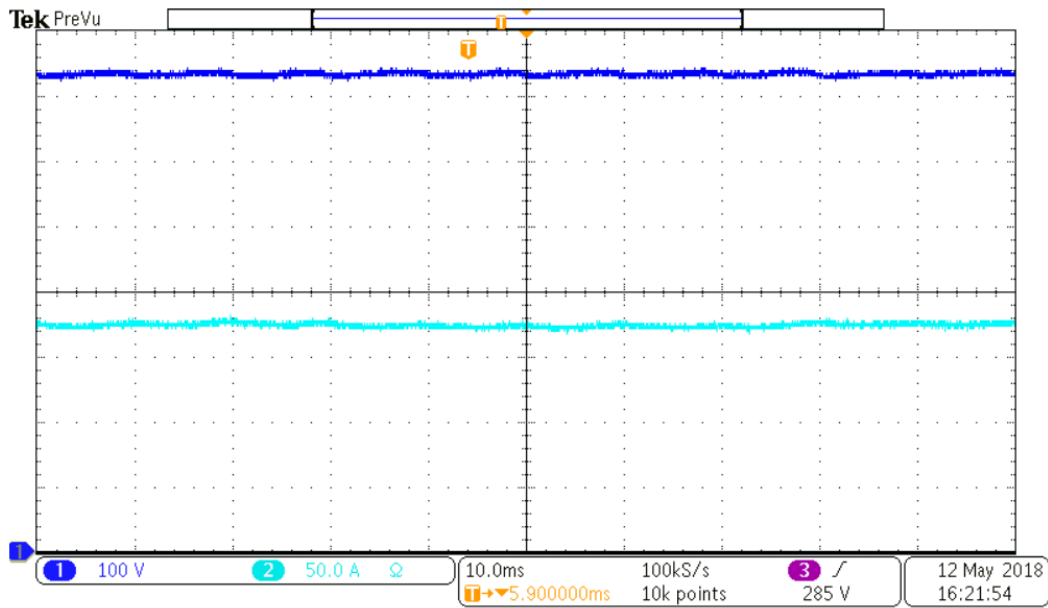


Figure 6. 5. Oscilloscope images of DC-link voltage and DC-link current

As a second test, generator side was again operated at 1800rpm using industrial motor drive with active front end converter and PLC communications. This time, braking was made to All SiC MOSFET based three phase traction inverter. At this speed, All SiC MOSFET based voltage source three phase PWM rectifier was provided 112.5kW

of power to grid. Waveforms of line to neutral voltage, line current, DC-Link voltage and DC-Link current saved in digital oscilloscope were shown in Figure 6. 6. Input and output power of All SiC MOSFET based voltage source three phase PWM rectifier were calculated in (6.3) and (6.4) according to oscilloscope measurements.

$$S_{IN} = \sqrt{3} * V_{AB,RMS} * i_{A,RMS} = \sqrt{3} * 400 * 163 = 112.93kVA \quad (6.3)$$

$$P_{OUT} = V_{DC} * i_{DC} = 750 * 150 = 112.5kW \quad (6.4)$$

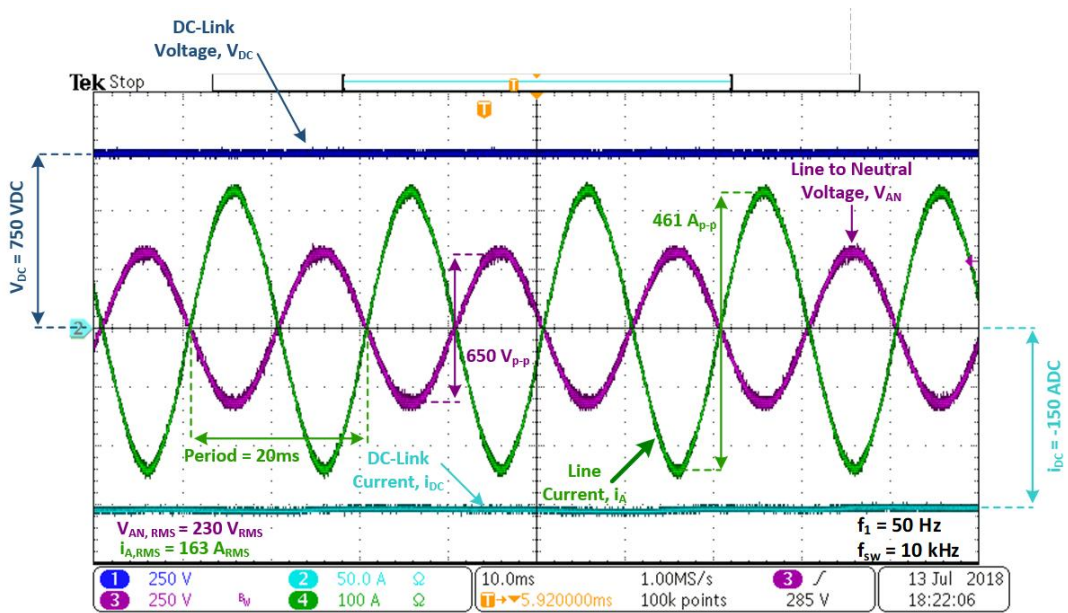


Figure 6. 6. Oscilloscope images of line to neutral voltage, line current, DC-link voltage and DC-link current in inversion mode

As a third test, power quality measurements were performed while generator side was again operated at 1800rpm using industrial motor drive with active front end converter and PLC communications. At this speed, All SiC MOSFET based voltage source three phase PWM rectifier was provided 112kW of power to All SiC MOSFET based three phase traction inverter. Probe connections of power quality analyzer used were illustrated in Figure 6. 7 clearly.

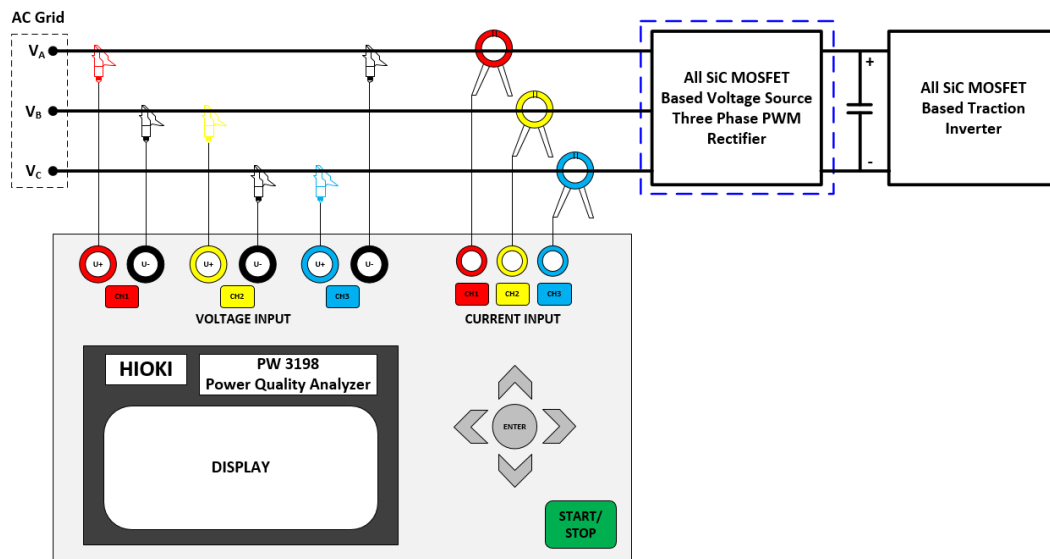


Figure 6. 7. Probe connections of power quality analyzer

Voltage probes of power quality analyzer were connected from line to line. Current probes were connected to each line. Snapshots for line to line grid voltages, line currents, THD value of line to line grid voltage, THD value of line current, harmonic lists according to order, apparent power of rectifier, active power of rectifier, reactive power of rectifier and power factor were saved. At the same time, data record was made during ten minutes. And then, 10 minutes of records were plotted using HIOKI 9624-50 PQA software for each data. Figure 6. 8 shows line to line grid voltages and line currents at the same graph. THD value of line to line voltage, V_{AB} and percentage of each harmonic according to fundamental value were given in Figure 6. 9. Figure 6. 10 illustrates THD value of line current, i_A and percentage of each harmonic according to fundamental value as in Figure 6. 9 . RMS values of line to line voltages, V_{AB} , V_{BC} , V_{CA} , RMS values of line currents, i_A , i_B , i_C , total active power of rectifier, total reactive power of rectifier, total apparent power of rectifier and power factor were displayed in Figure 6. 11 altogether. Difference between THD values of line to line voltages, V_{AB} , V_{BC} , V_{CA} can easily be seen in Figure 6. 12. Likewise, Figure 6. 13 shows distinctness of THD values of line currents, i_A , i_B , i_C .

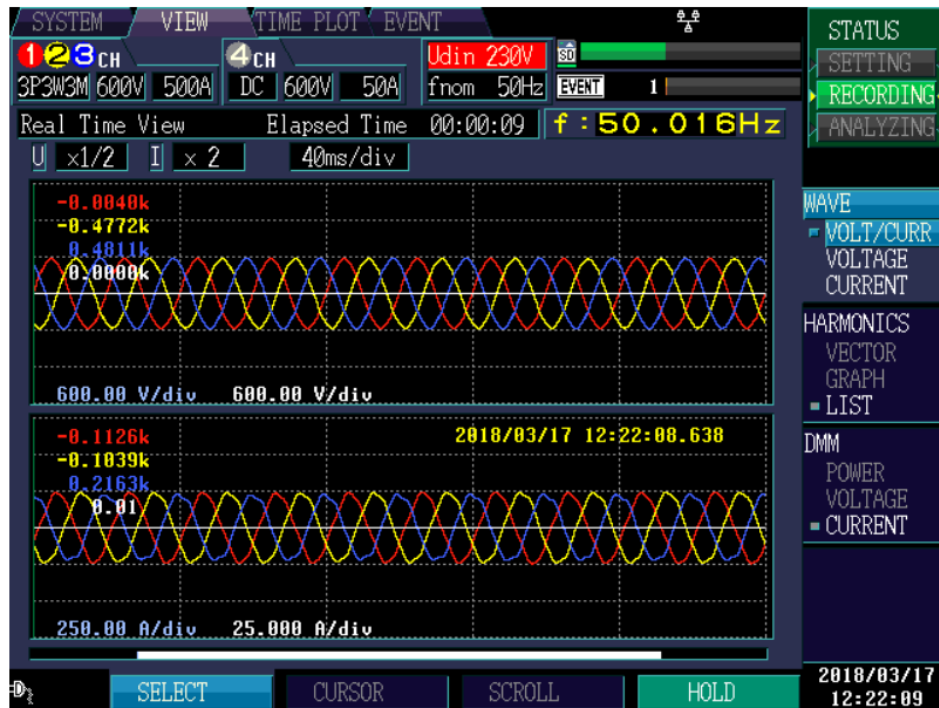


Figure 6. 8. Instant images of line to line voltages and line currents saved with power quality analyzer



Figure 6. 9. THD value of line to line voltage, V_{AB} and percentage of each harmonic according to fundamental value



Figure 6. 10. THD value of line current, i_A and percentage of each harmonic according to fundamental value



Figure 6. 11. RMS values of line to line voltages, RMS values of line currents, total active power of rectifier, total reactive power of rectifier, total apparent power of rectifier and power factor

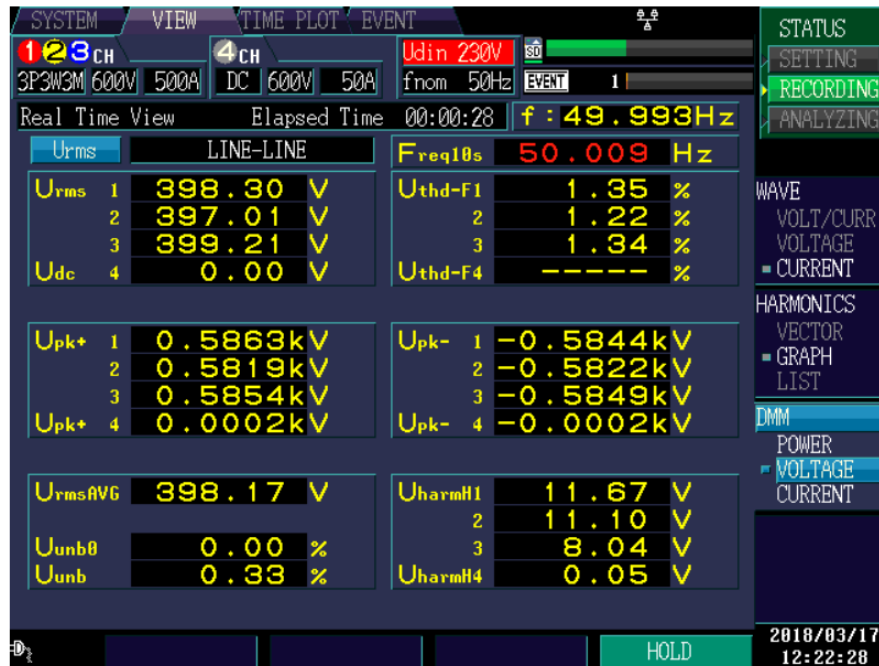


Figure 6. 12. THD values of line to line voltages, V_{AB} , V_{BC} , V_{CA}



Figure 6. 13. THD values of line currents, i_A , i_B , i_C

Line to line voltages, V_{AB} , V_{BC} , V_{CA} were recorded while all SiC MOSFET based voltage source three phase PWM rectifier was loaded at 122.5kVA of power for 10

minutes of duration. Recorded data was plotted using HIOKI 9624-50 PQA software as in Figure 6. 14.

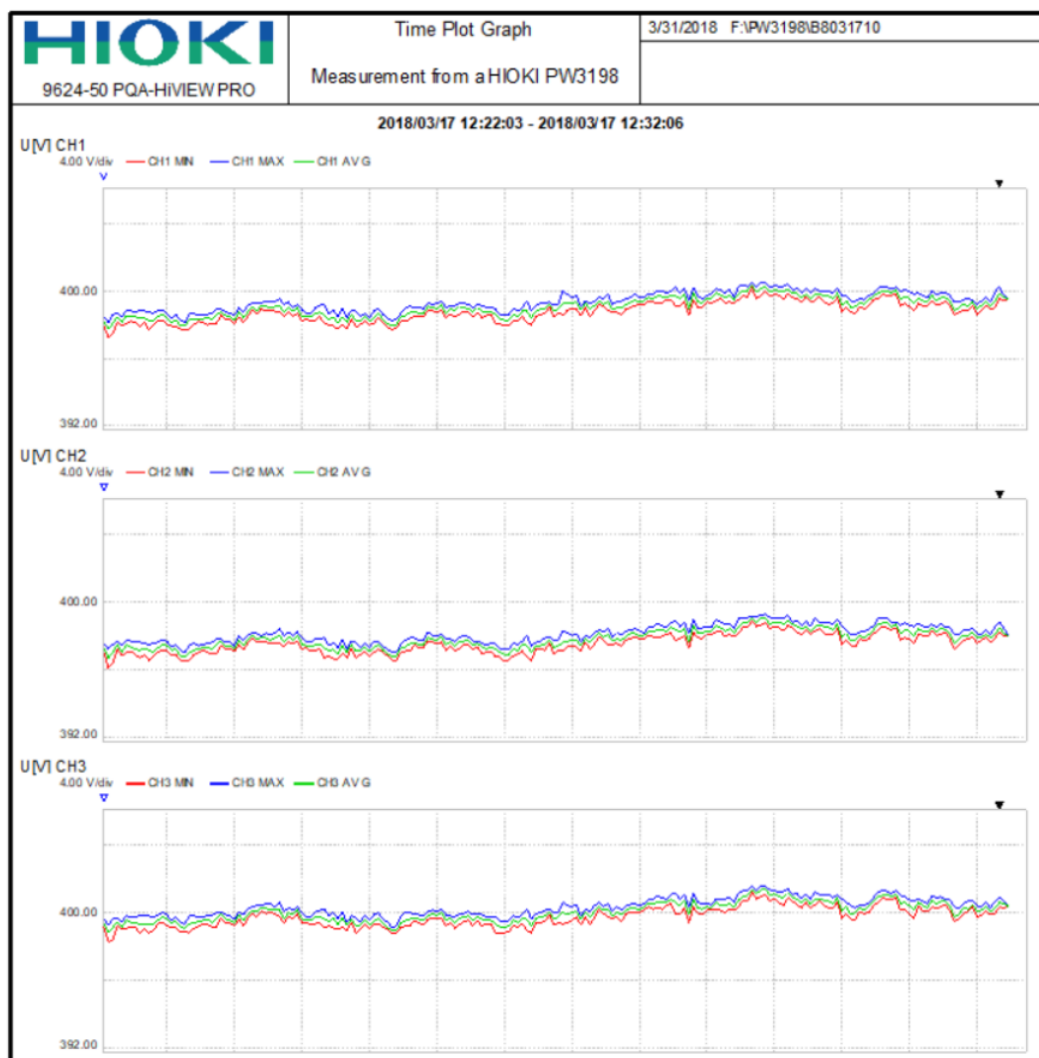


Figure 6. 14. 10 minutes of records of line to line voltages, V_{AB} , V_{BC} , V_{CA}

Line currents, i_A , i_B , i_C were recorded while all SiC MOSFET based voltage source three phase PWM rectifier was loaded at 122.5kVA of power for 10 minutes of duration. Recorded data was plotted using HIOKI 9624-50 PQA software as in Figure 6. 15.

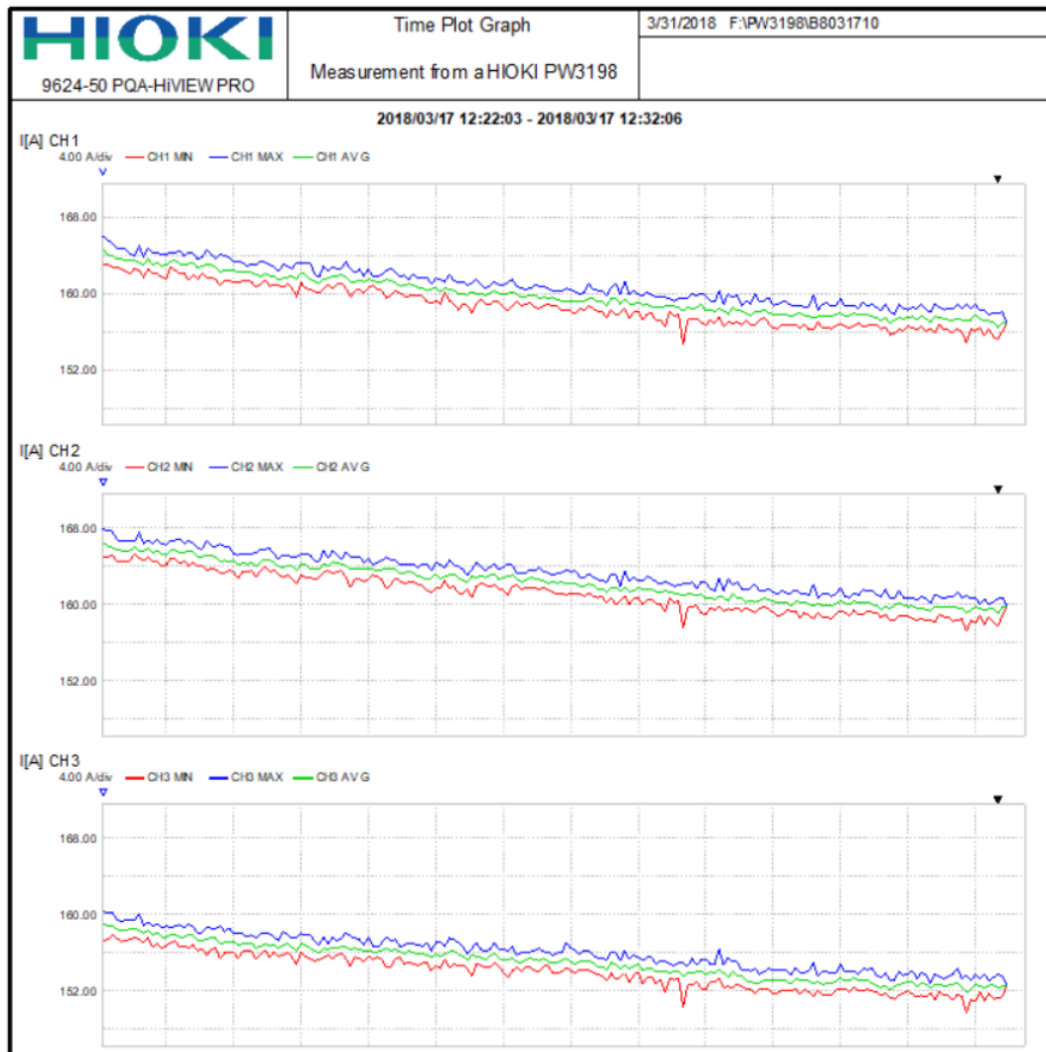


Figure 6. 15. 10 minutes of records of line currents, i_A , i_B , i_C

THD values of line to line voltages, V_{AB} , V_{BC} , V_{CA} were recorded while all SiC MOSFET based voltage source three phase PWM rectifier was loaded at 122.5kVA of power for 10 minutes of duration. Recorded data was plotted using HIOKI 9624-50 PQA software as in Figure 6. 16.

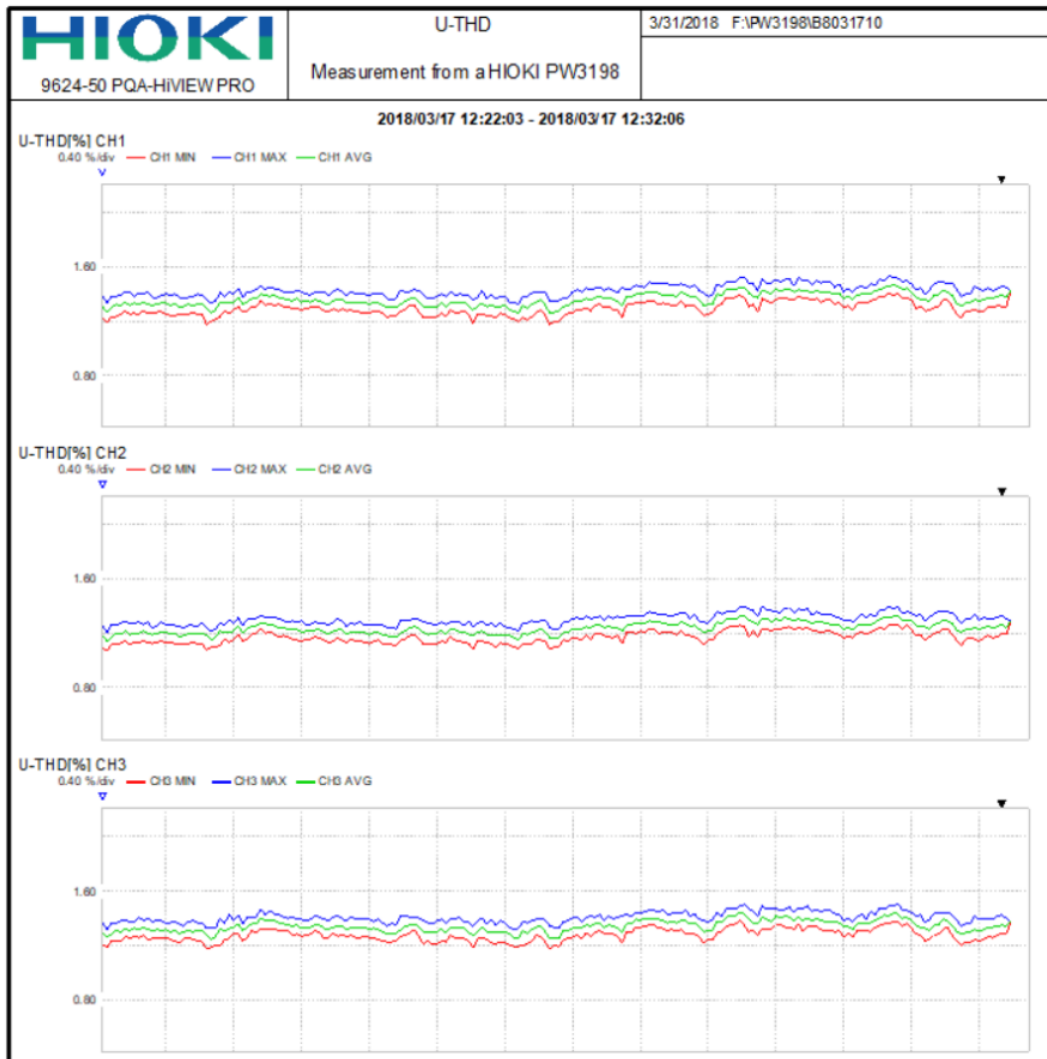


Figure 6. 16. THD values of line to line voltages, V_{AB} , V_{BC} , V_{CA} for 10 minutes of record

THD values of line currents, i_A , i_B , i_C were recorded while all SiC MOSFET based voltage source three phase PWM rectifier was loaded at 122.5kVA of power for 10 minutes of duration. Recorded data was plotted using HIOKI 9624-50 PQA software as in Figure 6. 17.

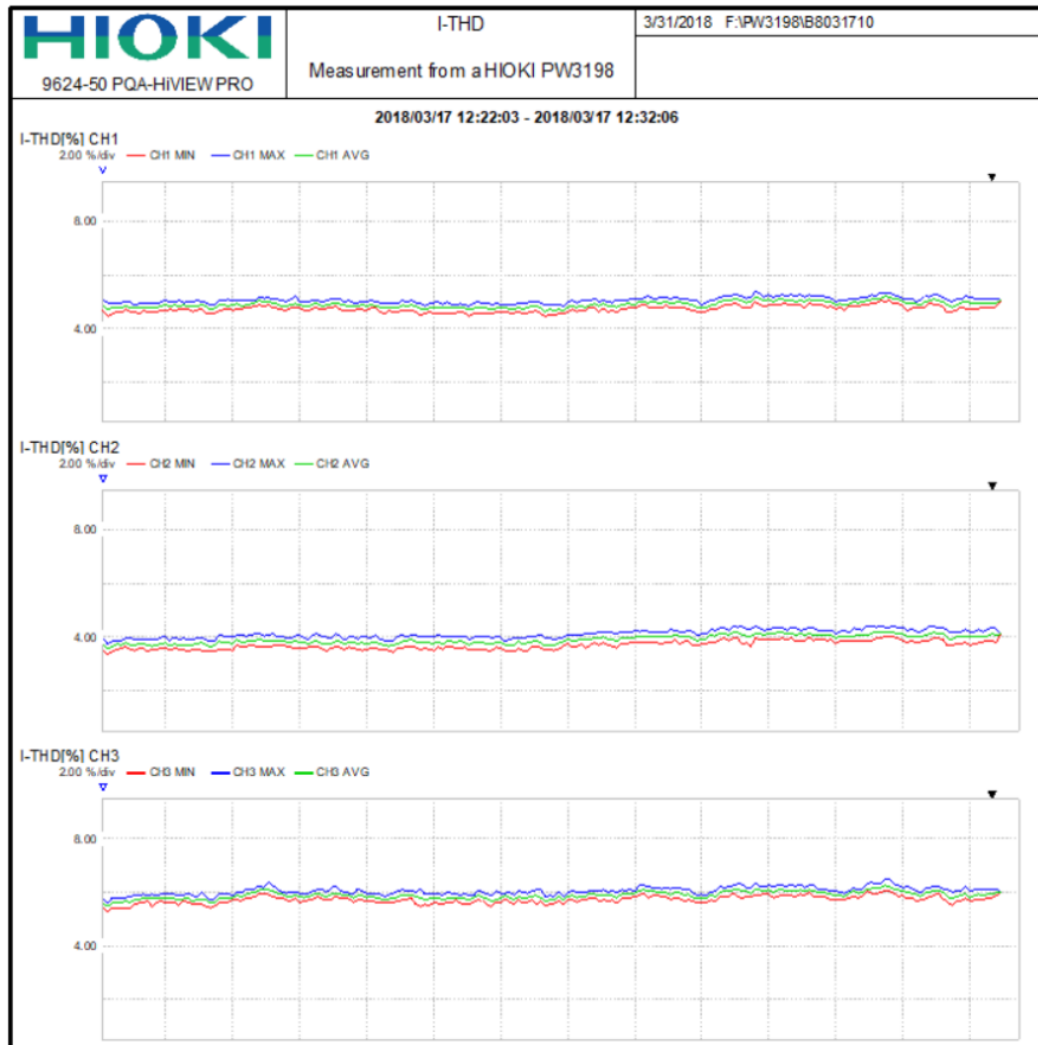


Figure 6. 17. THD values of line currents, i_A , i_B , i_C for 10 minutes of record

Finally, grid frequency was recorded while all SiC MOSFET based voltage source three phase PWM rectifier was loaded at 122.5kVA of power for 10 minutes of duration. Recorded data was plotted using HIOKI 9624-50 PQA software as in Figure 6. 18.

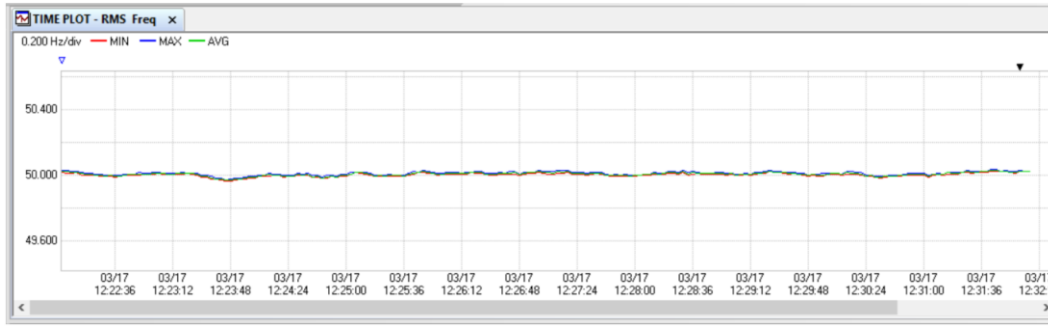


Figure 6. 18. Grid frequency variation for 10 minutes of record

As a final test, power quality measurements were performed while generator side was operated at 900rpm this time using industrial motor drive with active front end converter and PLC communications. At this speed, All SiC MOSFET based voltage source three phase PWM rectifier was provided 54.6kW of power to All SiC MOSFET based three phase traction inverter. Figure 6. 19 shows line to line grid voltages and line currents at the same graph. THD value of line to line voltage, V_{AB} and percentage of each harmonic according to fundamental value were given in Figure 6. 20. Figure 6. 21 illustrates THD value of line current, i_A and percentage of each harmonic according to fundamental value as in Figure 6. 20. RMS values of line to line voltages, V_{AB} , V_{BC} , V_{CA} , RMS values of line currents, i_A , i_B , i_C , total active power of rectifier, total reactive power of rectifier, total apparent power of rectifier and power factor were displayed in Figure 6. 22 altogether. Difference between THD values of line to line voltages, V_{AB} , V_{BC} , V_{CA} can easily be seen in Figure 6. 23. Likewise, Figure 6. 24 shows distinctness of THD values of line currents, i_A , i_B , i_C .

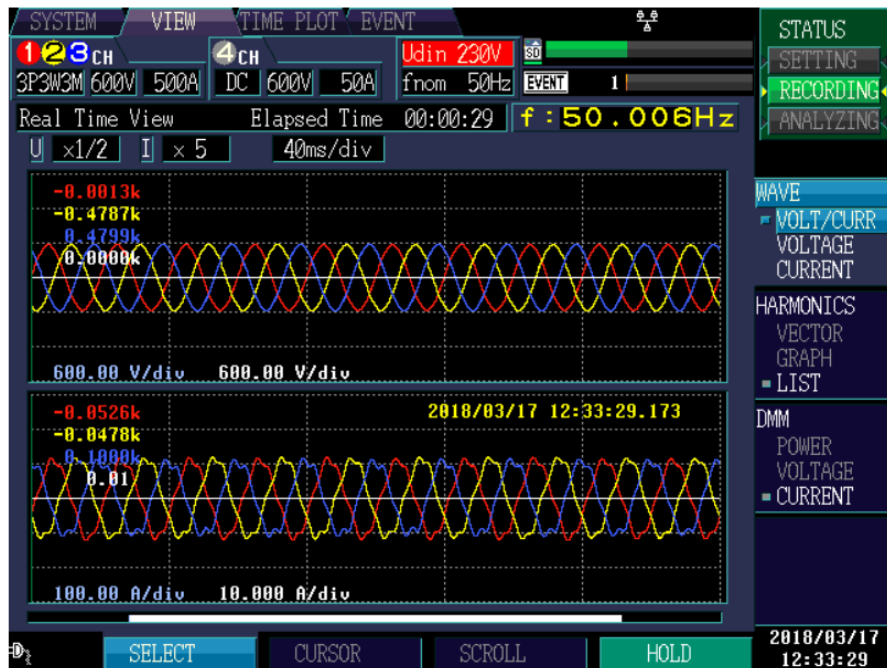


Figure 6. 19. Instant images of line to line voltages and line currents saved with power quality analyzer



Figure 6. 20. THD value of line to line voltage, V_{AB} and percentage of each harmonic according to fundamental value

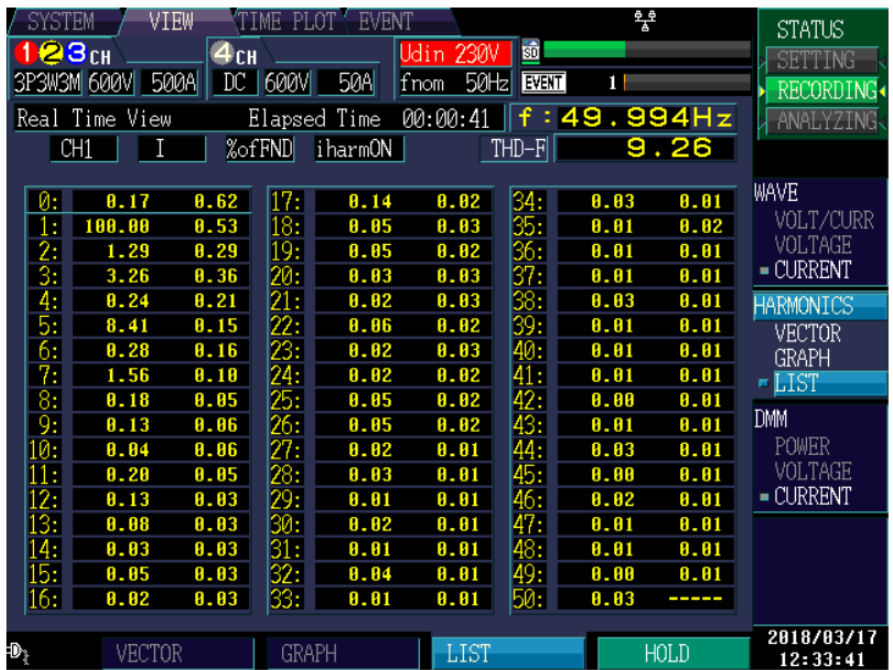


Figure 6. 21. THD value of line current, i_A and percentage of each harmonic according to fundamental value



Figure 6. 22. RMS values of line to line voltages, RMS values of line currents, total active power of rectifier, total reactive power of rectifier, total apparent power of rectifier and power factor

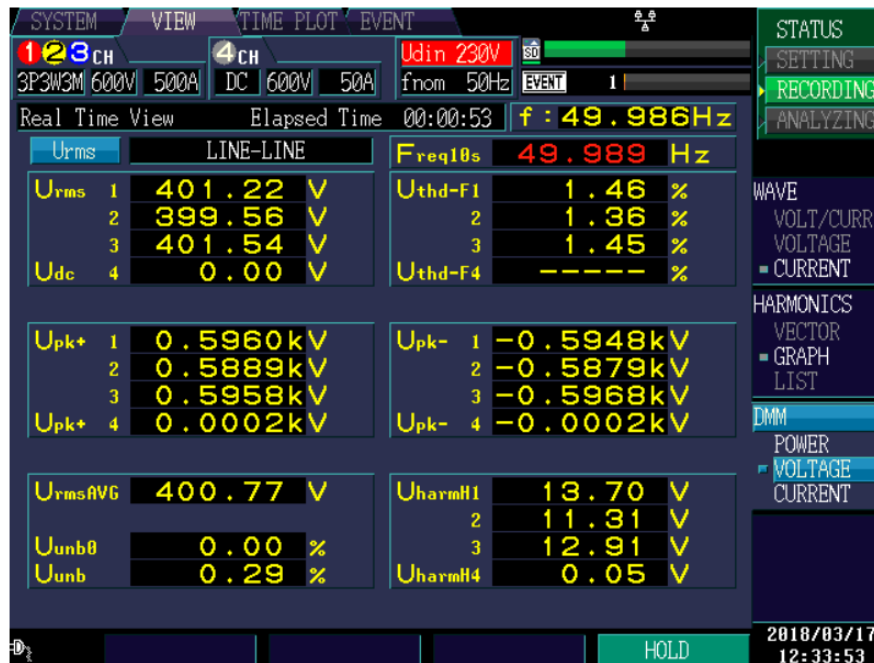


Figure 6. 23. THD values of line to line voltages, V_{AB} , V_{BC} , V_{CA}



Figure 6. 24. THD values of line currents, i_A , i_B , i_C

Line to line voltages, V_{AB} , V_{BC} , V_{CA} were recorded while all SiC MOSFET based voltage source three phase PWM rectifier was loaded at 54.6kVA of power for 10

minutes of duration. Recorded data was plotted using HIOKI 9624-50 PQA software as in Figure 6. 25.

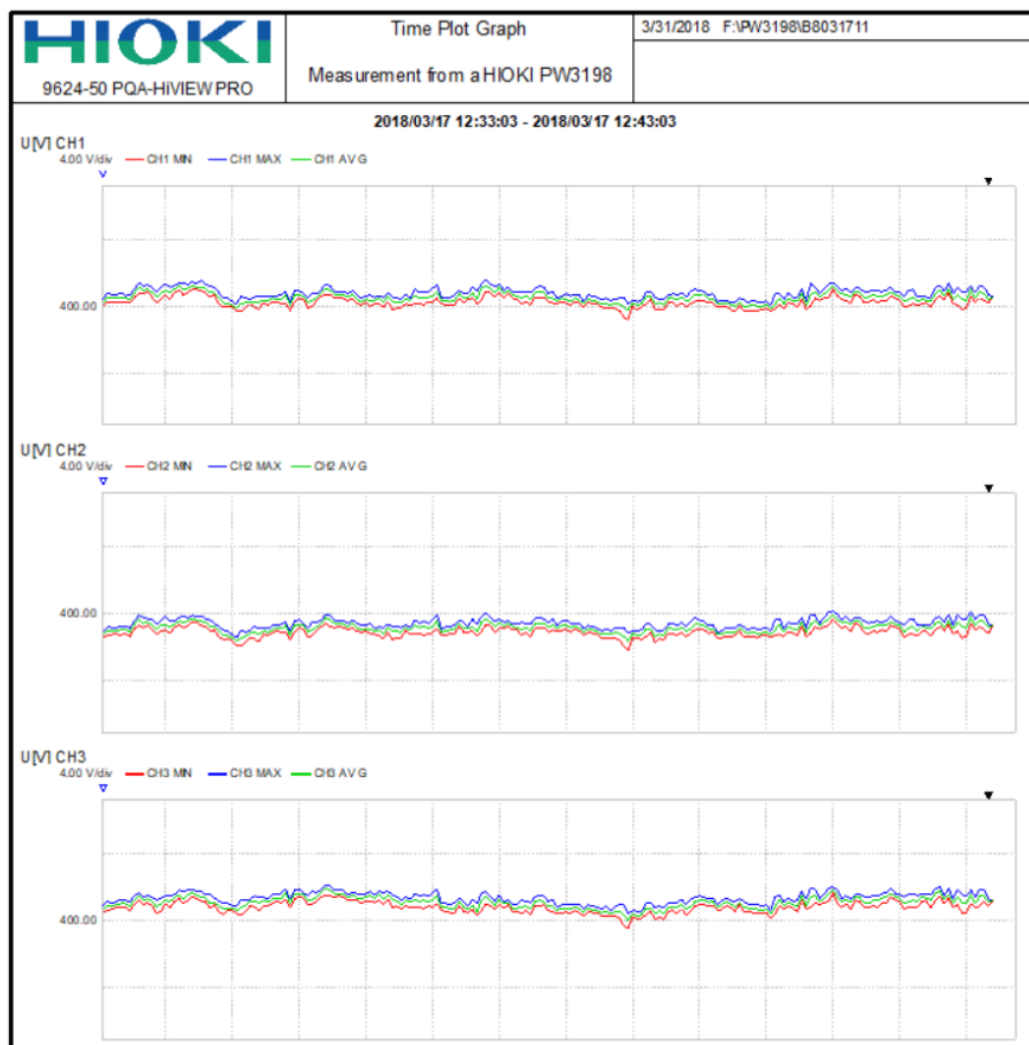


Figure 6. 25. 10 minutes of records of line to line voltages, V_{AB} , V_{BC} , V_{CA}

Line currents, i_A , i_B , i_C were recorded while all SiC MOSFET based voltage source three phase PWM rectifier was loaded at 54.6kVA of power for 10 minutes of duration. Recorded data was plotted using HIOKI 9624-50 PQA software as in Figure 6. 26.

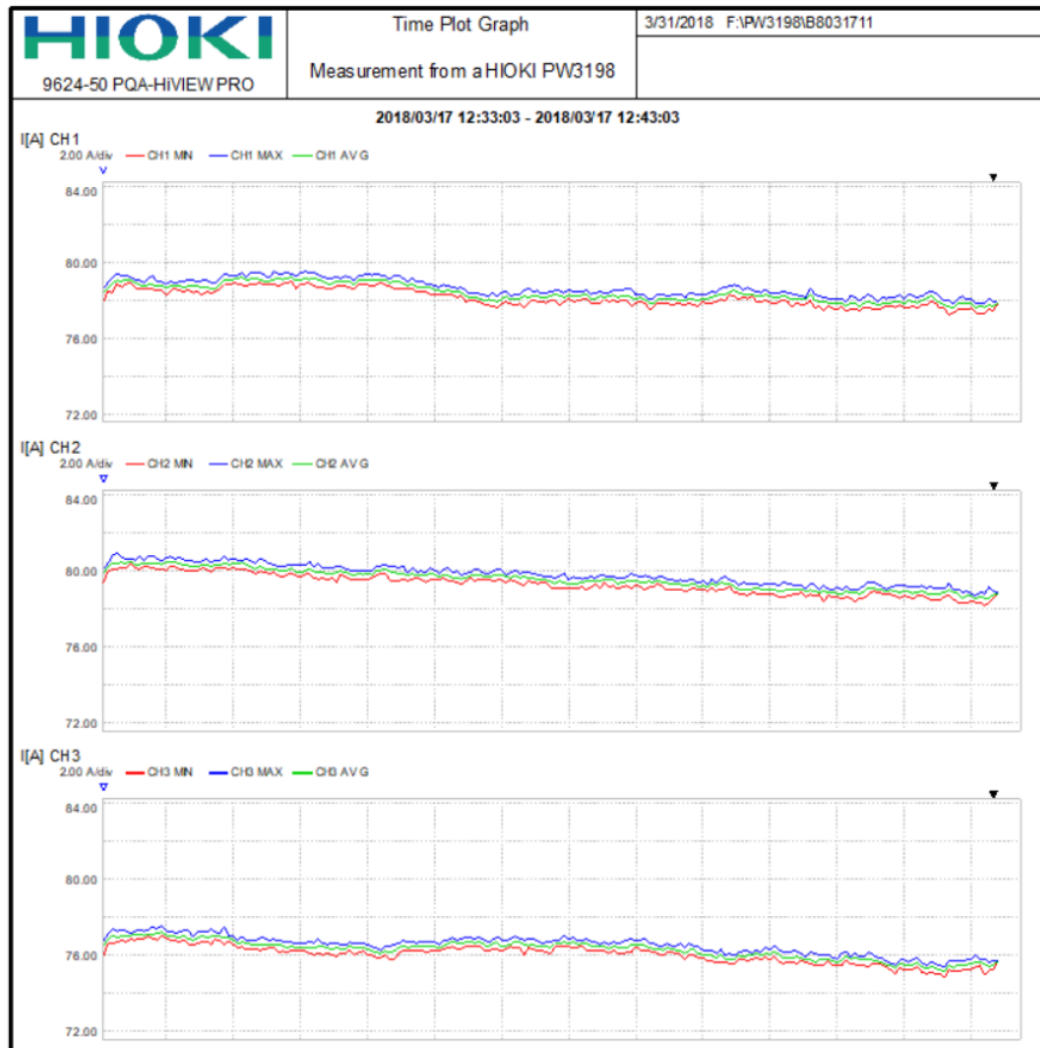


Figure 6. 26. 10 minutes of records of line currents, i_A , i_B , i_C

THD values of line to line voltages, V_{AB} , V_{BC} , V_{CA} were recorded while all SiC MOSFET based voltage source three phase PWM rectifier was loaded at 54.6kVA of power for 10 minutes of duration. Recorded data was plotted using HIOKI 9624-50 PQA software as in Figure 6. 27.

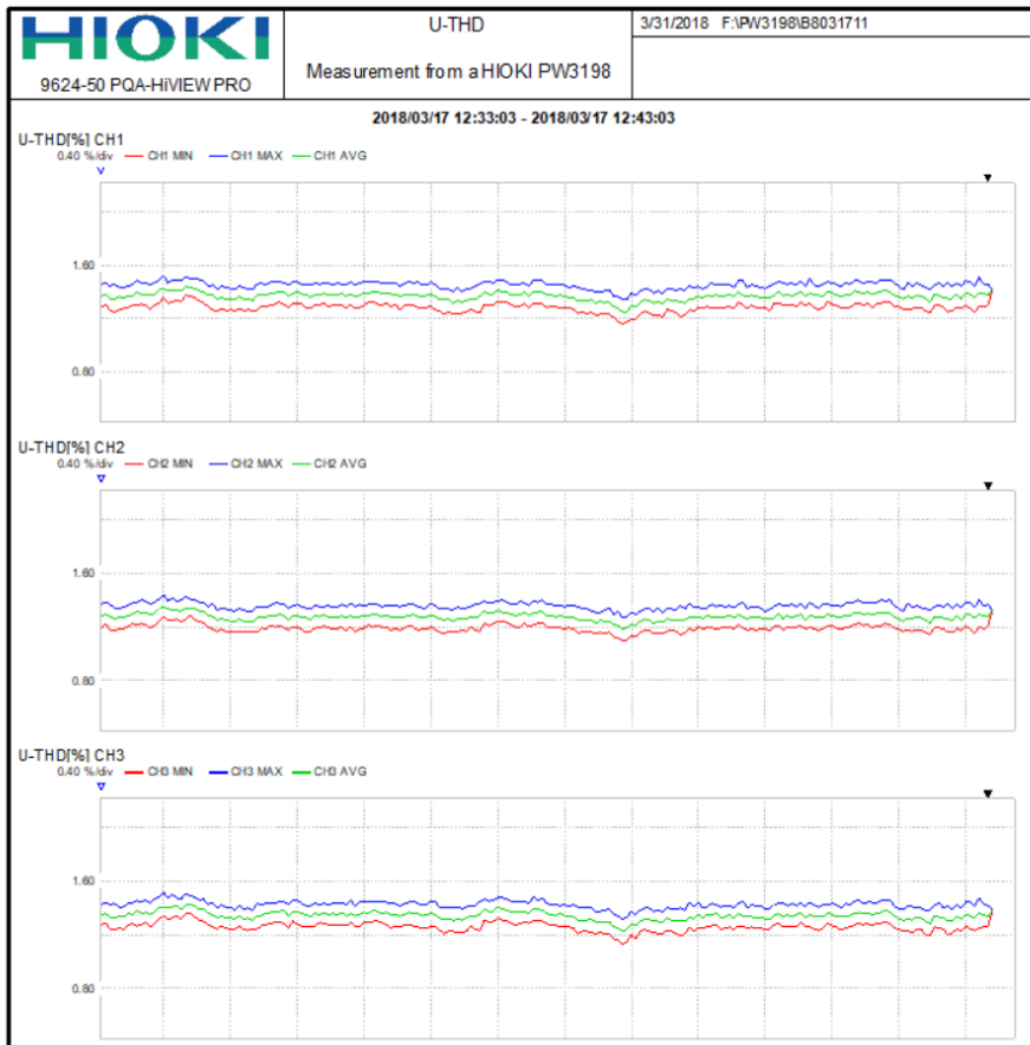


Figure 6. 27. THD values of line to line voltages, V_{AB} , V_{BC} , V_{CA} for 10 minutes of record

THD values of line currents, i_A , i_B , i_C were recorded while all SiC MOSFET based voltage source three phase PWM rectifier was loaded at 54.6kVA of power for 10 minutes of duration. Recorded data was plotted using HIOKI 9624-50 PQA software as in Figure 6. 28.



Figure 6. 28. THD values of line currents, i_A , i_B , i_C for 10 minutes of record

Finally, grid frequency was recorded while all SiC MOSFET based voltage source three phase PWM rectifier was loaded at 122.5kVA of power for 10 minutes of duration. Recorded data was plotted using HIOKI 9624-50 PQA software as in Figure 6. 29.

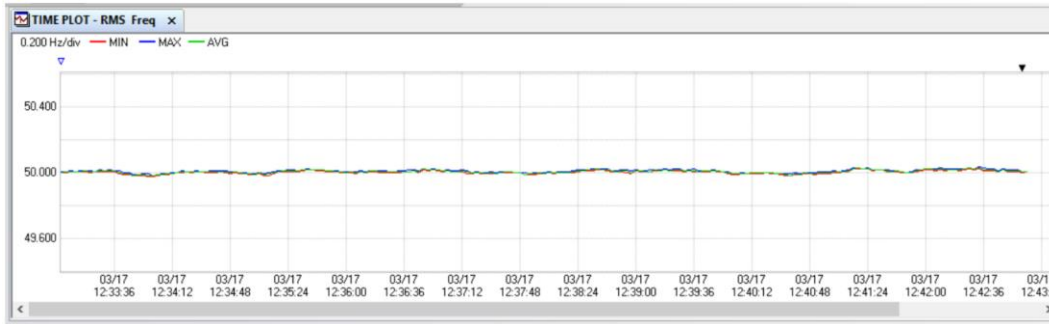


Figure 6. 29. Grid frequency variation for 10 minutes of record

At 112kVA of load test, THD values of V_{AB} , V_{BC} , V_{CA} were measured as 1.35 %, 1.22 % and 1.34 % respectively according to Figure 6. 12. Fifth harmonic was seen as most dominant order which is 0.99 % according to Figure 6. 9. Seventh and third harmonic were come after fifth harmonic which are 0.64 % and 0.37 %. THD values of i_A , i_B , i_C were measured as 4.80 %, 3.86 % and 5.88 % respectively according to Figure 6. 13. Fifth harmonic was seen as most dominant order which is 3.42 % according to Figure 6. 10. Third and second harmonic were come after fifth harmonic which are 3.26 % and 1.18 %.

At 54.6kVA of load test, THD values of V_{AB} , V_{BC} , V_{CA} were measured as 1.46 %, 1.36 % and 1.45 % respectively according to Figure 6. 23. Fifth harmonic was seen as most dominant order which is 1.02 % according to Figure 6. 20. Seventh and third harmonic were come after fifth harmonic which are 0.66 % and 0.41 %. THD values of i_A , i_B , i_C were measured as 8.84 %, 8.25 % and 10.82 % respectively according to Figure 6. 24. Fifth harmonic was seen as most dominant order which is 8.41 % according to Figure 6. 21. Third, seventh and second harmonic were come after fifth harmonic which are 3.26 %, 1.56 % and 1.29 %.

Results show voltage unbalance is present in grid because there is a second order harmonic having a considerably high percentage of THD in line current. To be able to decide whether THD values of line to line voltages, THD values of line currents and percentage of each harmonic are allowable or not, IEEE 519-2014 standard which is called as IEEE Recommended Practice and Requirements for Harmonic Control in

Electric Power Systems are used. Figure 6. 30 shows admissible value of percentage of each harmonic and admissible value of THD for line to neutral grid voltage. For 230V of line to neutral grid voltage, 5 % and 8 % are acceptable for percentage of each harmonic and percentage of THD respectively.

Bus voltage V at PCC	Individual harmonic (%)	Total harmonic distortion THD (%)
$V \leq 1.0$ kV	5.0	8.0
1 kV $< V \leq 69$ kV	3.0	5.0
69 kV $< V \leq 161$ kV	1.5	2.5
161 kV $< V$	1.0	1.5 ^a

^aHigh-voltage systems can have up to 2.0% THD where the cause is an HVDC terminal whose effects will have attenuated at points in the network where future users may be connected.

Figure 6. 30. Admissible value of percentage of each harmonic and admissible value of THD for line to neutral grid voltage

Above limitations were satisfied at both 54.6kVA of load test and 112kVA of load test. On the other hand, Figure 6. 31 indicates regulations for Total Demand Distortion (TDD) and each harmonic order. Since ratio of maximum short circuit current, I_{sc} to maximum demand load current, I_L is less than 20 at both load tests of all SiC MOSFET based voltage source three phase PWM rectifier, third, fifth and seventh order harmonics of line current should be less than or equal to 4 %.

Maximum harmonic current distortion in percent of I_L						
Individual harmonic order (odd harmonics) ^{a, b}						
I_{sc}/I_L	$3 \leq h < 11$	$11 \leq h < 17$	$17 \leq h < 23$	$23 \leq h < 35$	$35 \leq h \leq 50$	TDD
$< 20^c$	4.0	2.0	1.5	0.6	0.3	5.0
$20 < 50$	7.0	3.5	2.5	1.0	0.5	8.0
$50 < 100$	10.0	4.5	4.0	1.5	0.7	12.0
$100 < 1000$	12.0	5.5	5.0	2.0	1.0	15.0
> 1000	15.0	7.0	6.0	2.5	1.4	20.0

^aEven harmonics are limited to 25% of the odd harmonic limits above.

^bCurrent distortions that result in a dc offset, e.g., half-wave converters, are not allowed.

^cAll power generation equipment is limited to these values of current distortion, regardless of actual I_{sc}/I_L .

where

I_{sc} = maximum short-circuit current at PCC

I_L = maximum demand load current (fundamental frequency component)
at the PCC under normal load operating conditions

Figure 6. 31. Regulations for Total Demand Distortion (TDD) and each harmonic order

Third and fifth harmonic contents of line current for 112kVA of load test which are 3.42 % and 3.26 % were fulfilled the allowable value. At the same time, third harmonic content of line current for 54.6kVA of load test satisfied the admissible value. However, fifth harmonic content of line current for 54.6kVA of load test which is 8.41 % passed acceptable value which is 4 %. These results imply that distortion in line current is more at lower values of line current. For this reason, lowest THD value and harmonic content are obtained at rated load test.

CHAPTER 7

SIMULATIONS

In this chapter, simulation studies made for designed all SiC MOSFET based three phase voltage source PWM rectifier were mentioned. Built simulation models such as whole power circuitry, phase lock loop implementation, outer voltage control loop, inner current control loop and SVPWM implementation and related simulation results were shared in order to be explain the theory more clearly. Power circuitry and control blocks were given separately to be able to see the figures better. All simulations were made in MATLAB/Simulink simulation environment. 2016b version of MATLAB was used. On-state resistance value of selected SiC MOSFET module, forward voltage value of SiC diode and internal resistance value of SiC diode were directly used as switch parameters in Simulink in order to be able make simulation study as near as real one. At the same time, inductance and series DC resistance values of selected single phase AC line reactor were used in the power circuitry. Moreover, capacitance, ESR and ESL values of selected DC-Link capacitor were used in the series RLC branch built in Simulink. Figure 7. 1 shows power circuitry model of all SiC MOSFET based three phase voltage source PWM rectifier built in Simulink. Line to line grid voltages, line to neutral grid voltage, line currents, DC-Link current and DC-Link voltage were measured using Simulink scopes.

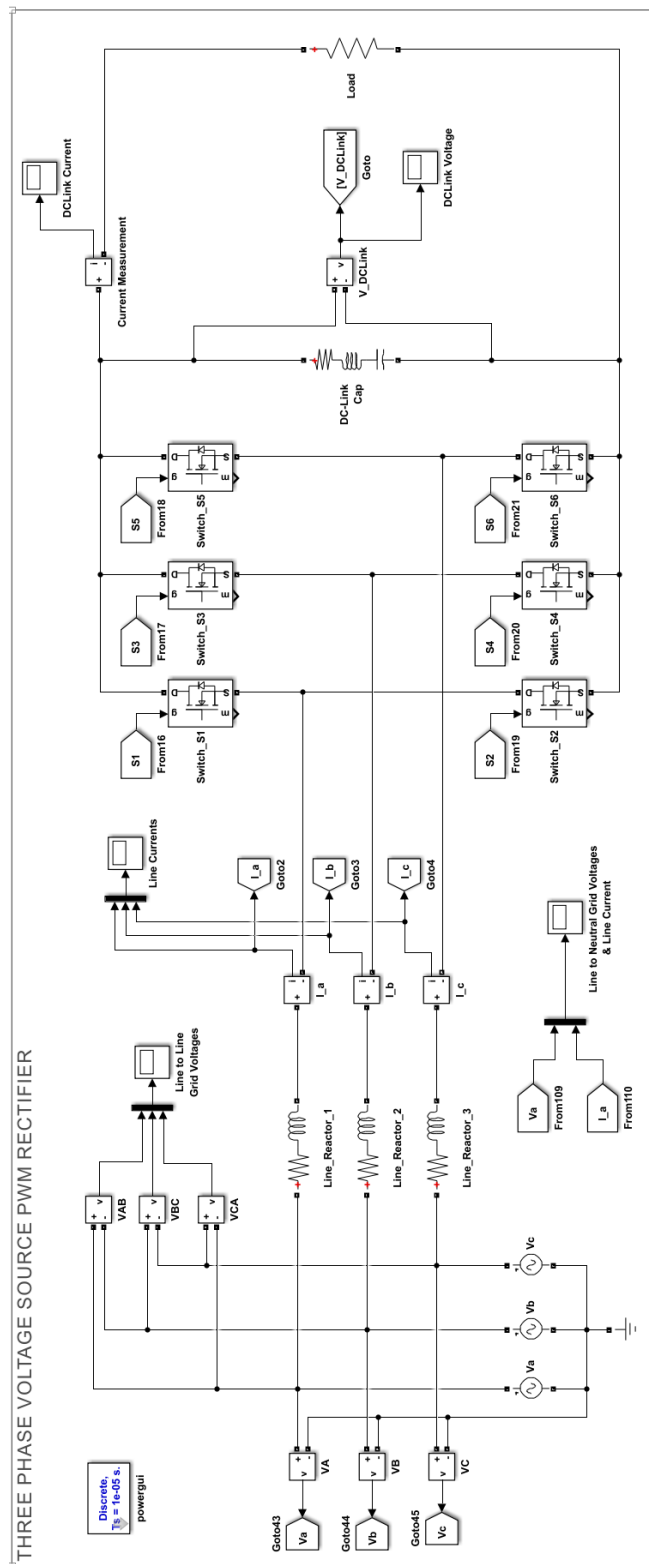


Figure 7. 1. Three phase voltage source PWM rectifier model build in Simulink

Besides, Figure 7. 2 shows implementation of PLL algorithm in MATLAB/Simulink. Clarke and Park transformation blocks and related control schema were seen clearly. Ready transformation blocks present in Simulink were not used for Clarke and Park transformation. These transformation blocks were formed using math operations given in the Simulink library.

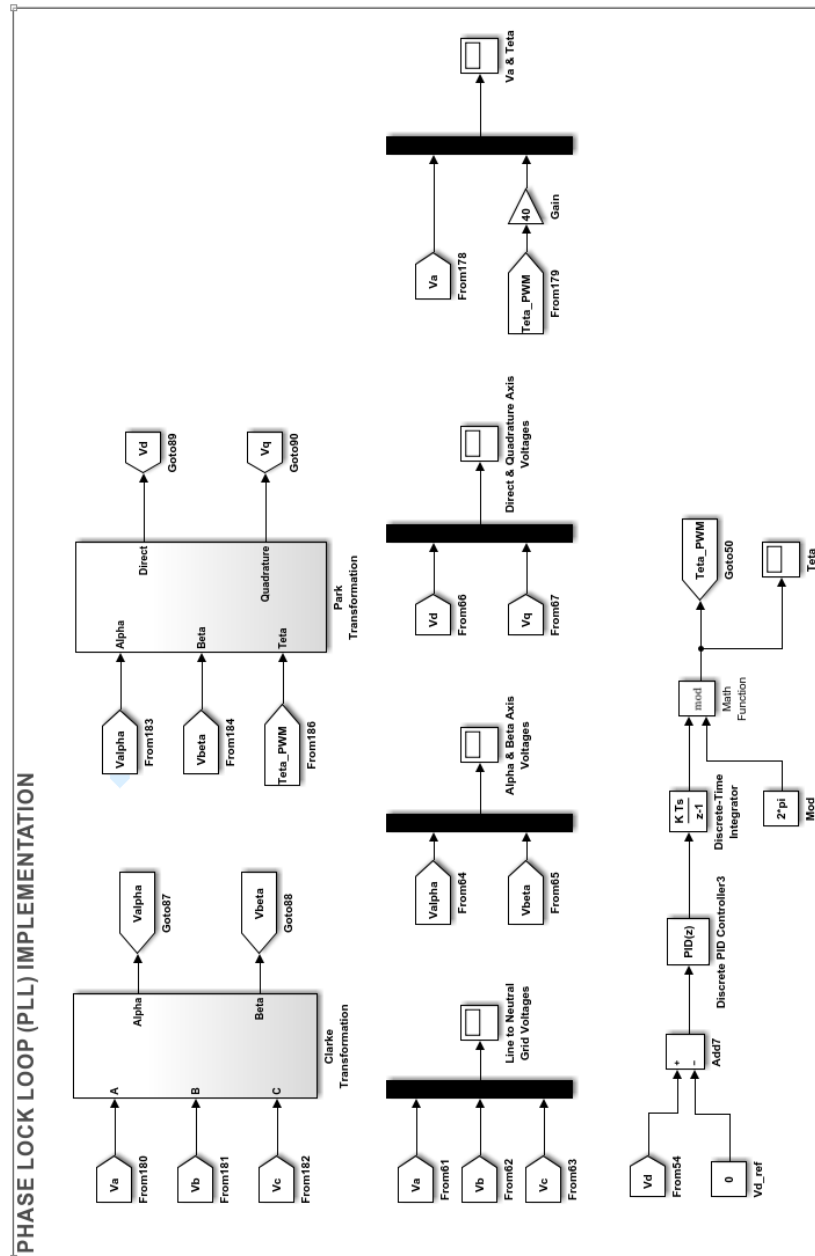


Figure 7. 2. Three phase PLL model built in Simulink

Figure 7. 3 shows line to neutral grid voltages shifted 120 degrees according to each other.

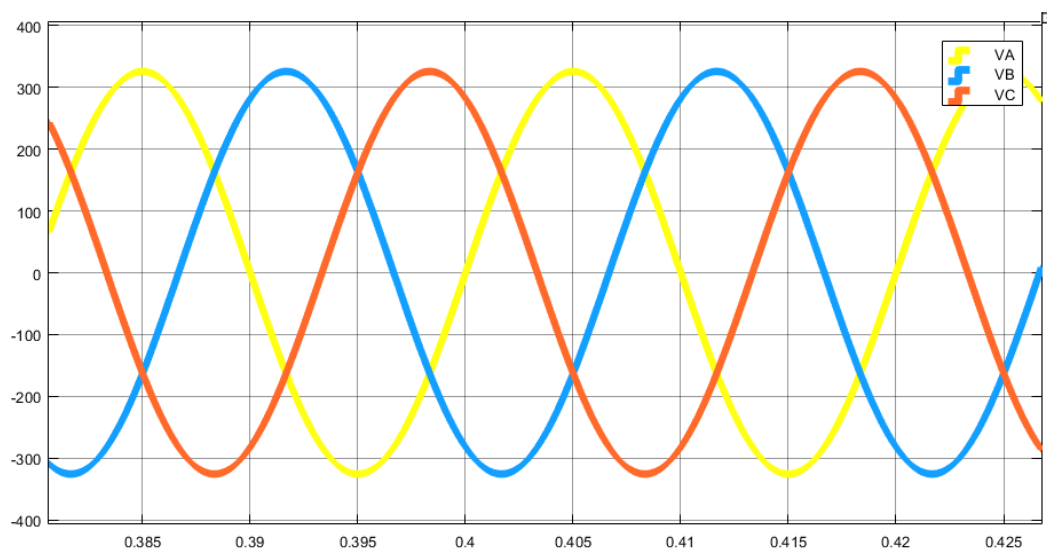


Figure 7. 3. Line to neutral voltages, V_A , V_B , V_C

Figure 7. 4 shows alpha & beta axis voltages formed as a result of Clarke transformation. Alpha & beta axis voltages are perpendicular to each other as seen in the Figure 7. 4. Yellow one shows alpha axis voltage, on the other hand blue one stands for beta axis voltage.

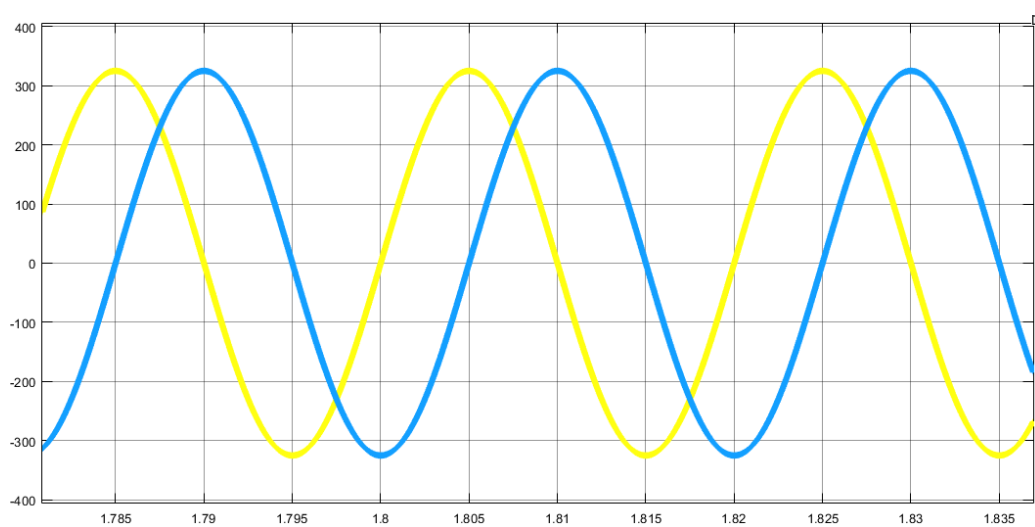


Figure 7. 4. Alpha & beta axis voltages

Figure 7. 5 shows direct & quadrature axis voltages formed as a result of Park transformation. Direct & quadrature axis voltages are DC values and also perpendicular to each other as seen in the Figure 7. 5. Yellow one shows direct axis voltage, on the other hand blue one stands for quadrature axis voltage.

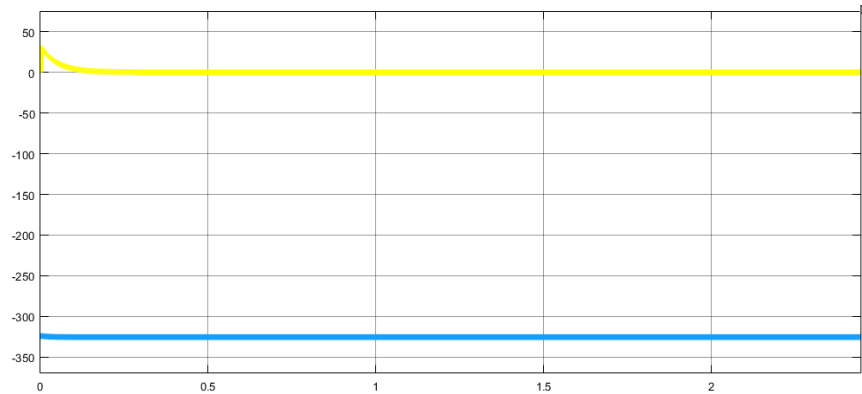


Figure 7. 5. Direct & quadrature axis voltages

Figure 7. 6 shows theta generated in PLL. First of all, direct axis voltage was subtracted from zero. Then, error was given as input to the PI controller. Output of PI controller was formed to w . Afterwards, theta was generated by taking the integral of w . However, this theta goes to infinity. For this reason, mod operation was made according to two pi. This theta resembles the ramp signal going from zero to two pi within the one period ($1/50\text{Hz} = 20\text{ms}$) as seen in the Figure 7. 6.

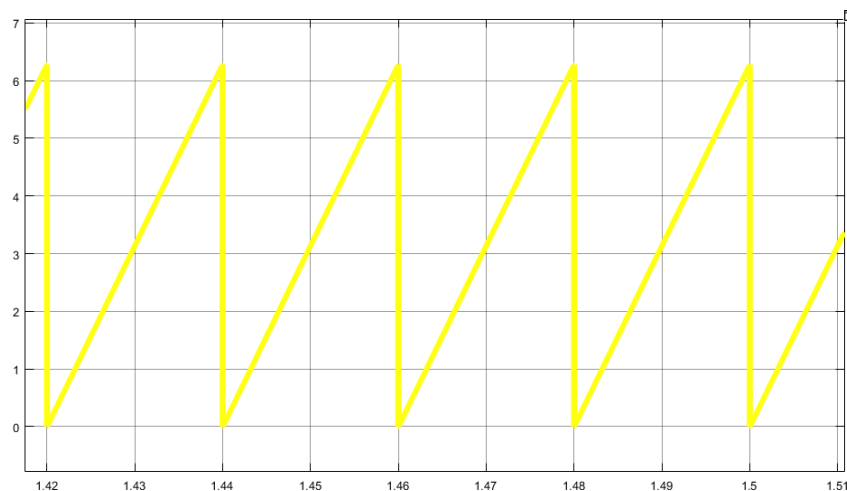


Figure 7. 6. Theta generated in PLL

Below, it is seen the line to neutral grid voltage, V_A and theta in a single figure. In order to be able to see line to neutral grid voltage, V_A and theta in a single figure, theta was multiplied with gain as shown in Figure 7. 2. It is expected that line to neutral grid voltage, V_A and theta should be synchronized in each period in successful PLL algorithm.

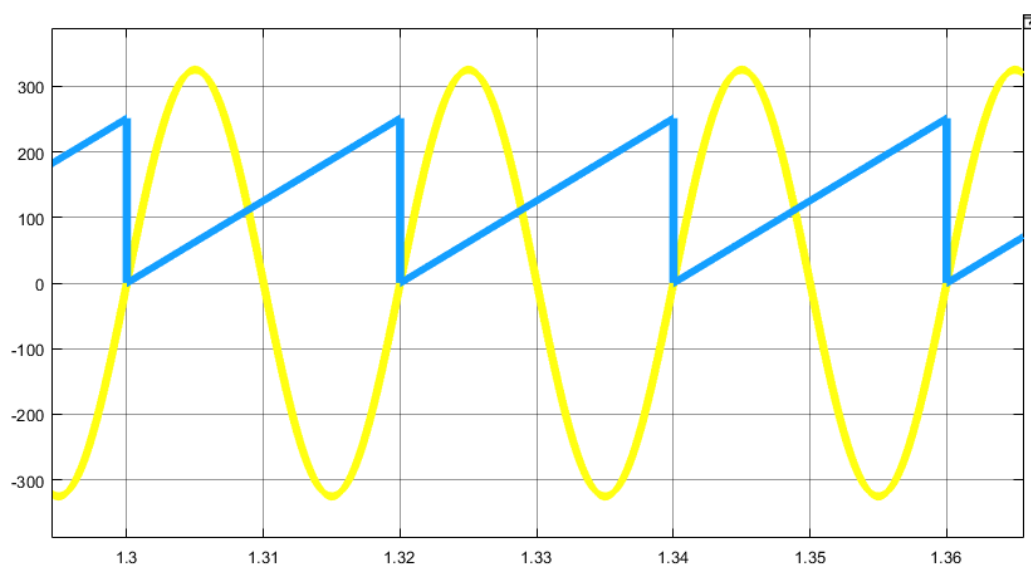


Figure 7. 7. Line to neutral voltage, V_A and theta

Figure 7. 8 shows the Simulink model belonging to outer voltage control loop and inner current control loop. In outer voltage control loop, DC-Link voltage reference which is 750 VDC was subtracted from measured DC-Link voltage. Result of the subtraction which is error was considered as input for the PI controller of outer voltage control loop. Output of PI controller was formed to the per unit reference quadrature axis current, $i_{q, \text{ref}, \text{pu}}$. In inner current control loop, line currents were converted to the per unit forms. Then, per unit line currents were converted to the per unit alpha & beta axis currents which are $i_{\alpha, \text{pu}}$ and $i_{\beta, \text{pu}}$ using Clarke transformation block. Later on, per unit alpha & beta axis currents were converted to per unit direct & quadrature axis currents which are $i_{d, \text{pu}}$ and $i_{q, \text{pu}}$ using Park transformation block. Afterwards, per unit reference quadrature axis current, $i_{q, \text{ref}, \text{pu}}$ formed in outer voltage control loop was subtracted from per unit quadrature axis

current, $i_{q, pu}$ formed in inner current control. Resulting error was passed from PI controller and then created per unit quadrature axis voltage, $V_{q, pu}$. At the same time, per unit reference direct axis current, $i_{d, ref, pu}$ which is zero was subtracted from per unit direct axis current, $i_{d, pu}$ formed in inner current control. Resulting error was passed from PI controller and then created per unit direct axis voltage, $V_{d, pu}$. These per unit quadrature & direct axis voltage which are $V_{q, pu}$ and $V_{d, pu}$ were converted to the per unit alpha & beta voltages which are $V_{\alpha, pu}$ and $V_{\beta, pu}$ by using Inverse Park transformation. Theta generated in PLL model was used in both Park transformation and Inverse Park Transformation. Parameters of PI controllers used in outer voltage control loop and inner current control loop should be optimized properly for good dynamic response at transients and good static response at steady state.

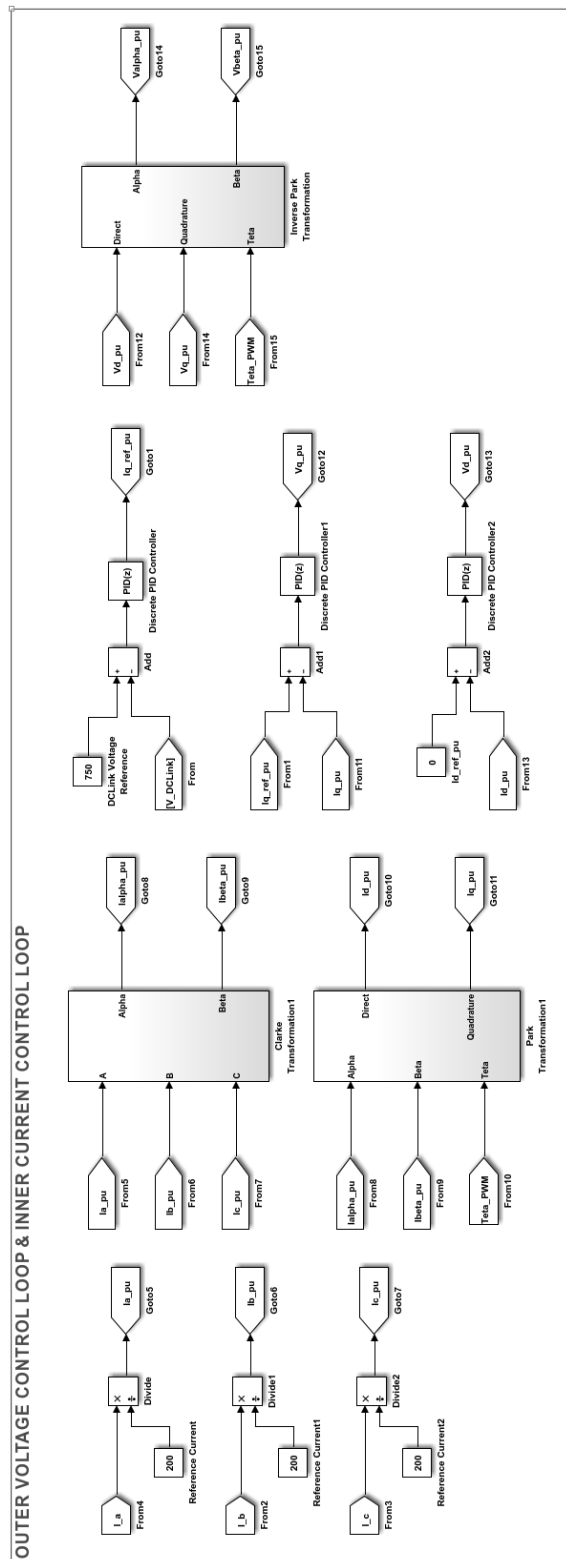


Figure 7. 8. Outer voltage control loop and inner current control loop models built in Simulink

Figure 7. 9 shows the sector selection model used in SVPWM implementation. A space voltage vector comprising vectorial sum of per unit alpha & beta axis voltages which are $V_{\alpha, pu}$ and $V_{\beta, pu}$ coming as a result of inner current control loop was formed. Later on, magnitude and angle of this space voltage vector were calculated. Afterwards, using its angle value, it was determined in which sector space vector exists.

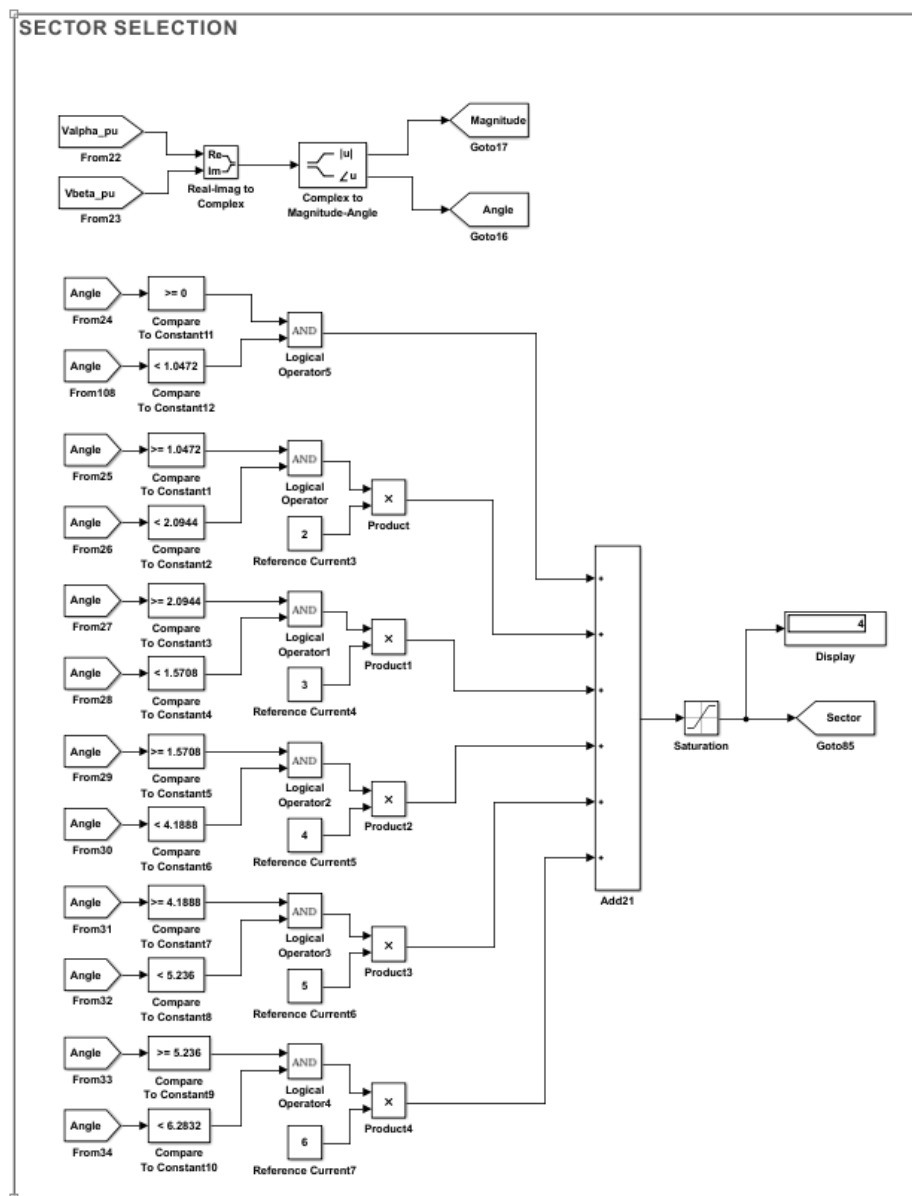


Figure 7. 9. Sector selection model built in Simulink for SVPWM

If space voltage vector is in Sector 1, Simulink model shown in Figure 7. 10 was used for SVPWM implementation. Blocks calculating the turn-on time of each vectors which are t_1 , t_2 , t_0 were determined using the formulas given in (5.5), (5.6, (5.7). Finally, switching states of each switches which are S_1, \dots, S_6 were determined by using two adjacent active vectors and turn-on times as shown in Figure 7. 10.

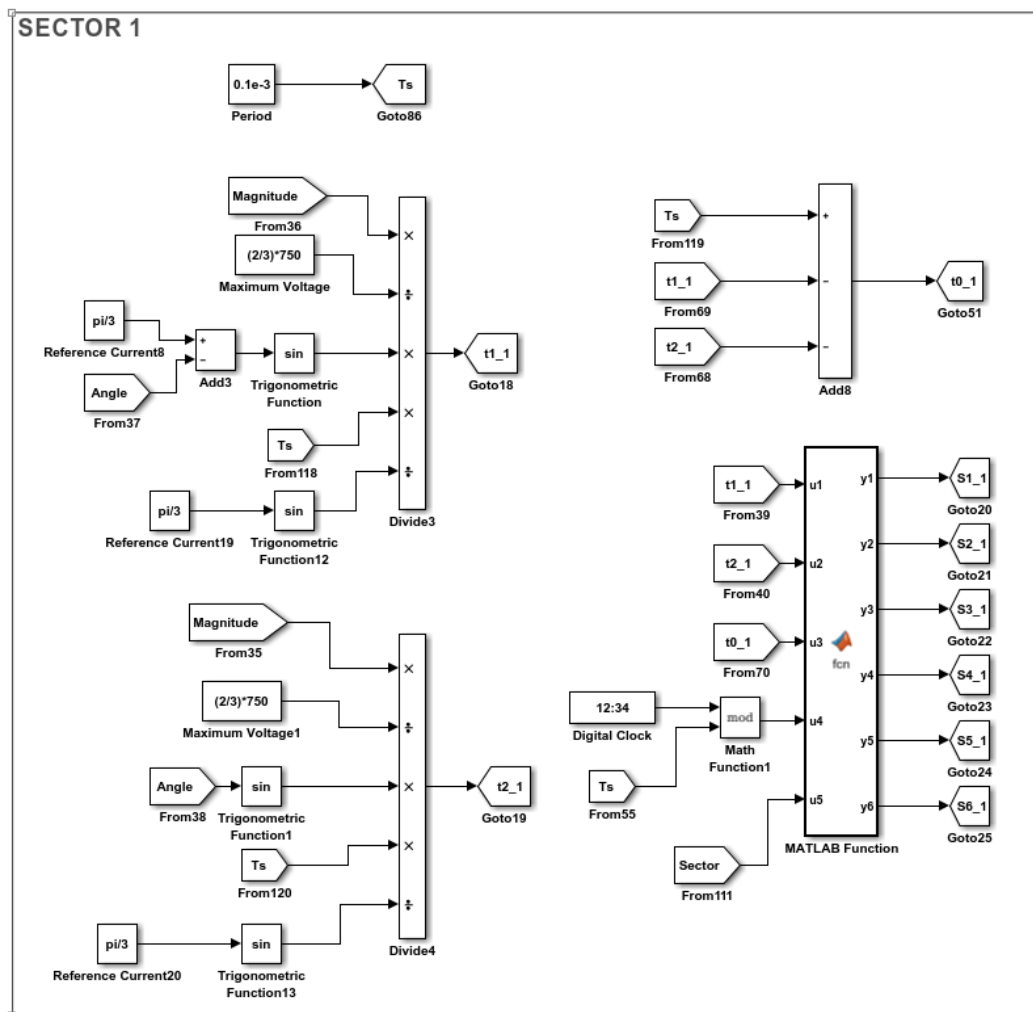


Figure 7. 10. Switching states of active vectors and zero vectors if reference vector is in Sector 1

If space voltage vector is in Sector 2, Simulink model shown in Figure 7. 11 was used for SVPWM implementation. Blocks calculating the turn-on time of each vectors which are t_1 , t_2 , t_0 were determined using the formulas given in (5.5), (5.6), (5.7). Finally, switching states of each switches which are S_1, \dots, S_6 were determined by using two adjacent active vectors and turn-on times as shown in Figure 7. 11.

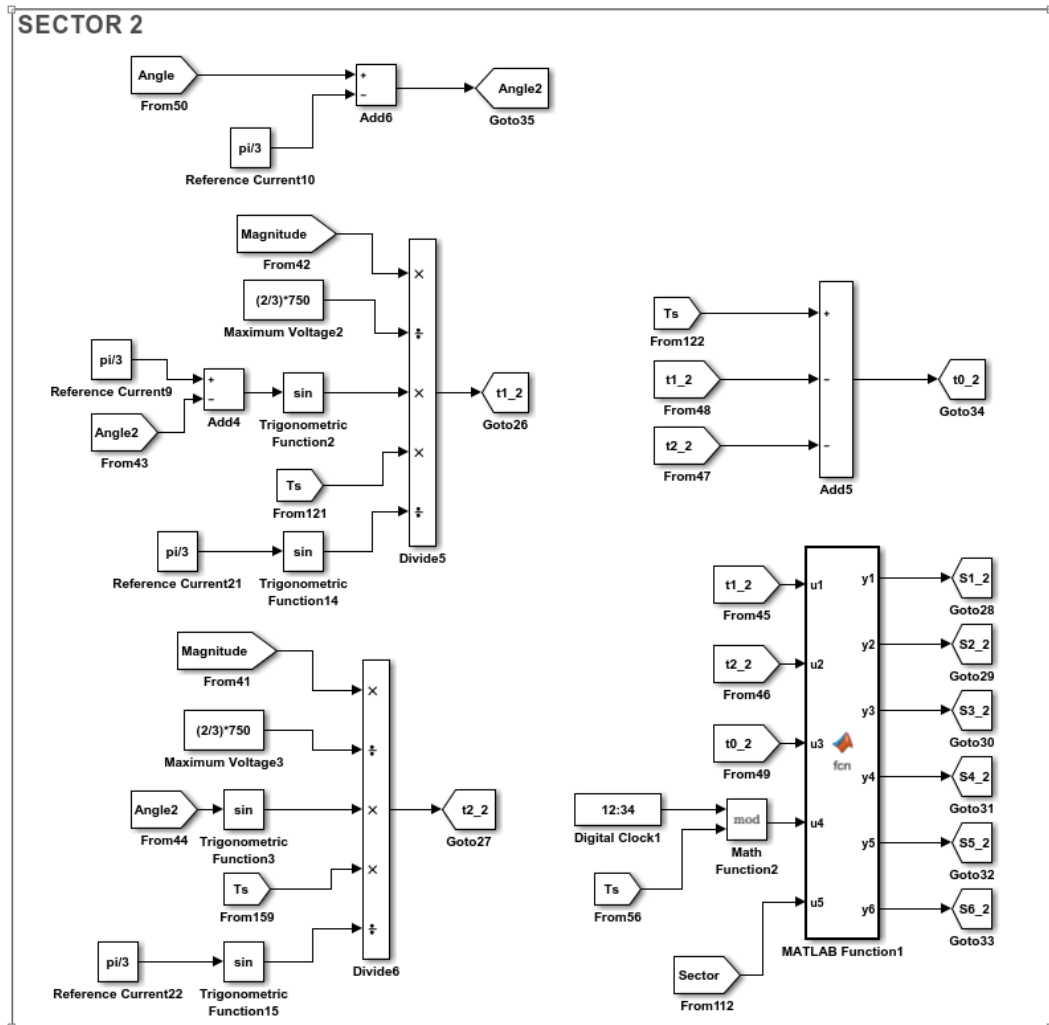


Figure 7. 11. Switching states of active vectors and zero vectors if reference vector is in Sector 2

If space voltage vector is in Sector 3, Simulink model shown in Figure 7. 12 was used for SVPWM implementation. Blocks calculating the turn-on time of each vectors which are t_1 , t_2 , t_0 were determined using the formulas given in (5.5), (5.6), (5.7). Finally, switching states of each switches which are S_1, \dots, S_6 were determined by using two adjacent active vectors and turn-on times as shown in Figure 7. 12.

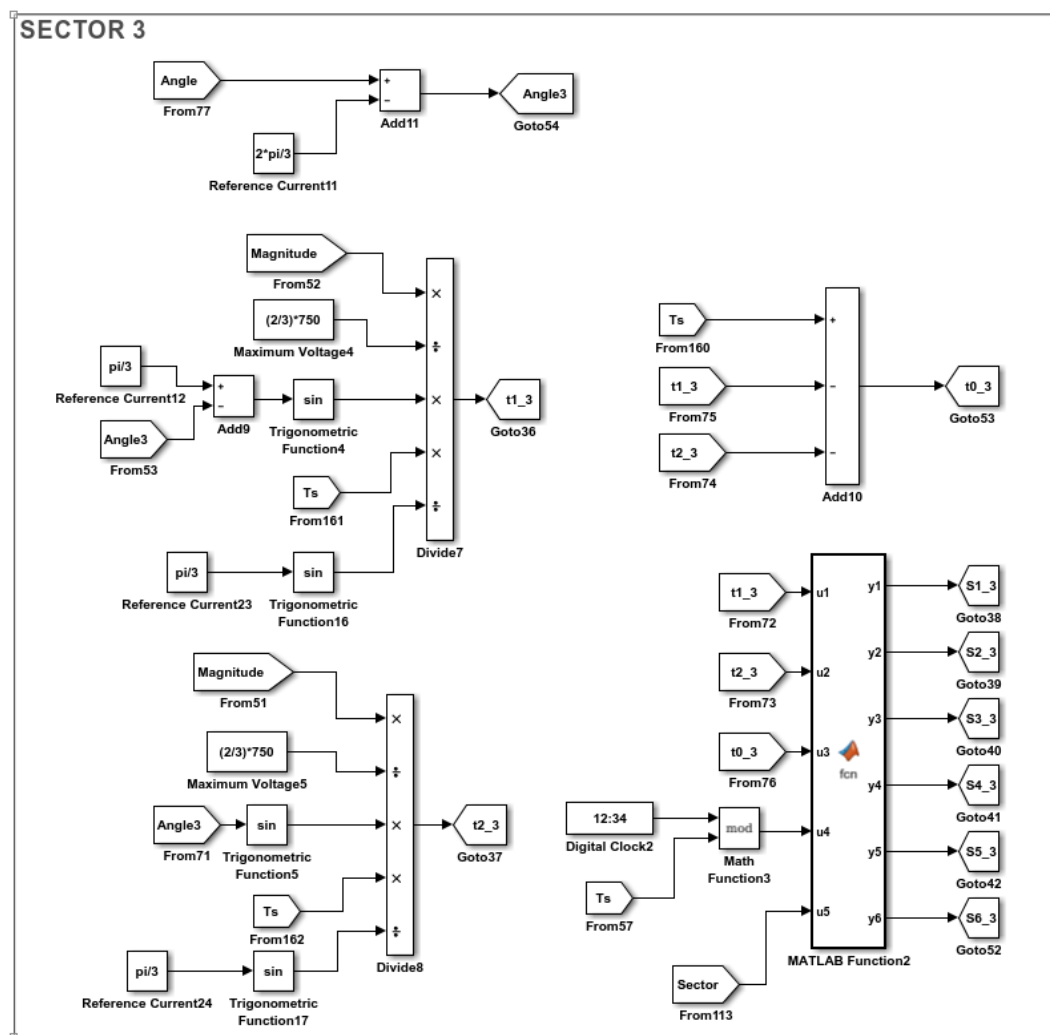


Figure 7. 12. Switching states of active vectors and zero vectors if reference vector is in Sector 3

If space voltage vector is in Sector 4, Simulink model shown in Figure 7. 13 was used for SVPWM implementation. Blocks calculating the turn-on time of each vectors which are t_1 , t_2 , t_0 were determined using the formulas given in (5.5), (5.6), (5.7). Finally, switching states of each switches which are S_1, \dots, S_6 were determined by using two adjacent active vectors and turn-on times as shown in Figure 7. 13.

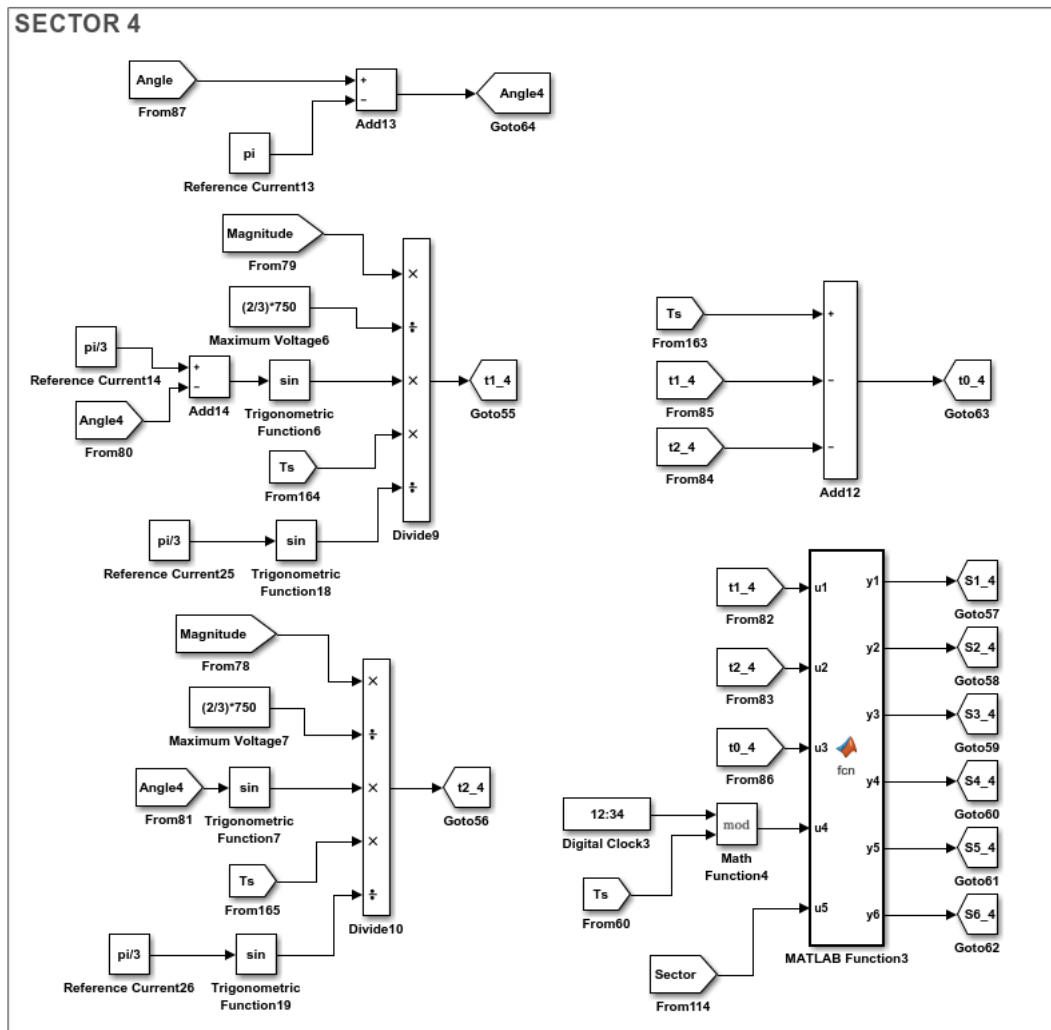


Figure 7. 13. Switching states of active vectors and zero vectors if reference vector is in Sector 4

If space voltage vector is in Sector 5, Simulink model shown in Figure 7. 14 was used for SVPWM implementation. Blocks calculating the turn-on time of each vectors which are t_1 , t_2 , t_0 were determined using the formulas given in (5.5), (5.6), (5.7). Finally, switching states of each switches which are S_1, \dots, S_6 were determined by using two adjacent active vectors and turn-on times as shown in Figure 7. 14.

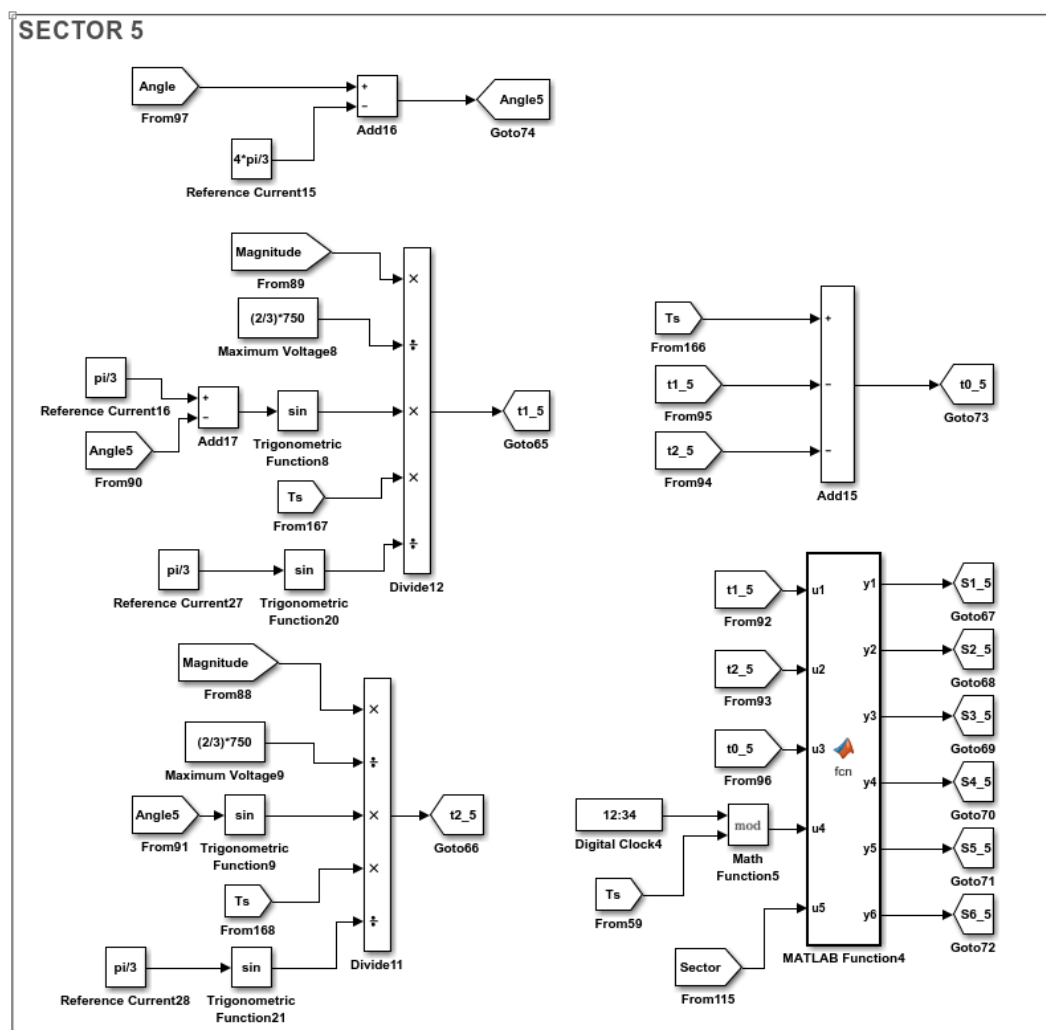


Figure 7. 14. Switching states of active vectors and zero vectors if reference vector is in Sector 5

If space voltage vector is in Sector 6, Simulink model shown in Figure 7. 15 was used for SVPWM implementation. Blocks calculating the turn-on time of each vectors which are t_1 , t_2 , t_0 were determined using the formulas given in (5.5), (5.6), (5.7). Finally, switching states of each switches which are S_1, \dots, S_6 were determined by using two adjacent active vectors and turn-on times as shown in Figure 7. 15.

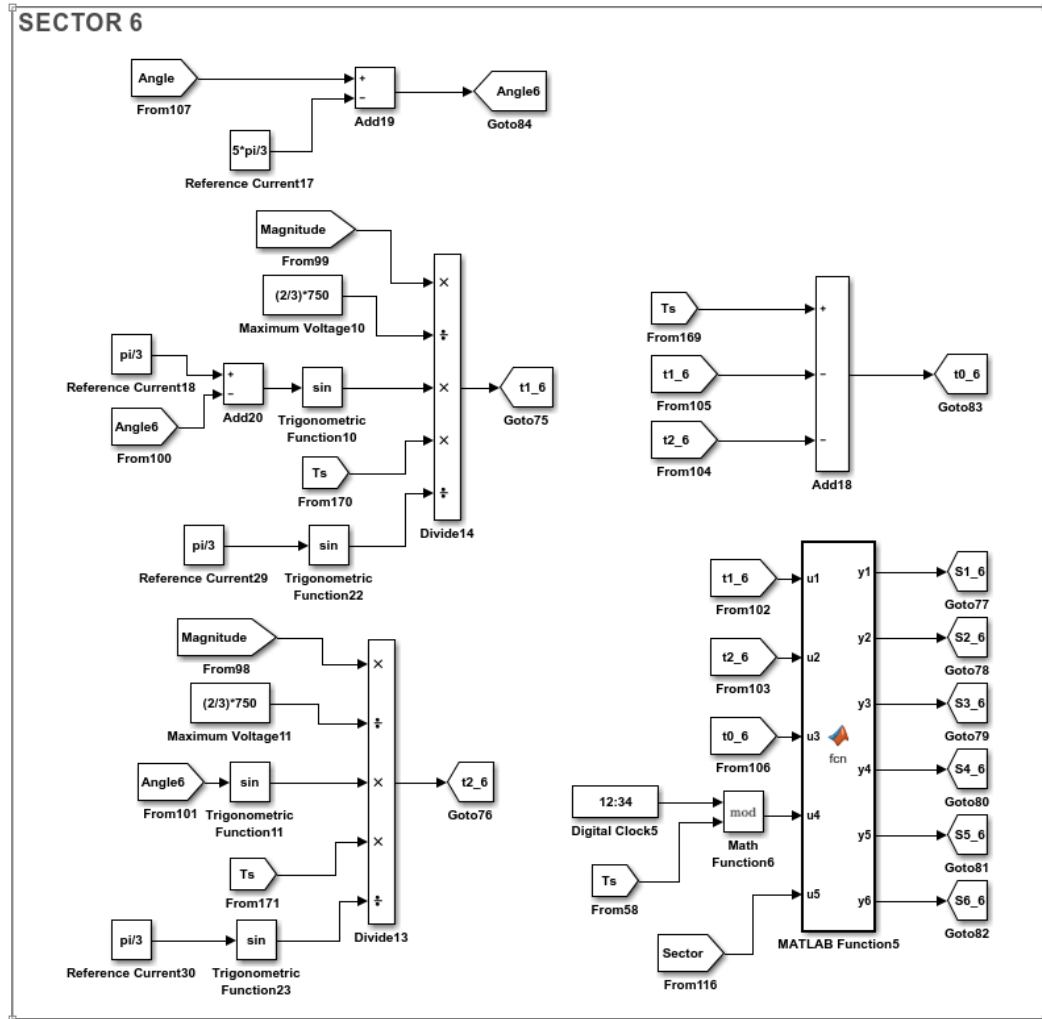


Figure 7. 15. Switching states of active vectors and zero vectors if reference vector is in Sector 6

CHAPTER 8

CONCLUSION AND FUTURE WORK

According to IEEE 519-2014 standard, grid connected converters have to satisfied both allowed THD value of line currents and also admissible percentage value of each harmonic compared to fundamental. Besides, it is expected that grid connected converters have properties of bidirectional power flow, unity power factor, pure sinusoidal line current and regulated output voltage in today's technology. Distorted line current comprises in line commutated rectifiers such as three phase diode bridge rectifier and three phase thyristor bridge rectifier which leads to significantly high harmonic content and consequently high THD value. Furthermore, line to neutral grid voltage which is in phase with line current, output voltage regulation and also power transfer to grid cannot be provided using these converters. Regenerative type PFC rectifiers such as single phase voltage source PWM rectifier and three phase voltage source PWM rectifier are used in the industry to satisfy properties above instead of line commutated rectifiers. Design of 130kVA of all SiC MOSFET based voltage source three phase PWM rectifier supplied from 400V, 50Hz grid was proposed in this thesis study. It was aimed to be used designed three phase voltage source rectifier in traction applications, battery charging applications and also wind turbine applications. Designed rectifier simulates 750VDC of catenary line. By this means, it is able to be used for supplying three phase traction inverter. Moreover, designed rectifier can be used together with bidirectional buck-boost converter for charging and discharging of a battery or a supercapacitor in rectification and inversion mode respectively. Likewise, it can be used in AC/DC side of a back to back converters especially in wind turbine applications. Besides, usage of SiC MOSFET as a power semiconductor switching device may be seen as innovative side of this thesis study. SiC MOSFET has superior properties compared to Si IGBT in terms of dielectric breakdown field, bandgap, doping concentration, drift velocity and thermal

conductivity. SiC MOSFET has lower on-state resistance, $R_{DS, ON}$ than Si IGBT and can be operate at higher switching frequencies than Si IGBT due to above properties. Furthermore, SiC MOSFET has no tail current and reverse recovery current which results in very small turn-off energy, E_{off} and zero reverse recovery energy. For this reason, SiC MOSFET has significantly smaller switching losses than Si IGBT. In this thesis study, SiC MOSFET was preferred instead of Si IGBT due to advantages mentioned above. Size and weight of passive components such as reactor and capacitor, and also size and weight of heatsink was able to reduced dramatically by switching at 10kHz thanks to SiC MOSFET. Efficiency and power density of designed rectifier were provided by reducing power losses and size of both passive components and cooling unit. Moreover, VOC and SVPWM was proposed as a control method and modulation technique respectively. VOC method was compared with DPC method in the scope of this thesis. Switching frequency should be constant to be able to select a suitable boost reactor, L_b easily. Since switching frequency is changing in DPC method, design gets hard. Besides, dynamic response of the system at transients and static response of the system at steady state are better in VOC method than in DPC method if it applied successfully. For this reason, VOC method was chosen as a control method. Regarding to modulation technique, SVPWM was contrasted with SPWM. Since number of switching is decreased in SVPWM, switching losses are less in SVPWM compared to SPWM. Moreover, better THD performance and unity power factor can be get in SVPWM because harmonics are able to be reduced significantly. One of the most important differences between SVPWM and SPWM is that better DC bus utilization is ensured via SPWM which results in more output voltages. Therefore, SVPWM was preferred as modulation technique in this thesis study. In other respects, designed rectifier panel was tested at full load and half load conditions by using three phase traction inverter as an active load. Bidirectional power transfer capability of designed rectifier, unity power factor operation, pure sinusoidal line current and 750VDC of regulated output voltage was proven via presented oscilloscope waveforms. Finally, it is proven to be satisfied regulations stated in IEEE 519-2014 standard with designed rectifier by presenting power quality analyzer measurements

such as THD value of line to neutral grid voltage, THD value of line currents and percentage values of each harmonic compared to fundamental. The following are considered for the future works.

- ✓ Design of liquid cooled all SiC MOSFET based three phase voltage source PWM rectifier can be considered.
- ✓ Heatsink can be changed with smaller one. Since a ready heatsink was bought, completely optimized heatsink in terms of size and volume could not found. Custom design can be made for increasing power density further.
- ✓ Switching frequency can be enhanced to 20kHz. In this way, size and weight of passive components such as boost reactor and DC-Link capacitor can be reduced further.
- ✓ Three phase three level voltage source PWM rectifier topology can be tried instead of two level topology. Since lower voltage switches can be used under favour of three level topology, Gallium Nitride (GaN) MOSFET can be considered instead of SiC MOSFET.
- ✓ Designed rectifier can be tested using bidirectional buck-boost converter instead of three phase traction inverter as a load. By this means, it may be proven that designed rectifier is also suitable for battery charging applications.
- ✓ Virtual Flux Oriented Control (VFOC) and Virtual Flux Based Direct Power Control (VFDPC) can be investigated and applied instead of VOC and DPC methods.
- ✓ If SiC MOSFETs having 3300V of drain-source voltage become widespread, all SiC MOSFET based voltage source three phase PWM rectifier having 1500VDC of regulated output voltage can be designed by using these switches for 1500VDC of catenary line applications.

By the way, the aim of this thesis study was to reveal a three phase voltage source PWM rectifier design using latest SiC MOSFET technology and use this design in traction application, battery charging & discharging applications. It was achieved this goal at the end of this thesis study. Designed all SiC MOSFET based three phase

voltage source PWM rectifier simulating the 750VDC of catenary line was used together with traction inverter and traction motor. At the same time, this converter was operated together with buck & boost converter for battery charging & discharging applications. Finally, this thesis study made a big contribution to me by increasing my knowledge in the fields of power converter design, control and algorithm development.

REFERENCES

- [1] Rodriguez, J. R., Dixon, J. W., Espinoza, J. R., Pontt, J., & Lezana, P. (2005). PWM Regenerative Rectifiers: State of The Art. *IEEE Transactions on Industrial Electronics*, 52(1), 5–22.
- [2] IEEE Std 519-2014: IEEE Recommended Practice and Requirements for Harmonic Control in Electric Power Systems, 2014.
- [3] Grman, L., Hrasko, M., Kuchta, J., & Buday, J. (2011). Single Phase PWM Rectifier in Traction Application. *Journal of Electrical Engineering*, 62(4), 206–212.
- [4] Li, X., He, Z., Wang, C., & Huang, H. (2013). The Application of Three-Phase PWM Rectifier in Battery Formation System. In *Proceedings 2013 International Conference on Mechatronic Sciences, Electric Engineering and Computer (MEC)*. Shengyang, China.
- [5] Buchert, K., & Fuchs, F. W. (2014). Comparison of Three Phase Rectifier Topologies in Small Wind Turbines. In *16th European Conference on Power Electronics and Applications*. Lappeenranta, Finland.
- [6] Trinadh, M., & Narsimha, R. (2015). Comparative Loss Evaluation of Si IGBT Versus Sic Mosfet (Silicon Carbide) for 3 Phase Spwm Inverter. *Indian Journal of Science and Technology*, 8(28).
- [7] Hosseini Aghdam, M. G., & Thiringer, T. (2009). Comparison of SiC and Si Power Semiconductor Devices To Be Used in 2.5 kW DC/DC Converter. In *2009 International Conference on Power Electronics and Drive Systems (PEDS)*. Taipei, Taiwan.
- [8] Biela, J., Schweizer, M., Waffler, S., & Kolar, J. W. (2010). SiC versus Si—Evaluation of Potentials for Performance Improvement of Inverter and DC–DC Converter Systems by SiC Power Semiconductors. *IEEE Transactions on Industrial Electronics*, 58(7), 2872–2882.

- [9] Sun, J., Xu, H., Wu, X., & Sheng, K. (2016). Comparison and Analysis of Short Circuit Capability of 1200V Single-Chip SiC MOSFET and Si IGBT. In 2016 13th China International Forum on Solid State Lighting: International Forum on Wide Bandgap Semiconductors China (SSLChina: IFWS). Beijing, China.
- [10] Infineon IGBT Power Losses Calculation Application Note, <https://tr.scribd.com/document/34307806/IGBT-Power-Losses-Calculation-Using-the-Data-Sheet-Parameters>, Last Access: 2019-01-01
- [11] Infineon MOSFET Power Losses Calculation Application Note, <https://tr.scribd.com/document/34308439/MOSFET-Power-Losses-Calculation-Using-the-Data-Sheet-Parameters>, Last Access: 2019-01-01
- [12] CREE CAS300M17BM2 SiC MOSFET Half Bridge Module Datasheet, <https://www.wolfspeed.com/downloads/dl/file/id/185/product/102/cas300m17bm2.pdf>, Last Access: 2019-01-01
- [13] Infineon FF225R17ME4_B11 Si IGBT Half Bridge Module Datasheet, https://www.infineon.com/dgdl/Infineon-FF225R17ME4_B11-DS-v02_01-en_de.pdf?fileId=db3a30432fbc32ee012fbf631bc73a55, Last Access: 2019-01-01
- [14] Mitsubishi Electric CM225DX-34T Si IGBT Half Bridge Module Datasheet, http://www.mitsubishielectric.com/semiconductors/content/product/powermodule/igbt/t_series/cm225dx-34t_e.pdf, Last Access: 2019-01-01
- [15] Semikron SEMiX353GB176HDs Si IGBT Half Bridge Module Datasheet, <https://www.semikron.com/products/product-classes/igbt-modules/detail/semix353gb176hds-27890500.html>, Last Access: 2019-01-01
- [16] Ziegler, S., Woodward, R. C., Herbert, H. C. I., & Lawrance, J. B. (2009). Current Sensing Techniques: A Review. *IEEE Sensors Journal*, 9(4), 354–376.

[17] LEM LF 510-S Current Transducer Datasheet, https://www.lem.com/sites/default/files/products_datasheets/lf_510-s.pdf, Last Access: 2019-01-01

[18] LEM LV 25-100 Voltage Transducer Datasheet, https://www.lem.com/sites/default/files/products_datasheets/lv_25-1000_e.pdf, Last Access: 2019-01-01

[19] Schneider Electric LC1F330 Contactor Datasheet, <https://www.schneider-electric.us/en/product/LC1F330/tesys-f-contactor---3p%283-no%29---ac-3---%3C%3D-440-v-330-a---without-coil/>, Last Access: 2019-01-01

[20] ABB TAL9-30-10 17-32V DC Contactor Datasheet, <https://new.abb.com/products/1SBL143061R5110/tal9-30-10-17-32v-dc-contactor>, Last Access: 2019-01-01

[21] ABB TAL26-30-10RT 17-32V DC Contactor Datasheet, <https://new.abb.com/products/1SBL243060R5110/tal26-30-10rt-17-32v-dc-contactor>, Last Access: 2019-01-01

[22] LEDWELL LW 2415M DC Power Supply, <http://www.ledwell.com.tr/ledwell-product-en.php?mid=24v-15amp-lw-2415m-adaptor-urun-323.html>, Last Access: 2019-01-01

[23] Blinov, A., Vinnikov, D., & Lehtla, T. (2011). Cooling Methods for High-Power Electronic Systems. *Scientific Journal of Riga Technical University. Power and Electrical Engineering*, 29(1), 79–86.

[24] Kang, S. S. (2012). Advanced Cooling for Power Electronics. In 2012 7th International Conference on Integrated Power Electronics Systems (CIPS). Nuremberg, Germany.

[25] Stibgen, M. (2004). Applying Laminated Busbars to Enhance DC Power Distribution Systems. In INTELEC 2004. 26th Annual International Telecommunications Energy Conference. Chicago, IL, USA.

- [26] EBMPAPST K3G 200-BD46-04 DC Fan Datasheet, https://www.ebmpapst.com/media/content/info-center/downloads_10/catalogs/compactfansen2011/compactfanssingle2011/DC_axial_fans_2016_01_EN.pdf, Last Access: 2019-01-01
- [27] Hava, A. M., Ayhan, U., & Aban, V. V. (2012). A DC Bus Capacitor Design Method for Various Inverter Applications. In 2012 IEEE Energy Conversion Congress and Exposition (ECCE). Raleigh, NC, USA.
- [28] Prodrive Technologies PT62SCMD17 SiC MOSFET Gate Driver Board Datasheet, <https://eu.mouser.com/datasheet/2/90/t62scmd17-838570.pdf>, Last Access: 2019-01-01
- [29] Filho, R. M. S., Seixas, P. F., Cortizo, P. C., Torres, L. A. B., & Souza, A. F. (2008). Comparison of Three Single-Phase PLL Algorithms for UPS Applications. *IEEE Industrial Electronics Society*, 55(8), 2923–2932.
- [30] Bobrowska, M., Rafal, K., Jasinski, M., & Kazmierkowski, M. P. (2011). Grid Synchronization and Symmetrical Components Extraction with PLL Algorithm for Grid Connected Power Electronic Converters – A Review. *Bulletin of the Polish Academy of Sciences, Technical Sciences*, 59(4).
- [31] Lechat, S. (2010). Voltage Oriented Control of Three-Phase Boost PWM Converters. Chalmers University of Technology.
- [32] Malinowski, M., Kazmierkowski, M. P., & Trzynadlowski, A. M. (2003). A Comparative Study of Control Techniques for PWM Rectifiers in AC Adjustable Speed Drives. *IEEE Transactions on Power Electronics*, 18(6), 1390–1396.
- [33] Haoran, S., Wei, X., Chenghua, F., & Yao, Y. (2013). Research on Three-phase Voltage Type PWM Rectifier System Based on SVPWM Control. *Research Journal of Applied Sciences, Engineering and Technology*, 5(12), 3364–3371.

[34] Ozkilog, M. C., Obdan, A. H., & Sarul, M. H. (2016). Comparison of Modulation Techniques of a Grid Side Converter in a Wind Energy Conversion System. *Journal for Control, Measurement, Electronics, Computing and Communications*, 57(2), 354–360.

[35] Nagar, K., Sharma, A. K., Palwalia, D. K., & Sharma, A. (2014). Harmonic Analysis of Three Phase SPWM and SVPWM Converters. *International Journal of Advanced Research in Electrical, Electronics and Instrumentation Engineering*, 3(11).

[36] Krishna, K. G., Kumar, T. K., & Rao, P. V. (2012). Better DC Bus Utilization and Torque Ripple Reduction by using SVPWM for VSI fed Induction Motor Drive. *International Journal of Computer and Electrical Engineering*, 4(2).

APPENDICES

A. CREE SiC MOSFET CHARACTERISTICS

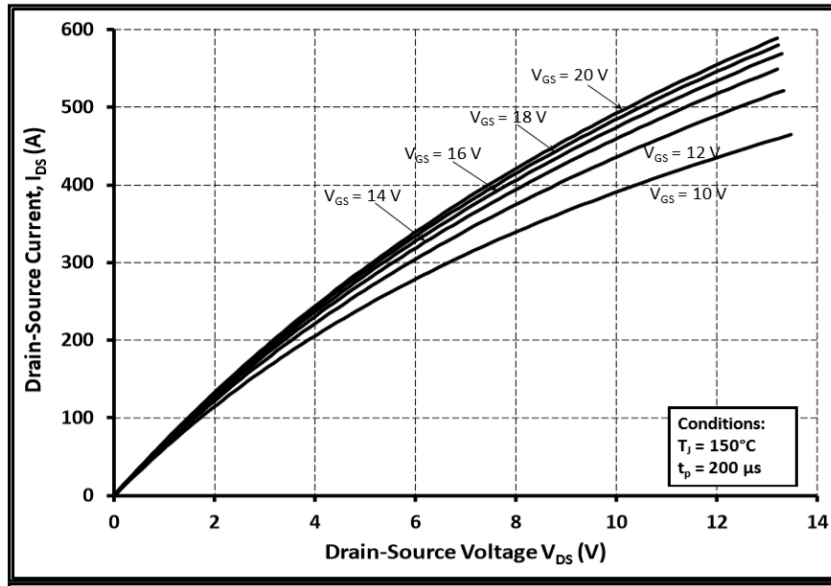


Figure A. 1. I_{DS} vs V_{DS} characteristics of SiC MOSFET

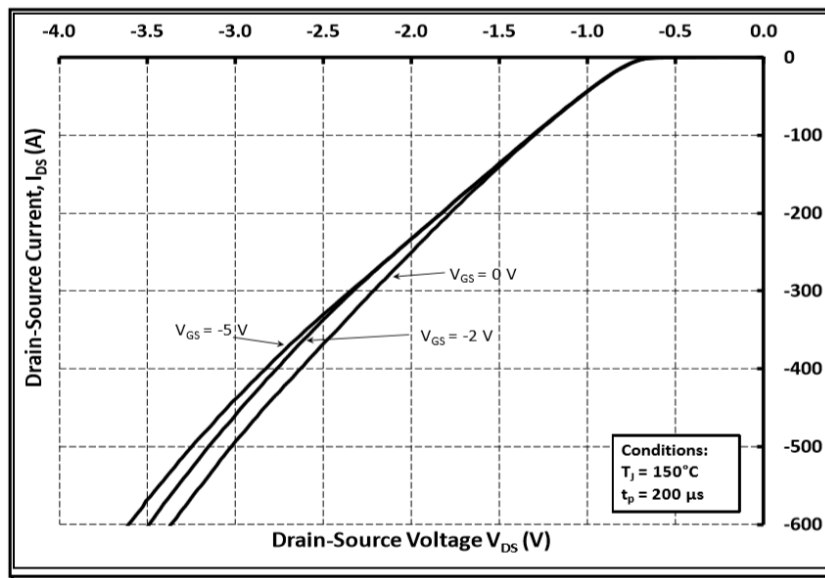


Figure A. 2. I_{DS} vs V_{DS} characteristics of FWD

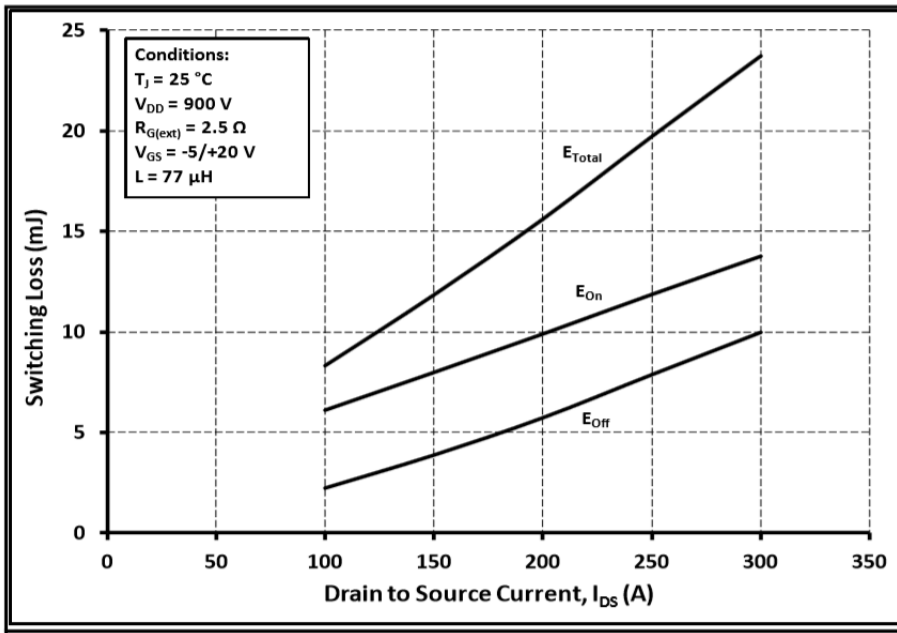


Figure A. 3. I_{DS} vs E_{ON} & E_{OFF} characteristics

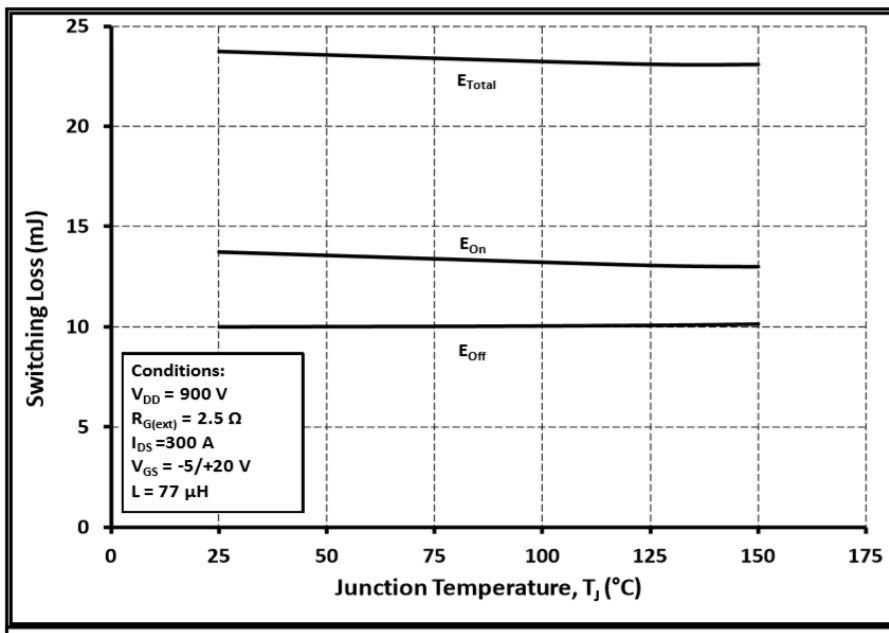


Figure A. 4. T_J vs E_{ON} & E_{OFF} characteristics

B. INFINEON Si IGBT CHARACTERISTICS

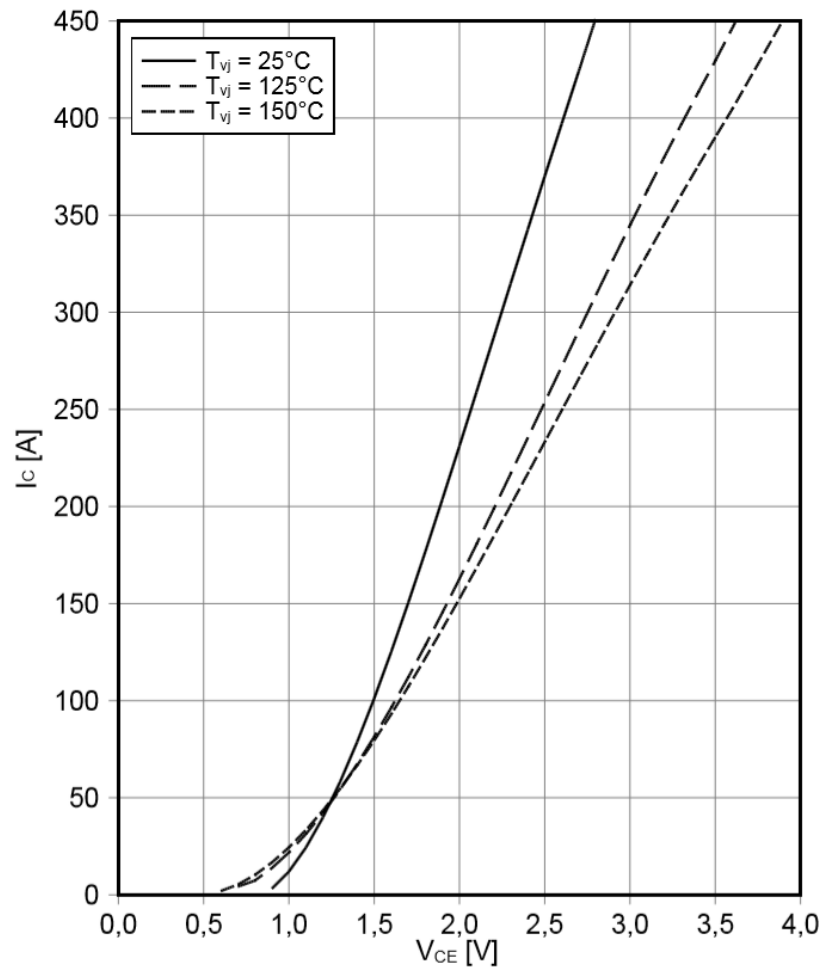


Figure B. 1. I_C vs V_{CE} characteristics of Si IGBT

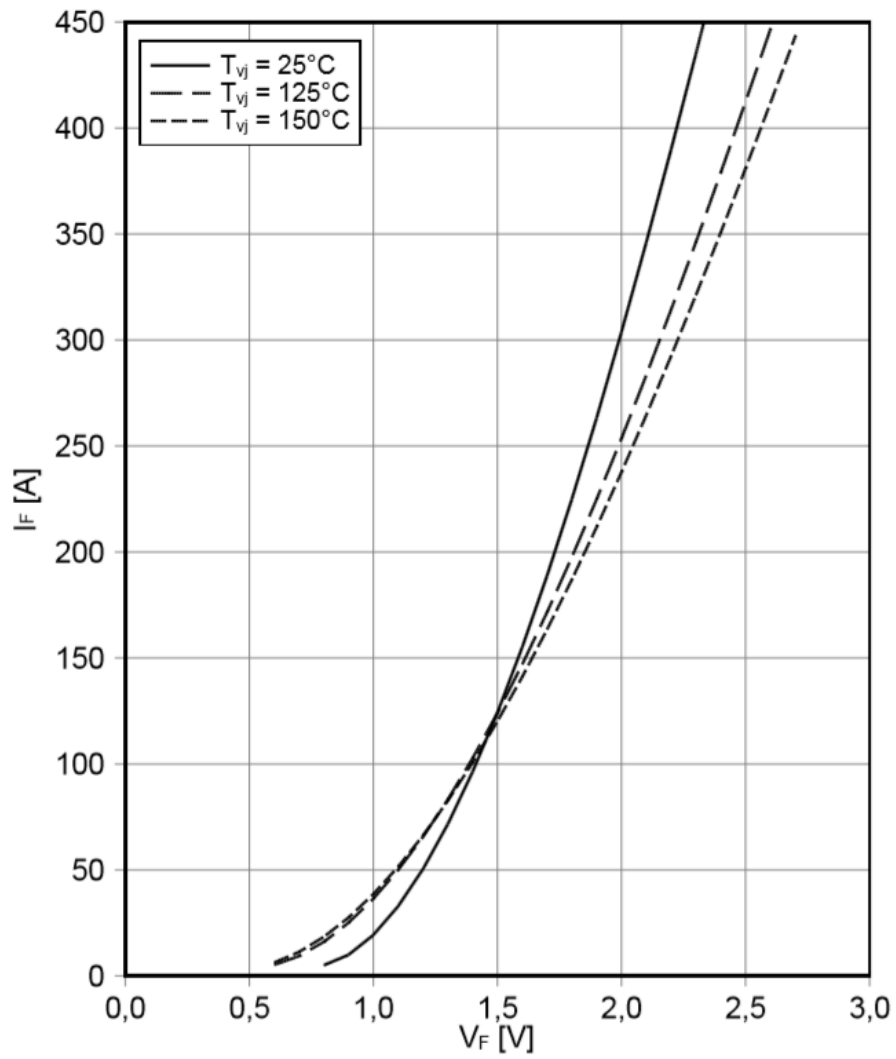


Figure B. 2. I_F vs V_F characteristics of FWD

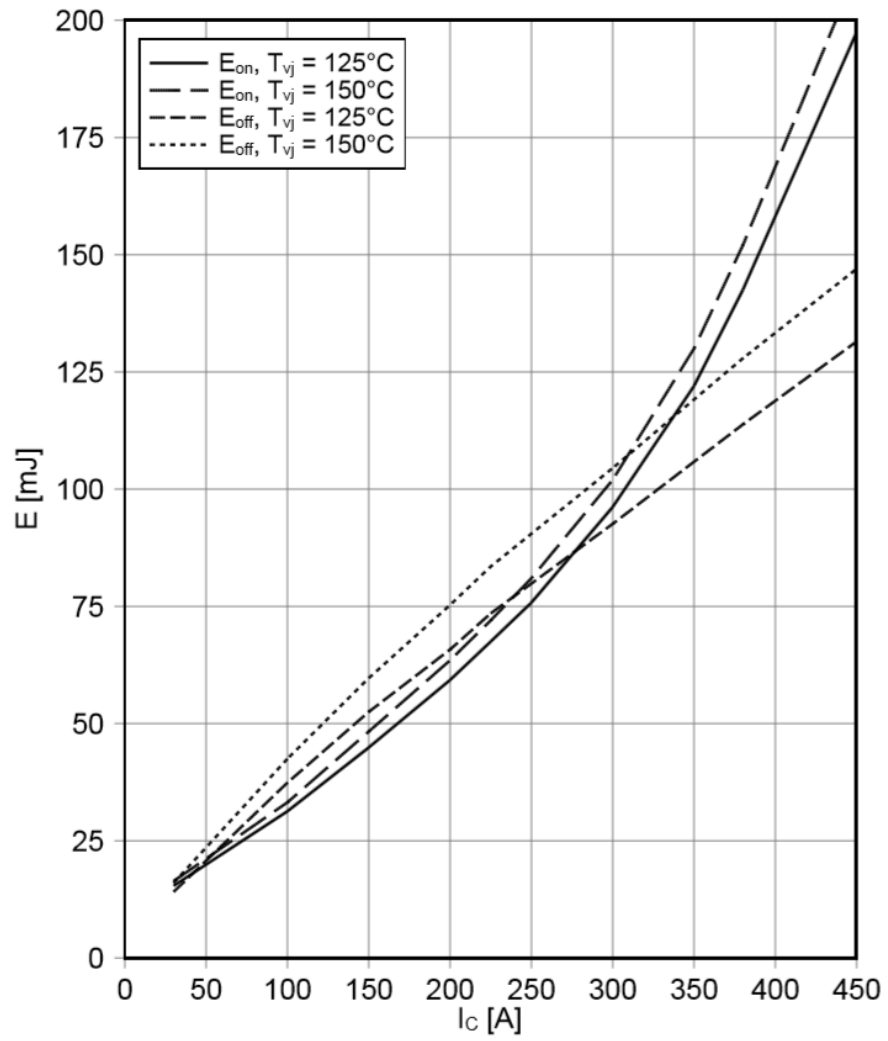


Figure B. 3. I_C vs E_{ON} & E_{OFF} characteristics

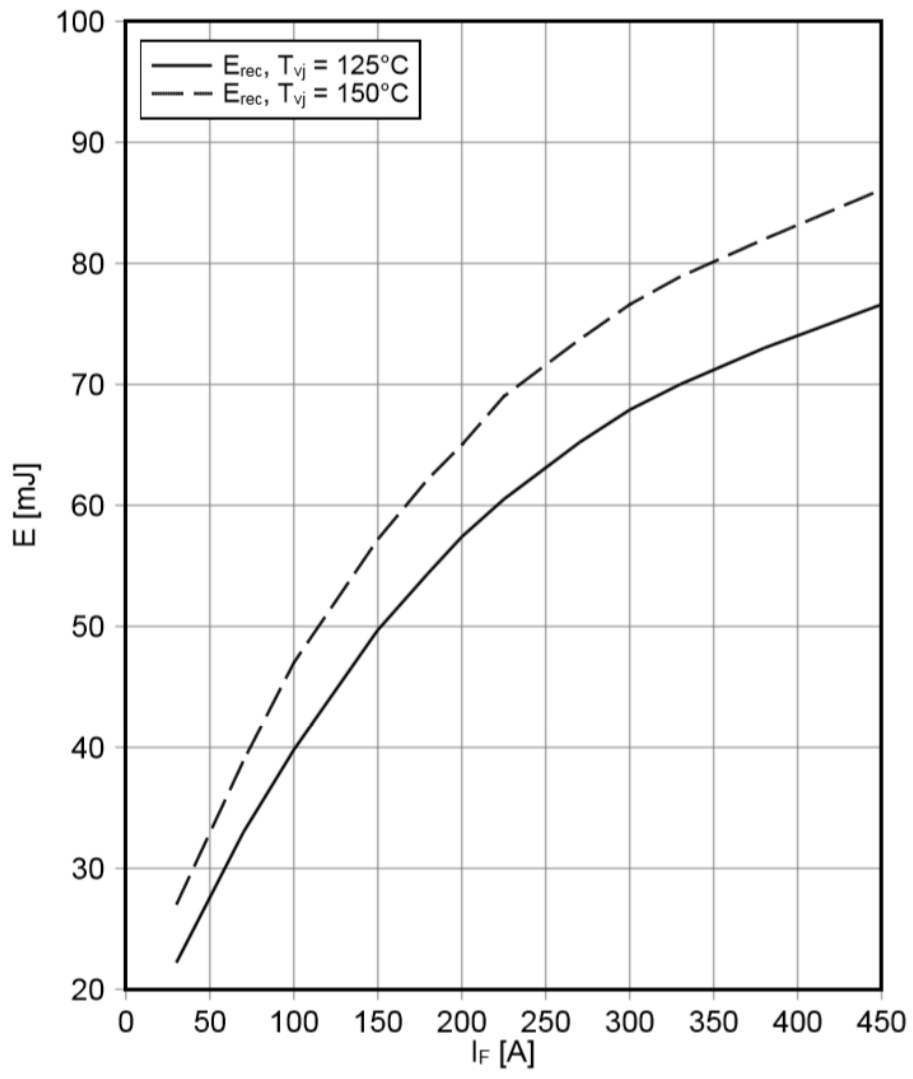


Figure B. 4. I_F vs E_{REC} characteristics

C. SEMIKRON Si IGBT CHARACTERISTICS

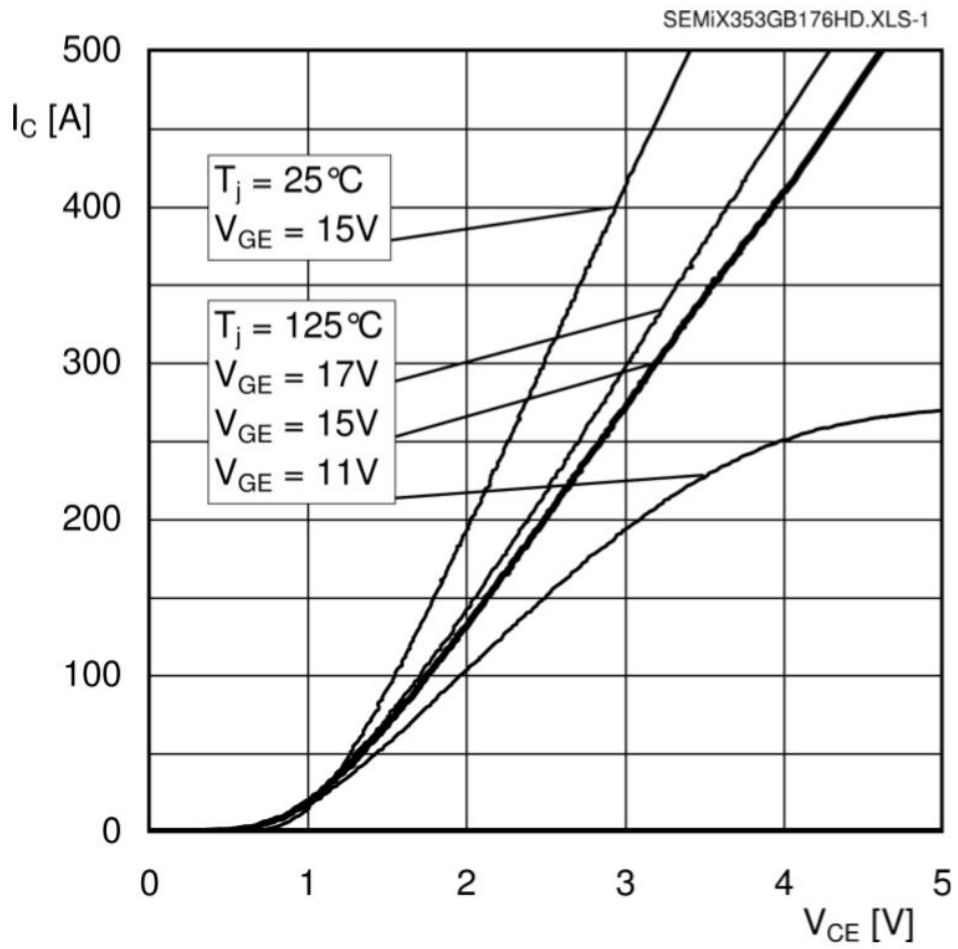


Figure C. 1. I_C vs V_{CE} characteristics of Si IGBT

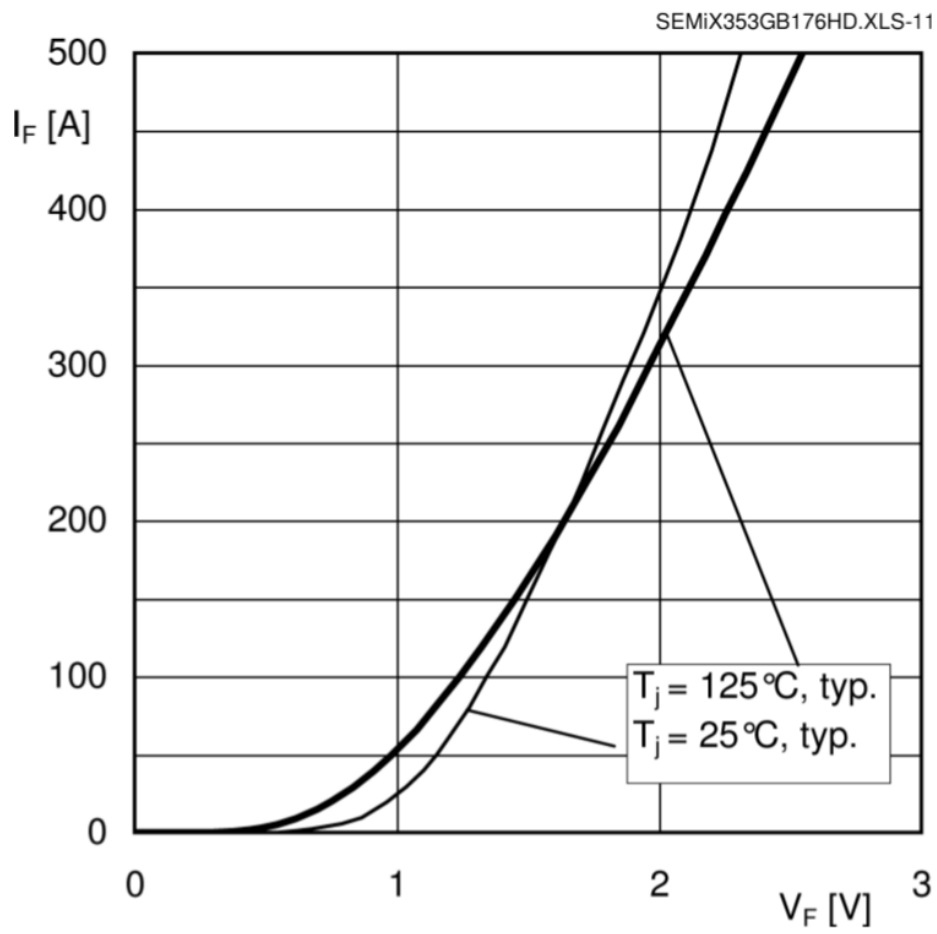


Figure C. 2. I_F vs V_F characteristics of FWD

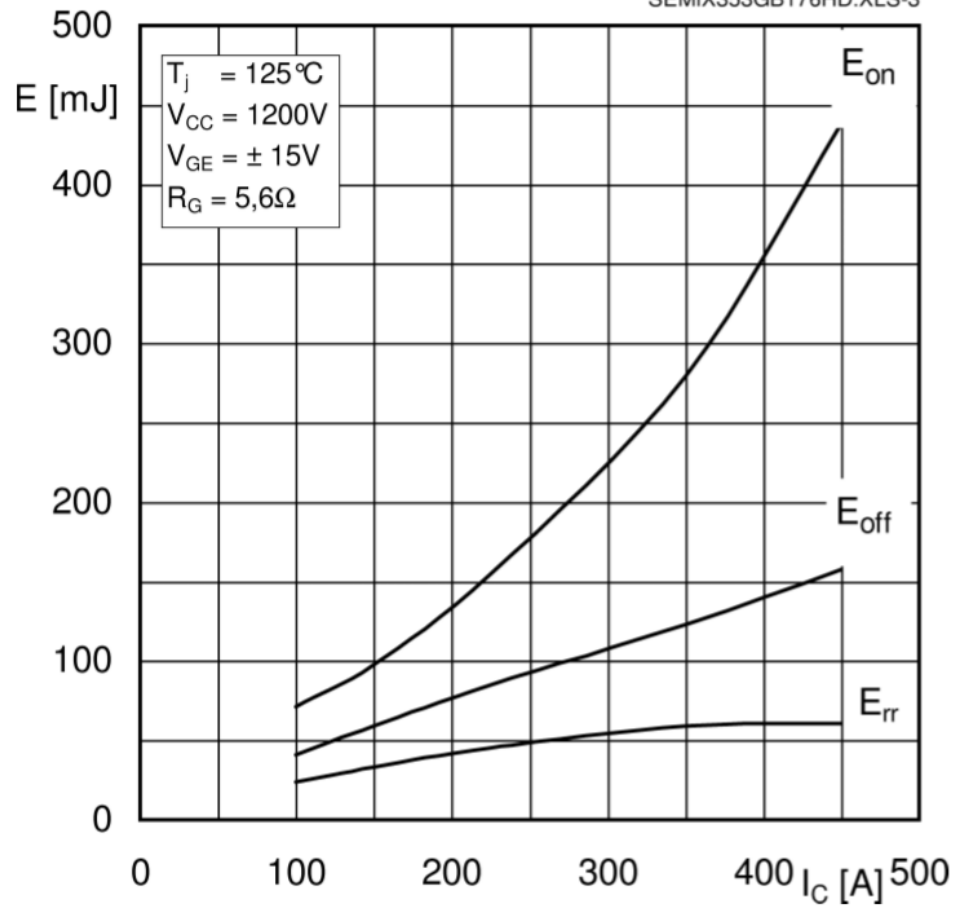


Figure C. 3. I_C vs E_{ON} & E_{OFF} & E_{REC} characteristics

D. MITSUBISHI Si IGBT CHARACTERISTICS

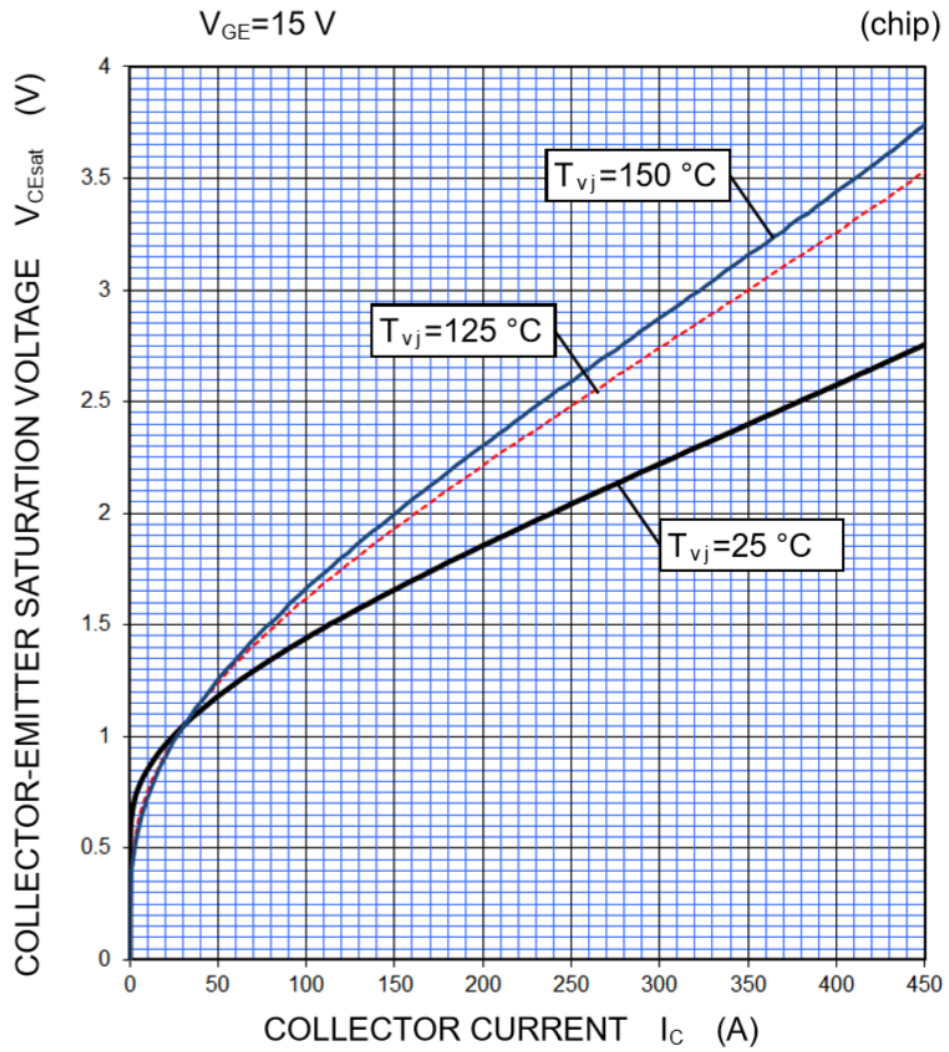


Figure D. 1. I_C vs V_{CE} characteristics of Si IGBT

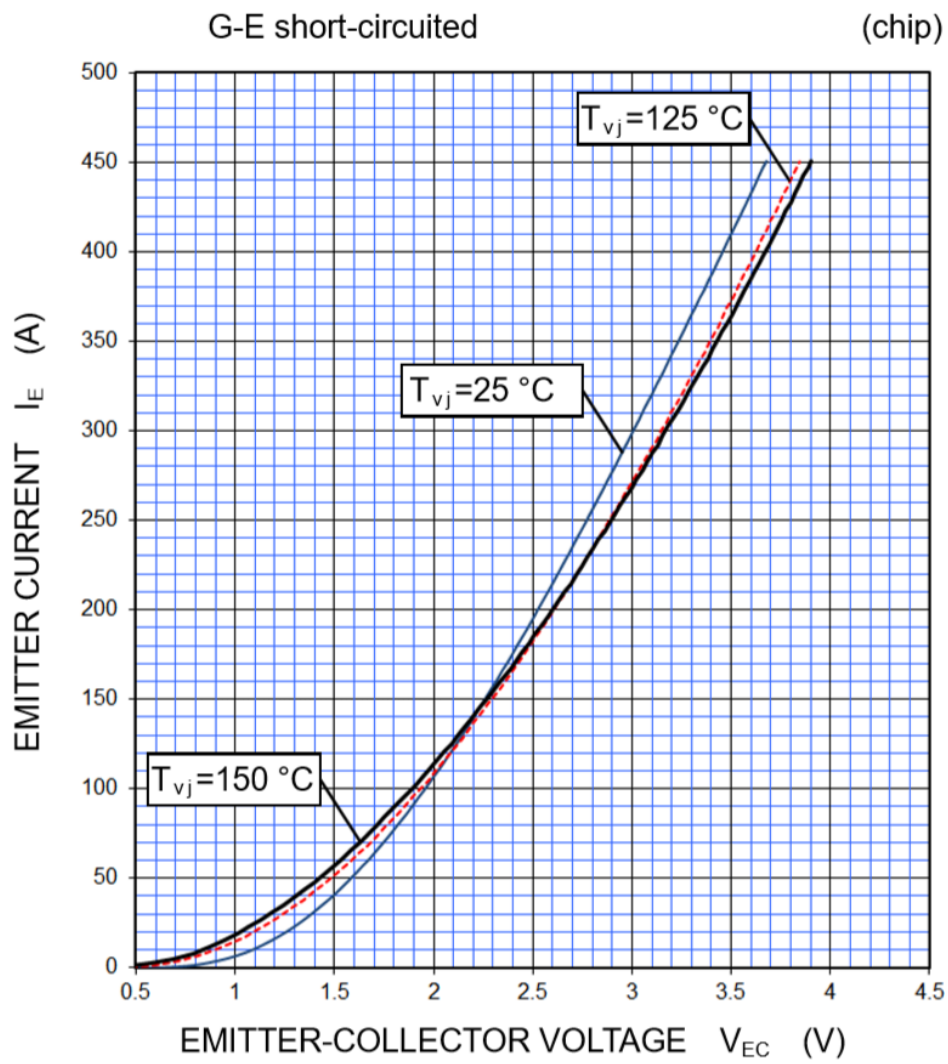


Figure D. 2. I_F vs V_F characteristics of FWD

$V_{CC}=1000\text{ V}$, $R_G=0\ \Omega$, $V_{GE}=\pm 15\text{ V}$, INDUCTIVE LOAD,
 —: $T_{vj}=150\text{ }^\circ\text{C}$, - - - - -: $T_{vj}=125\text{ }^\circ\text{C}$, PER PULSE

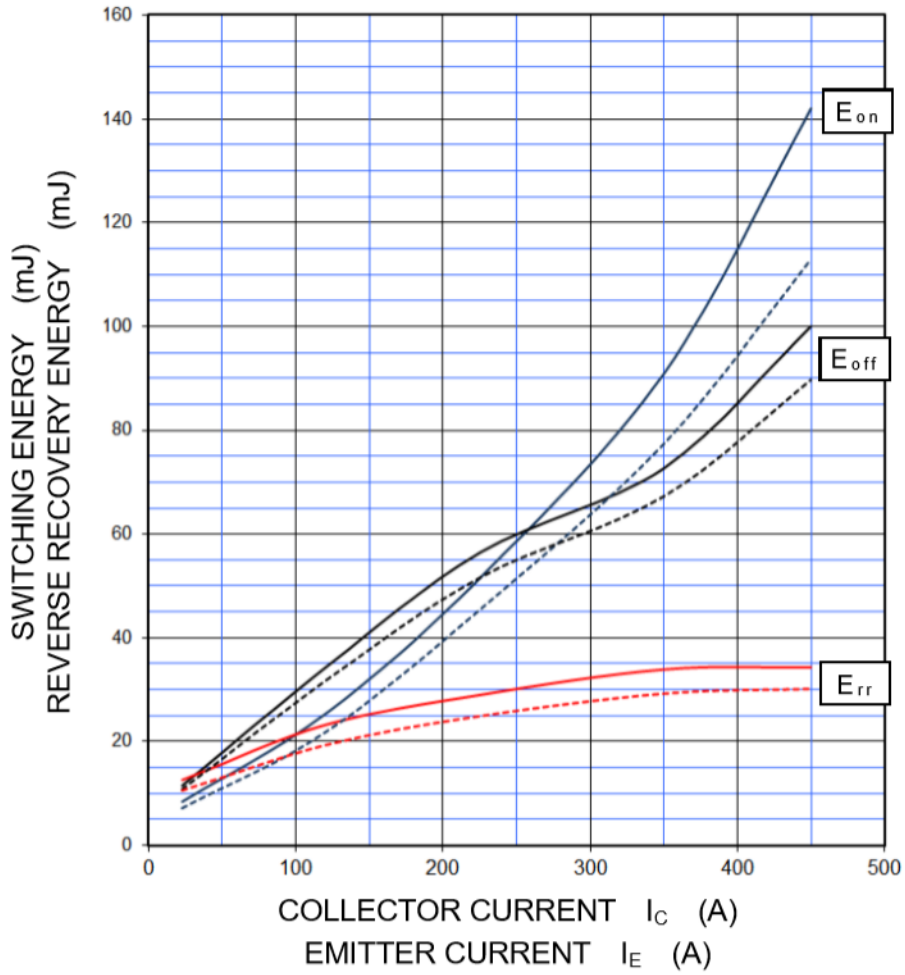


Figure D. 3. I_C vs E_{ON} & E_{OFF} & E_{REC} characteristic

